Natália Lage Domingues

Mixing in Single Screw Extrusion: Modelling and Optimization

Tese submetida com vista ao grau de Doutor

Departamento de Engenharia de Polímeros

Trabalho realizado sob a orientação de:

Prof. António Gaspar-Cunha

Prof. José António Covas

Junho 2011

Acknoledgments

This work would not be possible without the help of several entities and persons. Financial support, advisory support, collecting experimental data, organising several thousand of lines of numerical data, writings of articles and papers, were fundamental to the execution and successful completion of this work. A few people contributed with healthy discussions about some subjects related with this work, thus allowing for a better overall result. The names of contributors, in some form or another, are listed below, in alphabetic order.

A very special thanks to my son Lucas for switching the computer off several times during the final conception of this thesis, in the worst possible moments (just before auto save).

António Gaspar-Cunha, PhD (Advisor)

António Henrique Oliveira (Husband)

Cristina Teixeira (PhD student)

Francisco Mateus Ribeiro (Extruder Technician)

Fundação para a Ciência e Tecnologia (Financial suport, scolarship ref SFRH/BD/19605/2004)

Fundação Luso-Americana (Financial suport)

Guangzhou Jiechuang Trading Co., Ltd. (Raw materials supplier)

Ica Mana-Zloczower, PhD (Co-worker)

James Kaplan (Landlord)

João Paulo Peixoto (Extruder Technician)

José António Covas (Co-advisor)

Luciana Bava, PhD (Colleague)

Marco Camesasca, PhD (Co-worker)

Maria Clara Cramez, PhD (Material raw supplier)

Maria de Fátima Almeida (PhD student)

Maurício Malheiro (Microscopy Technician)

Miron Kaufman, PhD (Co-worker)

Nadya Denchev, PhD (Colleague)

Repsol (Raw materials supplier)

Summary

Given the importance of mixing in polymer processing, the aim of this work is to implement a mathematical model for quantifying the mixing behaviour in single screw extruders. The model developed considers the incorporation of solid or liquid additives into a polymeric matrix. For this purpose, the existing numerical routines capable of describing the flow in the melting and melt conveying zones of the extruder were coupled to specific programs incorporating the algorithms that quantify distributive and dispersive mixing in each system. In this way, a global modelling program for single screw extruders is developed, able to describe the flow, heat transfer and morphology development as a function of the materials properties, geometry and operating conditions.

Initially, a mathematical model is developed to predict the evolution of the morphology of immiscible liquid–liquid systems. It takes into account the stretching, breakup and coalescence phenomena and computes the dimensions of the dispersed phase in the polymeric matrix. Inserting this routine in the existing process modelling software, it becomes possible to compute the evolution of the drop dimensions along the melting and melt conveying zones. The experimental data obtained generally validated the theoretical predictions.

Subsequently, a model for solid agglomerate dispersion is proposed. As before, the numerical simulations of flow patterns in a rectangular channel were coupled to a Monte Carlo method of clusters, in order to predict rupture and erosion phenomena based on the value of the local fragmentation number. Mixing is characterized by the particle size distribution and Shannon entropy. In a further step, the model is used to predict the dynamics of filler size distribution in a plasticating single screw extruder. Again, the experimental results were generally in line with the predictions. The software is then used to investigate the effects of the process parameters on mixing.

Finally, the models of the evolution of the morphology of immiscible liquid-liquid systems and of the dispersion of solid agglomerates are adapted to compute global distributive and dispersive mixing indices in single screw extrusion. The effect of material properties, operating conditions and geometry of screw and die are discussed. For a given polymer system, the intensity of mixing is governed by the magnitude of the hydrodynamic stresses and by the residence time in the melt. The mixing indexes are used to optimize the process.

Sumário

A mistura é um tema importante na indústria dos polímeros. O objetivo deste trabalho é desenvolver e implementar um modelo matemático para quantificar a mistura numa extrusora monofuso. O modelo desenvolvido tem em consideração a incorporação de aditivos (sólidos ou líquidos) na matriz polimérica. As rotinas desenvolvidas que permitem quantificar as misturas distributiva e dispersiva num determinado sistema foram incorporadas num software de modelação de extrusão, o qual descreve o fluxo das zonas de fusão e transporte de fundido. Deste modo, conseguiu-se obter um software de modelação para extrusoras monofuso, capaz de prever o fluxo, transferência de calor e desenvolvimento da morfologia do sistema em função das propriedades dos materiais, geometria do parafuso/extrusora e das condições de processamento.

Num primeiro passo, o modelo matemático desenvolvido prevê a evolução da morfologia de sistemas de dois polímeros fundidos imiscíveis. Tem em consideração a deformação, quebra e coalescência de gotas, do polímero a dispersar, presentes no sistema, calculando a dimensão destas ao longo do parafuso. Com a incorporação deste modelo no sotware de modelação de extrusão torna-se possível calcular a evolução da dimensão de tais gotas ao longo das zonas de fusão e transporte de fundido. Realizaram-se observações experimentais, cujos resultados validam as previsões obtidas numericamente.

Num segundo passo, foi desenvolvido um modelo para prever a dispersão de aditivos sólidos numa matriz polimérica. Tal como no sistema anterior, este modelo calcula a dimensão de aglomerados sólidos, num canal rectangular, tendo em conta o número de fragmentação que regula a rutura e erosão dos sólidos. Neste modelo o momento em que o sólido sofre dispersão é calculado usando o método de Monte Carlo. A mistura é avaliada pela distribuição do tamanho das particulas sólidas e ainda pela entropia de Shannon. Consequentemente, este modelo foi aplicado às zonas de fusão e de transporte de fundido de uma extrusora monofuso, de modo a prever a evolução morfológica do sistema. Os resultados das observações experimentais são concordantes com as previsões calculadas. Deste modo, o software foi usado para estudar os efeitos dos parâmetros envolvidos no processamento de polímeros.

Por último, os modelos desenvolvidos para a previsão da morfologia de sistemas líquido-líquido imiscíveis e sólido-líquido foram adaptados de modo a calcular índices de mistura globais, tanto para mistura distributiva como para mistura dispersiva numa extrusora monofuso. Os efeitos das propriedades dos materiais, condições operatórias e geometrias do parafuso e fieira foram estudados. Para um dado sistema, a intensidade da mistura depende da magnitude das forças hidrodinâmicas e do tempo de residência do fundido. Por fim, o processo de extrusão é otimizado usando a informação destes índices de mistura.

Index

Nomenclature

Lower case Roman letters

d – Drop diameter

h – Critical value at which the liquid film breaks

k_m – Melt thermal conductivity

k_s – Solid thermal conductivity

mix_{disp} – Dispersive mixing index

mix_{dist} – Distributive mixing index

p – Viscosity ratio

p_i, p_j – Probabilities

r – Drop radius

r_c – Critical drop radius

t – Residence time

t_b – break-up time

t_{loc} – Local residence time

$\vec{v}$ – Vector velocity

x – x-direction

y – y-direction

z – z-direction

Upper case Roman letters

B – Width of the extending drop

Ca – Capillary number

Ca_{crit} – Critical capillary number

C_m – Melt specific heat

C_s – Solid specific heat

C_p – Thermal conductivity

D – Screw Diameter

D_b – Internal barrel diameter

Fa – Fragmentation number

H – Channel depth

H – Melting heat

L – Screw length

L – Length of the extending drop

M – Number of sub-regions

N – Screw speed; Number of drops/particles

N_{cur} – Current number of particles

N_{ini} – Initial number of particles

P – Pressure

P_{break} – Agglomerate break-up probability

P_{coal} – Probability of coalescence

P_{col} – Probability of collision

P_{exp} – Probability of film expulsion

T – Temperature

T_m – Melting temperature

T_s – Screw temperature

T_b – Barrel temperature

S – Shannon entropy

S_{max} – Maximum entropy

S_{norm} – Normalized Shannon entropy

V_{2D} – Two dimensional velocity profile

V_{3D} – Three dimensional velocity profile

V_{bx} – Barrel velocity in the x-direction

V_{bz} – Barrel velocity in the z-direction

V_x – Velocity at the x-direction

V_y – Velocity at the y-direction

V_z – Velocity at the z –direction

W – Channel width

Lower case Greek letters

α – Amplitude of the initial deformation;

Lower limit for the fragmentation number

β – Upper limit for the fragmentation number

δ – Random number

γ – Shear deformation

$\dot{\gamma}$ – Shear rate

ϕ – Volume fraction of the dispersed phase;

Material concentration

η – Blend viscosity

η_0, η_1, η_c – Matrix viscosity

η_d –Viscosity of the dispersed phase

λ – Index characterising the flow type

λ_N – Probability per unit time

ρ - Melt density

ρ_s – Solid density

σ_c – Cohesive strength

σ_h – Hydrodynamic stress

σ_{xy} – Shear stress *xy*-component

σ_{yz} – Shear stress *yz*-component

σ_{xz} – Shear stress *xz*-component

υ_{12} – Interfacial tension

Upper case Greek letters

Δt – Increment in time

Δx – x-axis increment

Δy – y-axis increment

Δz – z-axis increment

Ω – dominant growth rate of interfacial disturbances

List of figures

Chapter 1:

Chapter 2:

Chapter 3:

Chapter 4:

Chapter 5:

List of tables

1

Introduction

1 Introduction

Polymer single screw extrusion is a key polymer technique used to manufacture widespread plastics products such as pipes, profiles, films, electrical cables and filaments. Mixing plays an important role in the process. It determines the final morphology in many situations, such as when solid or liquid additives are to be incorporated, or when polymer blends are processed. Therefore, the capacity of predicting the degree of mixing reached in extrusion is of great practical importance.

Mixing involves the distribution/dispersion of the different material components in the matrix. If mixing of solids can be easy observable due to the size of the particles, this is not the case when the system involves melted polymers, since in this case the level of observation is at molecular scale. Most polymer systems combine two immiscible polymers, or a polymer with a solid and/or liquid additive. The degree of mixing depends is influenced by [1-7]:

a. The state of the material (e.g. solid or liquid);

b. The mechanism and kinetics of mixing (e.g. extruder type, screw geometry, operating conditions):

c. The nature and behaviour of the components (e.g. interfacial tension, viscosity, thermal conductivity);

There are a significant number of experimental and computational studies in the literature of the phenomena involved in mixing and of the development of mathematical models capable to quantify mixing. In the particular case of single screw extrusion, attention has been focused on the melt conveying zone, where the screw channel is filled with molten polymer [6-12].

The aim of this work is to develop computational predictions of mixing in systems where at least one of the components is in a liquid state. Thus, the study will be limited to the melting and melt conveying zone of a single screw extruder. More details about this thesis are presented in the forward sections.

2 Mixing Concepts

Mixing involves the distribution and/or the dispersion of the particles/materials existing in the system. Distribution consists in the spatial rearrangement of particles/materials, while dispersion consists in their size reduction. Since dispersion requires higher forces to break the particles, in practice one of two different situations can occur: a) distributive mixing without dispersion or b) the occurrence of both distributive and dispersive mixing.

Mixing is also important in cases were only a single material exists. In this case, the aim is to homogenise concentrations or melt temperature.

Figure 1 shows schematically the concept of distributive and dispersive mixing. The two mixing modes can occur simultaneously or sequentially during extrusion [13, 14].

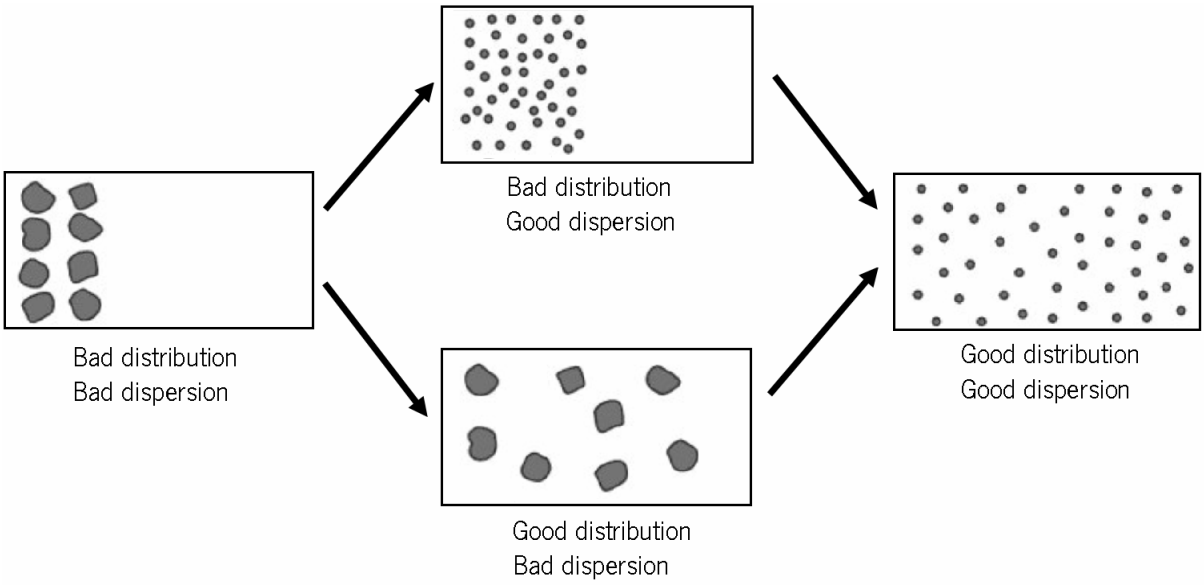

Figure 1: Concept of distributive and dispersive mixing [14].

The evaluation of the degree of mixing depends on the scale of observation, which is related to the size of the materials. Thus, a model able to describe the mixing at one scale is not necessarily applied in another scale [7, 14-15].

To promote mixing it is necessary to create relative movement between the different fluid/solid elements. Figure 2 illustrates the two types of deformation that can occur when a fluid moves due to external forces applied in a tri-dimensional space. Shear and elongational flows can exist simultaneously, sequentially or alone [7]. The relative importance of the shear and elongational flows for mixing was first demonstrated experimentally by Grace [16-17] for liquid materials. He established a relationship between the critical capillary number (Ca_{crit}) and the viscosity ratio (p), i.e., the ratio between the drop viscosity and the matrix viscosity, as can be seen in Figure 3. The capillary number quantifies the relative intensity of the viscous forces and interfacial tension. Break-up occurs when the viscous forces are sufficiently higher than the interfacial tension, i.e., when a critical capillary number is exceeded and acts during sufficient time [6, 17]. Taylor [18] and Hinch et al. [19-20] also studied the problem, their results being also included in Figure 3. They concluded that the best mixing under shear flow can be accomplished for viscosity ratios near 1, while

under elongational flow the range of viscosity ratios increases considerably. This means that elongational flow is much more efficient in promoting mixing [6-7, 16].

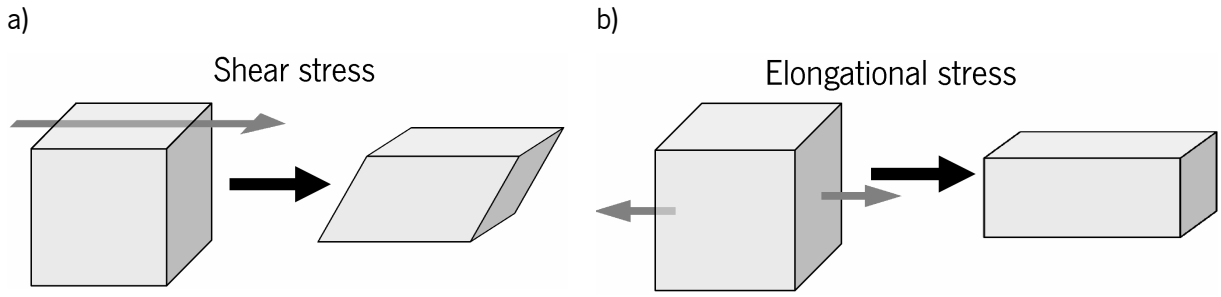

Figure 2: **a)** Shear flow and **b)** elongational flow.

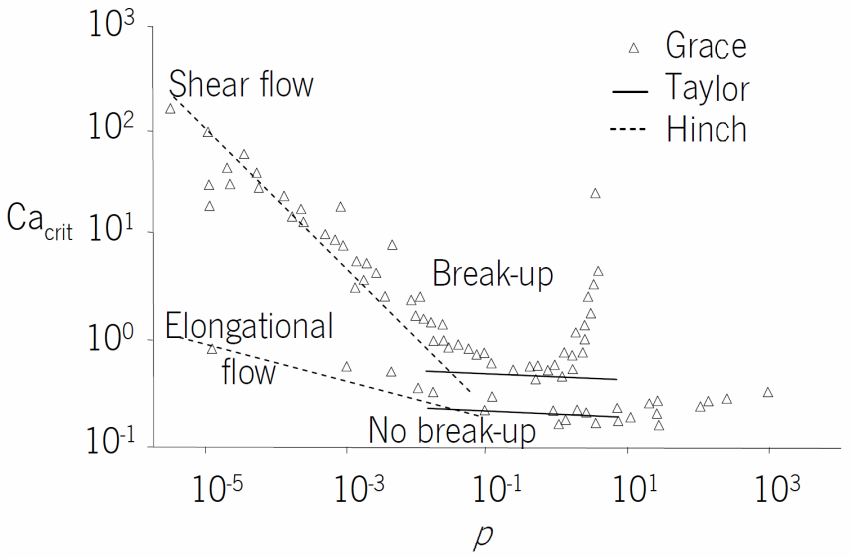

Figure 3: Grace Curve.

3 Single Screw Extrusion

The aim of this thesis is to apply the mixing concepts to quantify the mixing behavior in single screw extruders. In these machines, mixing occurs mainly when the polymer is melted, i.e., in the melt pool of the melting zone and in the melt conveying zone. In the latter it is necessary to assure that enough pressure is generated to pump the polymer through the die at the required rate. Due to its simpler modeling this functional zone has been the most studied [21-23]. With the models available, it is possible to calculate mass output, pressure, temperature, power consumption and residence time [23], knowing the material properties, the extruder geometry and the operating conditions. For that, mass, momentum and energy equations are

used, taking into account the following simplifications at melt pool of the melting zone and the melt conveying zone [21-23].

a. The density of incompressible fluids is constant during fluid flow:

$$\frac{\mathrm{D}\rho}{\mathrm{D}t}=0 \tag{1}$$

b. At the rectangular channel the velocity in the y direction is zero:

$$V_y=0 \tag{2}$$

c. The velocity profile depends only on the x and y direction:

$$\frac{\partial V_x}{\partial z}=\frac{\partial V_y}{\partial z}=\frac{\partial V_z}{\partial z}=0 \tag{3}$$

From simplification a. to c. the mass equation becomes:

$$\frac{\partial V_x}{\partial x}=0 \tag{4}$$

d. The mass forces of a fluid are zero:

$$\vec{f}=\vec{0} \tag{5}$$

e. Taking into account an incompressible fluid, it is assumes to have a stationary flow:

$$\frac{\mathrm{D}\vec{V}}{\mathrm{D}t}=0 \tag{6}$$

From simplification d. and e. the momentum equations become:

$$\frac{\partial P}{\partial x}=\frac{\partial}{\partial y}\left(\eta\frac{\partial V_x}{\partial y}\right) \tag{7a}$$

$$\frac{\partial P}{\partial y}=0 \tag{7b}$$

$$\frac{\partial P}{\partial z}=\frac{\partial}{\partial x}\left(\eta\frac{\partial V_z}{\partial x}\right)+\frac{\partial}{\partial y}\left(\eta\frac{\partial V_z}{\partial y}\right) \tag{7c}$$

f. Thermal conductivity (k) and specific heat (C_p) of the material are assumed to be constants.

g. The temperature does not depend on the fluid pressure:

$$\frac{\partial\left(V_x P\right)}{\partial x}=\frac{\partial\left(V_y P\right)}{\partial y}=\frac{\partial\left(V_z P\right)}{\partial z}=0 \tag{9}$$

h. Heat convection exists only at the z direction:

$$\frac{\partial T}{\partial x}=\frac{\partial T}{\partial y}=0 \tag{10}$$

i. Heat conduction exists at the *x* and *y* directions:

$$\frac{\partial^2 T}{\partial z^2} = 0 \tag{11}$$

Taking into account all the simplifications, the energy equation becomes:

$$\rho_m \, c_p \, V_z(y) \frac{\partial T}{\partial z} = k_m \left(\frac{\partial^2 T}{\partial x^2} + \frac{\partial^2 T}{\partial y^2} \right) + \eta \, \dot{\gamma}^2 \tag{12}$$

where the shear rate is given by:

$$\dot{\gamma} = \left[\left(\frac{\partial V_x}{\partial y} \right)^2 + \left(\frac{\partial V_z}{\partial x} \right)^2 + \left(\frac{\partial V_z}{\partial y} \right)^2 \right]^{1/2} \tag{13}$$

The boundary conditions are:

$$\begin{cases} V_x(y=0) = 0 \\ V_x(y=H) = -V_{bx} \end{cases} \qquad \begin{cases} V_z(x=0) = 0 \\ V_z(x=W) = 0 \\ V_z(y=0) = 0 \\ V_z(y=H) = V_{bz} \end{cases} \qquad \begin{cases} T(x=0) = T_s \\ T(x=W) = T_s \\ T(y=0) = T_s \\ T(y=H) = T_b \end{cases} \tag{14}$$

Given the complexity of the process (number of variables involved, screw geometry and Non-Newtonian nature of the polymers), it is appropriate to simplify the momentum and energy equations. Usually, melting conveying develops in the metering zone, where the channel depth is smaller and constant. Thus, it can be assumed to have an unwounded and rectangular channel where the polymer flows between two parallel plates of infinite dimensions [24], as described in Figure 4.

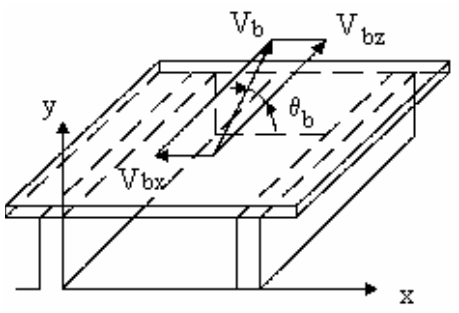

Figure 4: Simplified rectangular screw channel and velocities involved.

In single screw extrusion shear flow is predominant. Figure 5a shows the mechanism of deformation due to shear occurring in a channel cross-section [15]. The shear induced by the velocity profiles is not constant

along the section, and with the help of the velocity profiles, the material suffers stretching, folding and reorientation as illustrated in Figure 5b [6-7, 25].

a)

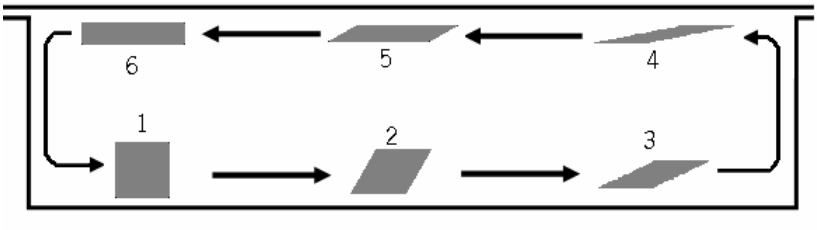

b)

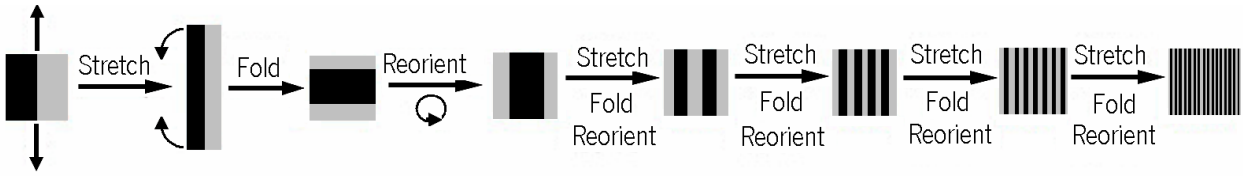

Figure 5: a) Shear deformation at a channel cross-section; b) Stretching, folding and reorientation phenomena in a cross channel section [25].

Taking into consideration the flow characteristics inside the screw channel it is important to identify how this can be used to quantify mixing given the materials properties, screw geometry and operating conditions.

The literature suggests that the degree of mixing increases with the generation of interfacial area between the individual material components and with the residence time [14]. Thus, the shear strain of the melted polymer will play an important role in the generation of this interfacial area. As stated above, the stress experienced by each polymer particle varies with its position in the screw channel. Therefore, a simple way to quantify the degree of mixing in an extruder can be the average strain [26-29]. Pinto and Tadmor [26] computed the Residence Time Distribution (RTD) and the "degree of mixing" (by means of a weighted-average total strain - WATS), assuming the isothermal flow of a Newtonian fluid between parallel plates. Bigg [27-28] developed a two-dimensional non-Newtonian isothermal model predicting the residence time and strain distributions.

Generically, there are differences between the mixing mechanisms in liquid-liquid and solid-liquid systems. In both cases, erosion and rupture phenomena develop. Erosion is the detachment of small fragments from the surface of the material, while rupture is the break-up of the material into two or more large fragments, as illustrated in figure 6.

In liquid-liquid systems the shear rate acts on the drop, causing its deformation, elongation and possible break-up. Erosion also occurs but is not significant, since it contributes less than 1% to the reduction of drop size [29]. For this reason, erosion in liquid-liquid systems will not be considered in this work. Coalescence happens when two drops merge due to the flow; consequently it increases the drops volume. These phenomena are shown schematically in Figure 6.

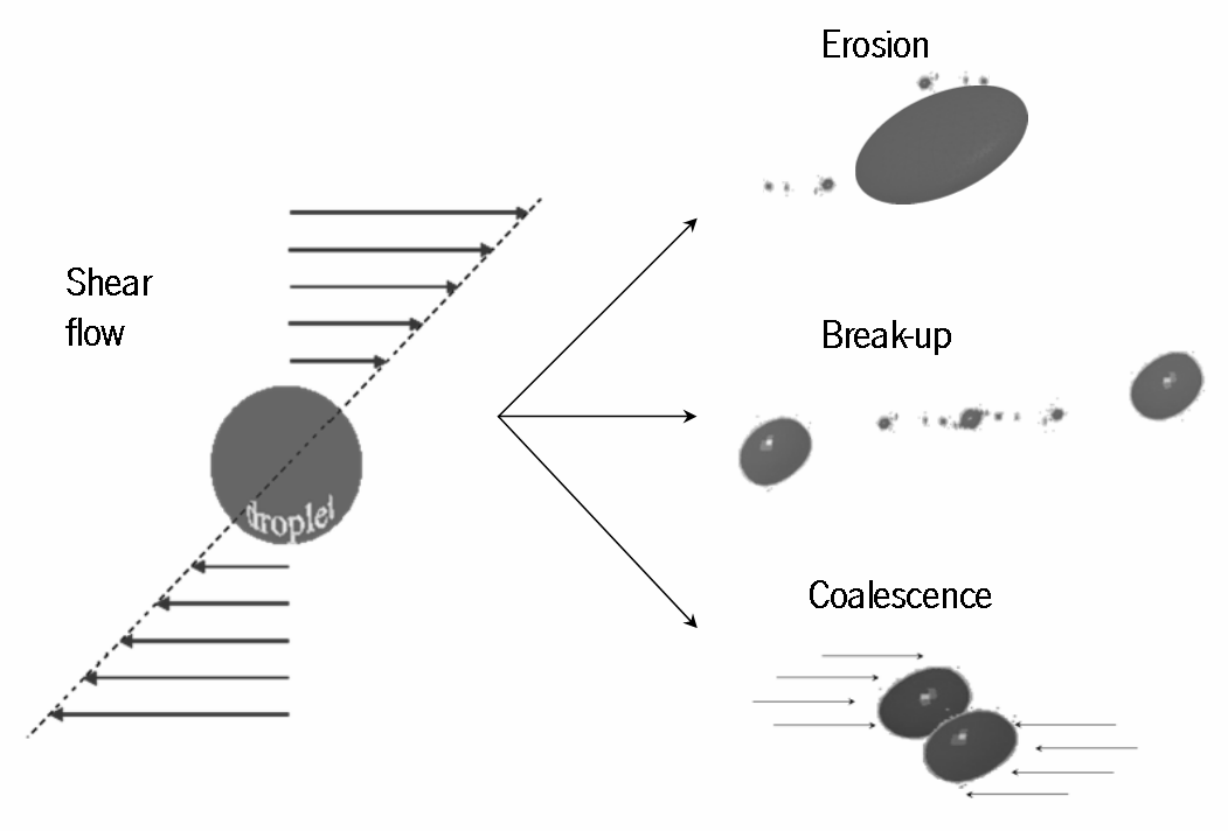

Figure 6: Dispersive mixing in liquid-liquid systems.

Concerning solid-liquid systems, dispersion occurs when the hydrodynamic forces induced by the flow are higher than the cohesive strength of the solid agglomerate. Erosion, in this case, is significant. Depending on the flow characteristics, solid agglomerates can erode 100%, i.e., they can be reduced to many single and indivisible particles. Rupture can also occur at a large scale. However, it is more difficult to induce rupture than erosion [13]. Figure 7 illustrates schematically these two phenomena. Similarly to the phenomena of coalescence, in solid-liquid systems flocculation can occurs, but due to the complexity involved in predicting its behavior it will not be taken it into account in this work.

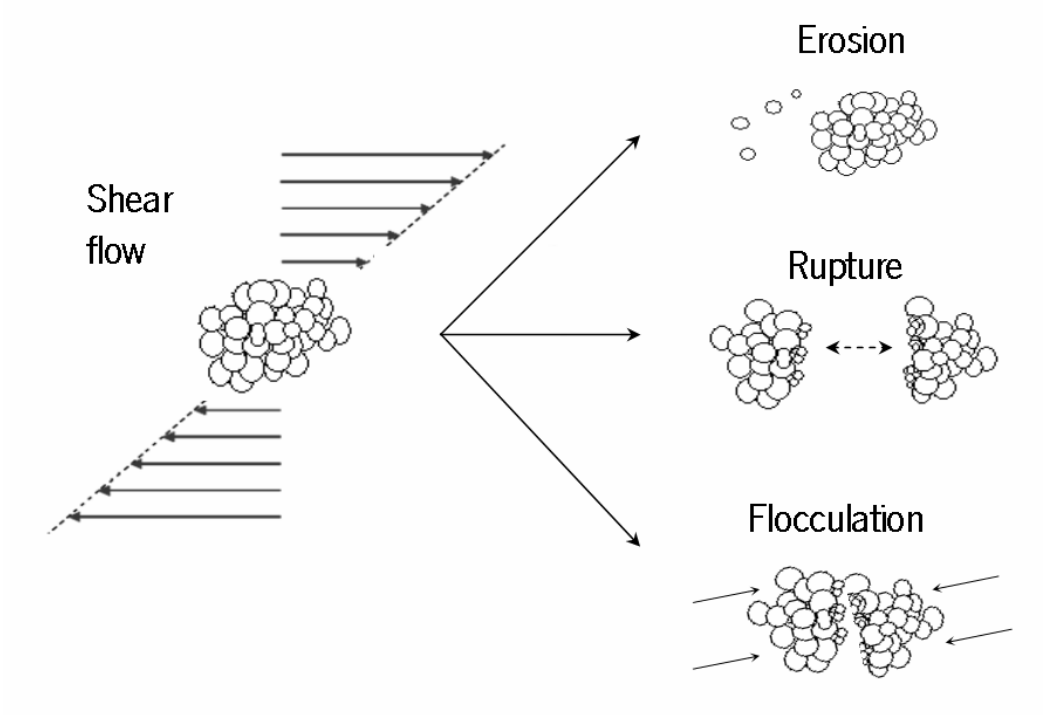

Figure 7: Dispersive mixing in solid-liquid systems.

4 Thesis Summary

The aim of this work is to develop computational mixing models able to predict mixing in a single screw extruder. Two different types of physical systems are considered: liquid-liquid and solid-liquid systems. The models developed should help to predict the mixing behaviour as a function of the materials properties, system geometry and operating conditions in order to use them in the development of a global software able to assists screw design and process optimization.

The work developed in presented in four chapters, describing computational and experimental steps to implement and validate the mixing models. Below a summary of each one of these chapters is presented.

Chapter II – Estimation of the Morphology Development of Immiscible Liquid–Liquid Systems during Single Screw Extrusion:

A mathematical model to predict the evolution of the morphology of immiscible liquid-liquid systems in single screw extruders is developed. The model is based on the literature and takes into account the deformation of the minor component in the system. The deformation of the material depends on the polymer properties and the flow and processing conditions. The minor component is constituted by drops uniformly

distributed in the polymeric matrix. Two phenomena affecting the system morphology are considered in the model, break-up and coalescence of drops. The morphology developed depends on the capacity of the flow in breaking the drops, but this only occurs if the deformation induced takes place during a sufficient time. The mixing model is superimposed on a two-dimensional flow modelling software able to compute the velocity profiles needed by the mixing routine. Thus, the mixing model is able to take into account the influence of process parameters, such as materials properties, screw geometry and operating conditions. Experimental work using an HDPE/PP blend is performed using different processing conditions to assess the predicting capabilities of the model. The average drop size is calculated and compared with the estimated average drop size. The limited experimental data obtained was generally in line with the theoretical predictions. Extensive computational studies were performed to analyse the influence of the material properties, such as viscosity ratio and interfacial tension, the operating conditions (screw speed and barrel temperature) and the screw geometry.

Chapter III – Modelling of Agglomerate Dispersion in Single Screw Extruders.

A model for solid agglomerate dispersion in single screw extruders is proposed. In solid-liquid systems the hydrodynamic forces are the responsible for two phenomena: erosion and rupture of solid agglomerates of single particles. The model proposed predicts the morphology of such systems, by computing the particle size distribution of the population of agglomerates present in the matrix. It combines numerical simulations of flow patterns in the metering section of a single screw extruder with a Monte Carlo method of clusters rupture and erosion mediated by a local fragmentation number. Particle size distributions and Shannon entropy are used for mixing characterization. The model is quite general and can be adapted to different polymer systems as well as for different processing equipment. It was applied on a rectangular channel simulating the metering zone of a single screw extruder, under isothermal conditions and using a three-dimensional flow modelling software. The analysis of this case study showed that the event of rupture or erosion depends not only on the hydrodynamic forces applied, but also on flow re-orientation. The agglomerate size distribution and the Shannon entropy are computed along the rectangular channel as well. The results evidence that a polymeric matrix containing solid additives tends to be homogenous in time. Such homogeneity is highly dependent on the operating conditions.

Chapter IV – Dynamics of Filler Size and Spatial Distribution in a Plasticating Single Screw Extruder - Modeling and Experimental Observations.

The model of agglomerate break-up developed in chapter III, incorporating both rupture and erosion, is employed to predict the dynamics of filler size distribution in a plasticating single screw extruder. As in chapter II, the mixing model for solid-liquid systems is superimposed on a two-dimensional flow modelling software. The comparison between the computational and experimental results obtained under different processing conditions on the filler spatial distribution along the extruder length, produced for a HDPE/silica system proved to be satisfactory. The method was also used to investigate the effect of material properties, operating conditions and extruder geometry on the dynamics of agglomerate dispersion along a single screw extruder. Generally, dispersion levels were primarily governed by the magnitude of the hydrodynamic stresses developed in the extruder and the residence time in the melt.

Chapter V – A Quantitative Approach to Assess the Mixing Ability of Single Screw Extruders for Polymer Extrusion.

Models to predict the evolution of the morphology of immiscible liquid-liquid systems and of solid agglomerate dispersion in single screw extruders are adapted to compute global distributive and dispersive mixing indices. The mixing indices proposed reflect the distributive and dispersive mixing degree in systems containing a liquid or solid additive. The two types of polymeric systems are studied separately. In the case of liquid-liquid systems, the dimensions of the dispersed phase are computed along the melting and melt conveying zones of the screw and take into account the affine deformation, break-up and coalescence of drops. The model of agglomerate break-up incorporates both rupture and erosion, whilst the filler spatial distribution is estimated along the same two screw zones.

The effect of material properties (e.g., interfacial tension, viscosity ratio, matrix viscosity, cohesive forces and thermal conductivity), operating conditions (e.g., screw speed and barrel temperature) and geometry of the screw and die (e.g., length of metering zone, compression ratio, channel depth and die geometry) are investigated. For a given polymer system, the intensity of mixing is governed by the relative magnitude of the hydrodynamic stresses and the residence time in the melt. The mixing indices proposed are used to optimize the process.

This thesis gave origin to the following international journal publications and conference presentations:

International Journals:

1. Domingues N, Camesasca M, Kaufman M, et al., *Modeling of Agglomerate Dispersion in Single Screw Extruders*. International Polymer Processing. 2010; 25(3):251-257.
2. Domingues N, Gaspar-Cunha A, Covas JA., *Estimation of the morphology development of immiscible liquid–liquid systems during single screw extrusion*. Polymer Engineering and Science. 2010; 50(11):2194-2204.
3. Domingues N, Gaspar-Cunha A, Covas JA, et al., *Dynamics of Filler Size and Spatial Distribution in a Plasticating Single Screw Extruder – Modeling and Experimental Observations*. International Polymer Processing. 2010; 25(3):188-198.
4. Domingues N, Gaspar-Cunha A, Covas JA., *Global Mixing Indices for Single Screw Extrusion*. International Journal of Material Forming. 2008; 1:723-726.
5. Domingues N, Gaspar-Cunha A, Covas JA., *Modelling of Mixing in Single Screw Extruders*. Materials Science Forum. 2006; 514:1409-1413.

Conference presentations:

1. Domingues N, Gaspar-Cunha A, Covas JA., *Re-visiting extrusion scale-up*. In: 11th Esaform Conference on Material Forming. Lyon, France; 2008.
2. Domingues N, Gaspar-Cunha A, Covas JA., *Global Mixing Indices for Single Screw Extrusion*. In: 11th Esaform Conference on Material Forming. Lyon, France; 2008.
3. Domingues N, Gaspar-Cunha A, Covas JA., *The use of global mixing indices to assess mixing efficiency in single screw extrusion*. In: PPS 24 - Proceedings of the Polymer processing Society Annual Meeting. Salerno, Italy; 2008.
4. Domingues N, Gaspar-Cunha A, Covas JA, et al., *Numerical and experimental study of agglomerate dispersion in polymer extrusion*. In: PPS 24 - Proceedings of the Polymer processing Society Annual Meeting. Salerno; 2008.

5. Domingues N, Gaspar-Cunha A, Covas JA., *The use of Global Mixing Indices to Assess Mixing Efficiency in Single Screw Extrusion*. In: Plastic Extrusion Asia 2008 Conference. Bangkok, Thailand; 2008.

6. Domingues N, Gaspar-Cunha A, Covas JA., *Predicting Distributive and Dispersive Mixing in Polymer Extrusion*. In: César de Sá J, Santos A, eds. NUMIFORM'07, Materials Processing and Design: Modelling, Simulation and Applications. Porto, Portugal: American Institute of Physics; 2007: 1531-1537.

7. Domingues N, Gaspar-Cunha A, Covas JA, Manas-Zloczower I., *Computational and Experimental Study of Mixing in a Single Screw Extruder*. In: Cueto E, Chinesta F, eds. 10th Esaform Conference on Material Forming. Zaragoza, Spain; 2007.

8. Domingues N, Camesasca M, Kaufman M, et al., *Modelling Agglomerate Dispersion in Single Screw Extruders*. In: ANTEC 2006 - 64th SPE Annual Technical Conference; 2006: 942-946.

References

1. J.L. White, *Polymer Mixing – Technology and Engineering*, Hanser Publishers, Germany (2001)

2. T.A. Osswald, *Polymer Processing Fundamentals*, Hanser Publishers, Munich (1998)

3. L.A. Utracki, *Polymer Alloys and Blends – Thermodynamics and Rheology*, Hanser Publishers, Munich (1989).

4. J.T. Lindt and A.K. Ghosh, *Fluid mechanics of the formation of polymer blends. Part I: Formation of lamellar structures*, Polym. Eng. Sci., **32**, 1802-1813 (1992).

5. Y. Suetsugu, *The effect of mixing on some properties of compounds and composites*, In Mixing and Compounding of Polymers, Manas-Zloczower, I., Tadmor, Z. (Eds), Hanser Publishers, Munich, 521 (1994).

6. H.E.H. Meijer, J.M.H. Janssen, *Mixing of Immiscible Liquids*, In Mixing and Compounding of Polymers, Manas-Zloczower, I., Tadmor, Z. (Eds), Hanser Publishers, Munich, 85, Hanser Publishers, Munich (1994)

7. J.M. Ottino, *The Kinematics of Mixing: Stretching, Chaos and Transport*, Cambridge Univ. Press. UK (1989)

8. P.H.M. Elemans, J.M. van Wunnik, "The Effect of Feeding Mode on Dispersive Mixing Efficiency in Single-Screw Extrusion", Polym. Eng. Sci., **41**, 1099-1106 (2001)

9. M. Gale, *Mixing in Single Screw Extruders*, Chemetech Publishing (2009)

10. R.I. Janes, P.J. Winch, *Mixing and shear predictions for a single-screw extruder, using computational simulation*, IMA Journal of Management Mathematics, **5**, 399-415 (1993)

11. C. Rauwendaal, *Mixing in Polymer Processing*, Marcel Dekker Inc., New York (1991)

12. S. Tyagi, A.K. Ghosh, *Morphology Development during Blending of Immiscible Polymers in Screw Extruders*, Polym. Eng. Sci, **42**, 1309-1321 (2002)

13. I. Manas-Zlockzower, *Analysis of Mixing in Polymer Processing Equipment*, Rheology Bulettin, **66** (1997)

14. Z. Tadmor, C.G. Gogos, *Principles of Polymer Processing*, 2nd Ed., John Wiley & Sons, Inc., New Jersey (2006)

15. C. Rauwendall, *Polymer Extrusion*, Hanser Publisers, Munich (1986)

16. H.P. Grace, *Dispersion Phenomena is High Viscosity Immiscible Fluid Systems and Application of Static Mixers as Dispersion Devices in such Systems*, Chemical Engineering Communications, 14, 225 (1982)

17. L. Delamare and B. Vergnes, Polym. Eng. Sci., 36, 1685 (1996).

18. G. I. Taylor, *The Viscosity of Fluid Containing Small Drops of another Fluid*, Proceedings of the Royal Society of London, Series A, 138 (834), p. 41 (1932)

19. E. J. Hinch, A. Acrivos, *Steady Long Slender in Two-Dimensional Straining Motion*, Journal of Fluid Mechanics, 97 (3), p. 401 (1979)

20. E. J. Hinch, A. Acrivos, *Long Slender Drops in a Sample Shear Flow*, Journal of Fluid Mechanics, 98 (2), p. 305 (1980)

21. K. Amellal, P.G. Lafleur, B. Arpin, *Polymer Rheology and Processing*, ed.s A.A. Collyer, L.A. Utracki, Elsevier, 277 (1989)

22. Z. Tadmor, I. Klein, *Engineering Principles of Plasticating Extrusion*, Van Nostrand Reinhold, Ney York (1970)

23. Cunha, A.G., *Modelling and optimization of single screw extrusion*, PhD Thesis, University of Minho, Portugal (1999)

24. J.F. Carley, R.S. Mallouk, J.M. McKelvey, *Experimental Studies of Melt Extrusion*, Ind. Eng. Chem., **45**, 5, 974 (1953)

25. A. J. deMello, *Control and detection of chemical reactions in microfluidic systems*, in Nature Review, 442, pp. 394-402 (2006)

26. G. Pinto, Z. Tadmor, *Mixing and Residence Time Distribution in Melt Screw Extruders*, Polym. Eng. Sci., 10, pp. 279-288 (1970).

27. D.M. Bigg, *Mixing in a Single Screw Extruder*, PhD. Thesis, University of Massachusetts (1973).

28. D.M. Bigg, S. Middleman, *Mixing in a Screw Extruder. A Model for Residence Time Distribution and Strain,* Ind. Eng. Chem. Fundam., 13, pp. 66-71 (1974).

29. Y. Renardy, V. Cristini and J. Li, *Drop fragment under shear with inertia*, International Journal of Multiphase Flow, **28**, 1125 (2002)

II

Estimation of the Morphology Development of Immiscible Liquid–Liquid Systems during Single Screw Extrusion [1]

[1] Article published at Polymer Engineering & Science, volume 50, Issue 11, pages 2194-2204, November 2010
Authores: N. Domingues, A. Gaspar-Cunha, J. A. Covas

1 Introduction

Plasticating extrusion is an important processing technique for the manufacture of plastics products. Presently, due to the continuous development of more performing material systems, single screw extruders rarely process pure homopolymers. Instead, they must melt, mix/blend and pump more complex material systems, such as polymers with a number of specialized additives, polymer blends, or highly filled compounds.

When the solid feedstock starts melting, blending and mixing of the components begin, the evolution of these phenomena along the screw axis depending on the local thermo-mechanical environment. It is well known that the morphology of a blend of two immiscible polymers, or the degree of dispersion of solid agglomerates, determine the performance of the final compound under service conditions [1, 2]. Therefore, it is of practical importance to be able to correlate the physical properties of the polymer system to be processed and the processing conditions (screw and die geometry, screw speed and barrel temperature profile) with the development of morphology, or with the levels of the dispersion of solids in the matrix (see, for example [3]).

Previous studies of this topic have largely concentrated on studying blend morphology development along the screw. Lindt and Ghosh [4] showed theoretically and experimentally that during melting the scale of segregation between the blend components is reduced by several orders of magnitude within a short helical channel increment. Tyagi and Ghosh [5] monitored the average size of the dispersed phase along the length of the screw to conclude that the evolution from polymer pellets to threads and to droplets result from repetitive cycles of flow through zones inducing high deformation rates or being predominantly quiescent (denoted as strong and weak zones by Janssen and Meijer, respectively [6]). Huang *at al.* [7] monitored the morphology evolution of Polypropylene / Polyamide-6 blends with different viscosity ratios using sampling devices and concluded that this ratio determines the rate of striations break-up into droplets. Jun *at al.* [8] developed an experimental apparatus that mimics the flow in the metering zone of a single screw extruder to follow the deformation and break-up mechanism of an immiscible drop suspended in a low viscosity silicone oil. The formation of elongated threads and a complex break-up sequence (again dictated by strong/weak shear) was reported.

As for correlations of morphology with properties and processing conditions in single screw extrusion, Yeh *at al.* [9] studied the effect of material characteristics and process conditions on the barrier properties of a High Density Polyethylene/Nylon polymer blend. Huang *at al.* [10] found out that both the geometry and screw speed could affect significantly the final morphology of high density polyethylene / polyamide-6 blends.

Predicting the morphology evolution of a liquid-liquid system in a single screw extruder requires coupling a description of the flow and heat transfer in this type of machine to a morphology evolution model. In contrast with twin screw extrusion, where a number of computational models have been proposed [11-16], previous efforts for single screw plasticating extrusion are not abundant. In their initial attempt, Wilczynski *at al.* [17] took only into consideration the melt conveying zone of the screw, disregarded the occurrence of coalescence and assumed as valid along the screw the rheological behavior of the final blend. Later, coalescence was included [18]. With a view to predict mixing in a single screw extruder, DeRoussel e*t al.* [19] computed particle advection, stretching, coalescence and breakup along the melt conveying zone, where the cross-channel flow was modeled using a weighted-residual solution approach proposed by Chella and Ottino [20].

This work aims at using the breath of scientific know-how developed so far on the development of multiphase liquid-liquid morphologies during flow to estimate the morphology development of physical polymer blends, or of polymers and additives, along a single screw extruder. The analysis encompasses the melting and the melt conveying zones of the plasticating sequence and considers the relevant deformation, break-up and coalescence phenomena. The morphology evolution model follows generally that proposed by Chesters [13] and used by Delamare and Vergnes [14] for twin screw extruders. Since a melting model considering the presence of two materials is not currently available in the literature, melting of the major polymer was considered, a certain number of drops (determined by the concentration) of the minor component being inserted at the pace of melting, as uniformly distributed in the freshly generated melt; the evolution of the dimensions of these entities were estimated along the screw channel.

2 Model of Morphology Evolution

2.1 Mathematical Model

During the flow of a two-phase liquid-liquid system, the minor component may suffer morphological changes depending on local conditions. Following the same approach of most previous efforts on predicting morphology development, these changes will be modeled here focusing on the individual behavior of many single drops suspended in the flow. This means that the formation upon melting of threads that will then break into droplets reported by a few authors [4, 5] is assumed here as the direct formation of droplets suspended in a melt, which is the most common assumption.

In the general case of the affine deformation of a drop in a simple shear flow, stretching of the drop proceeds slowly, the long axis of the extending drop (L) growing in accordance with the following equation [6, 21]:

$$L = \begin{cases} \left(1 + \frac{\gamma^2}{2} + \frac{\gamma}{2}\sqrt{4+\gamma^2}\right)^{0.5} \cdot d & \text{if} \quad \gamma < 5 \\ \gamma \cdot d & \text{if} \quad \gamma \geq 5 \end{cases} \tag{1}$$

where γ is shear deformation and d is the initial drop diameter. Similar expressions could be written for B, the drop width.

Dispersion may involve erosion, break-up and coalescence phenomena. The first consists in the removal of small fragments from the drop surface. Since these usually represent less than one percent of the original drop volume [21], this mechanism will be disregarded here. The event of drop break-up is determined by the magnitude of the capillary number (Ca), which quantifies the relative intensity of the viscous forces (η_c is matrix viscosity, $\dot{\gamma}$ is shear rate and r is drop radius) and the interfacial tension (υ_{12}) acting across the interface between two immiscible liquids:

$$Ca = \frac{\eta_c \dot{\gamma} r}{\upsilon_{12}} \tag{2}$$

Break-up occurs when the viscous forces are sufficiently higher than the interfacial tension, *i.e.*, when a critical capillary number is exceeded and acts during sufficient time ($t \geq t_b$, where t_b is the required drop break-up time) [14, 21]:

$$t_b = \frac{2\eta_c r}{\upsilon_{12}\Omega(\lambda, p)} Ln\sqrt{\frac{r}{\alpha}} \ ; \tag{3}$$

here Ω is the dominant growth rate of interfacial disturbances [21, 22], λ is a index that characterizes the flow type (1 for extensional, 0.5 for shear and 0 for rotational flow), p is the ratio (η_d/η_c) between the viscosity of the dispersed phase (η_d) and that of the matrix (η_c) and α is the amplitude of the initial deformation. Since Ω is usually defined graphically [21, 22], an analytical approximation is proposed here:

$$\Omega(\lambda, p) = \lambda \ \frac{a + cp^{0.5} + ep + gp^{1.5} + ip^2}{1 + bp^{0.5} + dp + fp^{1.5} + hp^2 + jp^{2.5}} \tag{4}$$

with a = 0.10, b = 66.95, c = 56.94, d = 289.59, e = 42.63, f = 1533.34, g = 248.80, h = 413.15, i = -12.49 and j = 1050.83.

Grace [22] established a well-known correlation between Ca_{crit} and p for a spherical drop suspended in a homogeneous steady flow. Stegeman [23] proposed an analytical approximation that works adequately for p approximately equal to 1 (for example, when p ranges in the interval 10^{-6} - 10^{3}, errors vary between 22.5% and 94.4% for shear flow and between 7.10% and 47.36% for extensional flow). A different empirical approximation to the Grace curve is proposed here, involving the following equations for shear flow: for $p \leq 1$

$$Ca_{crit} = a + bp^{0.5} + \frac{c}{p^{0.5}} \tag{5a}$$

with a = - 0.64, b = 0.84 and c = 0.32; and for $p > 1$

$$Ca_{crit} = e^{a+bp+cp^2} \tag{5b}$$

with a = – 0.46, b = - 0.44 and c = 0.38. In the case of extensional flow:

$$Ca_{crit} = \frac{a + cp^{0.5} + ep + gp^{1.5}}{1 + bp^{0.5} + dp + fp^{1.5}} \tag{5c}$$

with a = 1.12, b = 58.53, c = 18.56, d = 93.70, e = 16.25, f = - 0.01, and g = 0.46. The error ranges for p in the interval 10^{-6} - 10^{3} are now 0.5% - 20.5% and 2.4% - 23.8% for shear and extensional flows, respectively.

The Reynolds number plays an important role in the drop break-up mode [23]. Whereas for high values of the ratio of inertial to viscous forces the initial drop deforms extensively and bursts into numerous droplets, in polymer extrusion (characterized by low Reynolds numbers), the drop is expected to break into two equal smaller circular droplets, each one following the same fate until a critical radius (r_c) is reached. A third smaller circular droplet is also created from the initial neck of the drop (and reportedly has a volume of 10 to 17% of that of the initial drop volume [24] - an average value, 13.5%, will be assumed here). The radius r_c can be determined from the following equation:

$$\frac{r_c}{r} = \frac{Ca_{crit}}{Ca} \tag{6}$$

Elmendorp and Van der Vegt [25] showed that coalescence phenomena become significant when the volumetric fraction of the dispersed phase is greater than 0.5%. Also, the probability of coalescence increases

as the drop dimension decreases [26]. Chesters [13] and Delamare and Vergnes [14] considered the collision of two identical spherical drops moving jointly in a shear flow. Two successive steps were assumed:

i) collision of the two drops;

ii) exclusion of the polymer film separating them, which will flow into the main stream.

The coalescence probability was defined as the product of the probability of the two drops colliding, P_{col}, with the probability of film exclusion between the drops, P_{exp}:

$$P_{coal} = P_{col} \cdot P_{exp} \tag{7}$$

with

$$P_{col} = \exp\left(-\frac{\pi}{8\,\dot{\gamma}\,\phi\,t_{loc}} \right) \tag{8}$$

and

$$P_{exp} = \exp\left[-\frac{9}{8}\left(\frac{r}{h} \right)^2 Ca^2 \right] \tag{9a}$$

$$P_{exp} = \exp\left[-\frac{\sqrt{3}}{4}\left(\frac{r}{h} \right) p.Ca^{3/2} \right] \tag{9b}$$

$$P_{exp} = \exp\left[-\frac{3}{2}\mathrm{Ln}\left(\frac{r}{h} \right) Ca \right] \tag{9c}$$

for stationary, partially mobile and mobile interfaces, respectively. When the viscosity ratio (p) is much lower than 1 the interfaces can be considered as mobile, while for $p >> 1$ they are taken as stationary; ϕ is the volume fraction of the dispersed phase, t_{loc} is the local residence time and h is the critical value at which the liquid film breaks, which is given by [14]:

$$h = \left(\frac{10^{-20} r}{8\pi\upsilon_{12}} \right)^{1/3} \tag{10}$$

2.2 Algorithm

The phenomena taken into consideration above must be interrelated with a description of the flow developing along an extrusion screw from hopper to die, taking into account operating conditions and screw geometry. Figure 1 shows the corresponding algorithm. The process modeling routine computes velocity and temperature profiles along the screw considering a 2D mesh at each increment Δz, once the local development of solids conveying, melting, or melt conveying is detected [27].

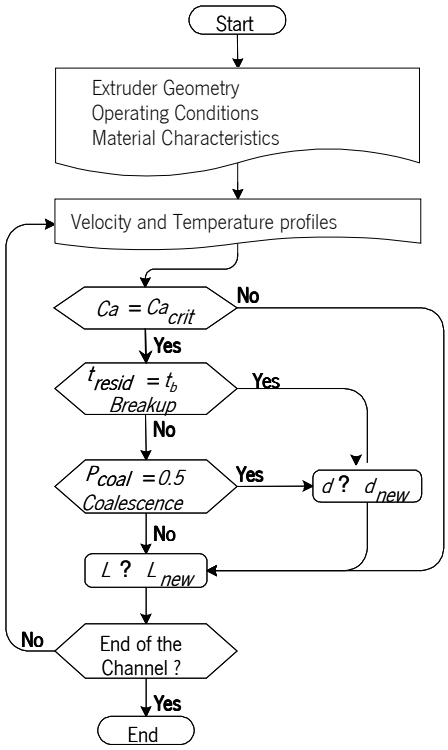

Figure 1: Algorithm for morphology prediction of a liquid-liquid system.

As soon as melting is initiated and progresses, a given number of drops - proportional to the concentration of the dispersed phase and to the pace of melting - is inserted as uniformly distributed in the melted portion of each cross-section Δz under consideration, using the 2D mesh adopted for the flow calculations. Thus, if no changes in morphology would occur, the number of suspended drops would increase along the melting stage from none to the number resulting from their concentration in the blend/compound. In practice, and depending on local flow conditions, the number of drops at each channel cross-section may vary due to the break-up and/or coalescence of existing units, plus the insertion of new ones. During melt

conveying the process continues, except that no new drops are inserted. Throughout the melting and melt conveying the process is applied either for the new drops inserted or formed after break and for the existing treads.

The capillary number (Ca) and critical capillary number (Ca_{crit}) at each channel mesh element of a given cross section are evaluated via equations 2 and 5, respectively. If $Ca < Ca_{crit}$, a drop will not break. Otherwise, a break-up time t_b is computed from equation 3. If $Ca \geq Ca_{crit}$ during a time greater than t_b, break-up occurs. In this case, each existing droplet is replaced by three droplets (two equal droplets plus a third smaller droplet) that are considered for the statistical average at each channel cross-section, although with relative weights associated with their sizes. The coalescence probability (P_{coal}) is also estimated at local level from equation 7 and taken into account if not lower than 0.5. Obviously, it also contributes to the statistical average. This sequence is repeated iteratively, until reaching the end of the screw.

For the sake of simplicity (and shorter computing times), and as in most previous works [14, 16], the algorithm does not provide effective interconnectivity between flow and morphology, *i.e.*, it was assumed that pressure, temperature and velocity profiles along the screw are not influenced by the presence of the second phase. Such coupling would require the availability of a constitutive equation capable of considering the effect on the viscosity of the percentage, size and size distribution of the minor phase, as a function of temperature and shear rate. The use of experimental data to determine the parameters of such a relation would not only require the execution of difficult and lengthy experiments, but would also preclude the practical usefulness of the method.

Utracki [28] proposed a two-parameter equation to describe the viscosity of an immiscible blend as a function of concentration, ϕ_j and viscosity of the components, η_j:

$$\log \eta = \sum_j \phi_j \log \eta_j \tag{11}$$

Accordingly, the viscosity of the blend is only 10% above or below that of the matrix when the viscosity ratio of the components is within 0.1 and 10 for concentrations up to 5%, the range of viscosity ratios decreasing with an increase in concentration, as shown in Figure 2 for concentrations up to 15%. Therefore, the grey area in Figure 2 identifies the concentrations ϕ_j and viscosity ratios p that minimize the errors resulting from the lack of interdependence between flow and morphology.

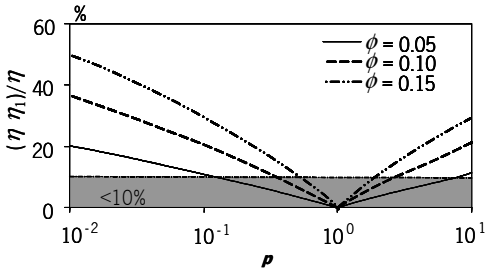

Figure 2: Influence of viscosity ratio (p) and concentration of the minor phase (ϕ) on the variation of the viscosity of the blend (η) in relation with the viscosity of the matrix (η_1).

3 Flow Modeling

As in most equivalent analyses, flow in the screw channel is assumed to develop along a rectangular canal (unwound helix) whose depth changes in the z direction, on top of which a flat surface (inner barrel wall) slides at constant velocity (given by the screw speed) and kept at a set temperature. Material pressure, velocity and temperature are computed for small down channel increments (Δz), considering a 2D mesh at each increment. The routine starts by computing pressure at the base of the hopper. Then, one assumes the development of a non-isothermal drag flow of an elastic solid plug in the initial turns of the screw [29], with heat conduction and dissipation at all surfaces. When the material near to the barrel interface reaches its melting temperature, a melt film appears and a set of equations for the delay zone is solved [30]. In fact, this stage is sub-divided in two steps. In the first one, a melt film separates the solid plug from the barrel surface. Later, this film will surround the four solid plug surfaces [31]. This is followed by melting, where the five zone model proposed by Lindt *et al.* [32, 33] is adopted.

The precise description of the flow of molten polymer during melting and melt conveying requires a full 3D analysis. However, if the overall modeling of the plasticating sequence from hopper to die and associated morphology development are to be used for practical design and optimization purposes, which may require its repetitive use [27], the necessary computational times would become unacceptable. The pattern of the helical streamlines, whose features are determined by their location in the channel cross-section, are well known, have a decisive contribution to the evolution of the morphology, and create a stagnant line along the z direction at y = 2H/3 (see Figure 3a). In a simpler 2D representation, where the physical presence of the channel flights is ignored, the flow of drops in the x direction would cause their collision against the lateral walls, followed by vanishing from flow. To deal with this problem, one may imagine that when a drop reaches the channel side wall (for example, at locations 1 and 1' in Figure 3b), is automatically repositioned in the

subsequent corresponding flow path line in the opposite direction (*i.e.*, when drops reach points 1 or 1', they will be sited in points 2 or 2', respectively). The stagnation line at y = 2H/3 now extends over the entire channel width. In fact, most analysis of mixing (e.g., WATS developed by Pinto and Tadmor [34] adopted this description. Chella and Ottino [20] used this simplified flow description, as well as a more complex approximate analytical steady-state creeping flow solution, to predict mixing in a rectangular cavity flow and in a single screw extruder, having concluded that the results provided by the two methods were comparable, the former being preferable in practice due to its relative simplicity.

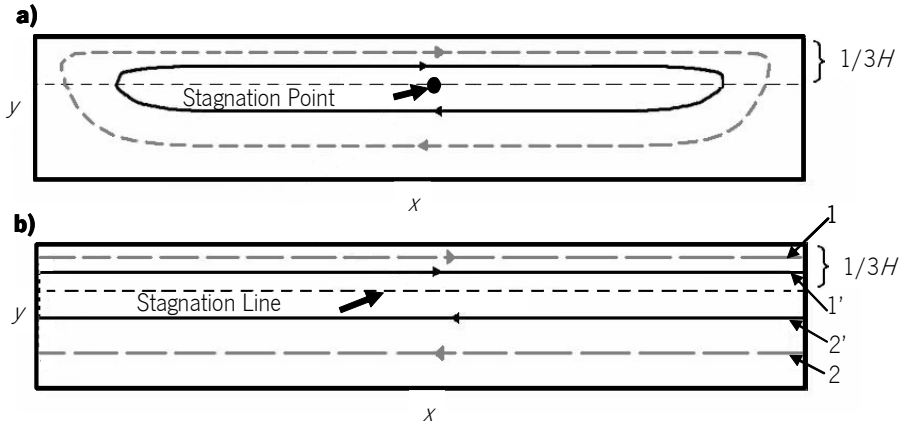

Figure 3: Cross-channel flow in a screw channel. **a)** helicoidal path; **b)** simplified path.

Melt conveying and pressure flow along the screw and die, respectively, are thus assumed as non-isothermal 2D, the melt rheological behavior being described by the Carreau-Yasuda law [35]. The governing equations for the melt flow in the screw, *i.e.*, continuity, linear momentum and energy conservation are, respectively:

$$\frac{\partial V_x}{\partial x} + \frac{\partial V_z}{\partial z} = 0 \tag{12}$$

$$\frac{\partial P}{\partial x} = \frac{\partial}{\partial y}\left(\eta \frac{\partial V_x}{\partial y}\right) \tag{13a}$$

$$\frac{\partial P}{\partial y} = 0 \tag{13b}$$

$$\frac{\partial P}{\partial z} = \frac{\partial}{\partial x}\left(\eta \frac{\partial V_z}{\partial x}\right) + \frac{\partial}{\partial y}\left(\eta \frac{\partial V_z}{\partial y}\right) \tag{13c}$$

$$\rho C_p V_z \frac{\partial T}{\partial z} = k\left(\frac{\partial^2 T}{\partial x^2} + \frac{\partial^2 T}{\partial y^2}\right) + \eta\dot{\gamma}^2 \tag{14}$$

where V_x, V_y and V_z are velocities in the x, y and z direction, P is pressure, T is temperature, ρ is melt density, η is viscosity, and k and C_p are thermal conductivity and specific heat, respectively. Melt flow is taken as incompressible and fully developed in the down and cross channel directions and the temperature field is fully developed in the cross channel and down-channel directions (i.e., $\partial T / \partial x = 0$ and $\partial T / \partial y = 0$). Since pure shear flow develops, λ is equal to 0.5. The boundary conditions are:

$$\begin{cases} V_x(y=0) = 0 \\ V_x(y=H) = -V_{bx} \end{cases} \qquad \begin{cases} V_z(x=0) = 0 \\ V_z(x=W) = 0 \\ V_z(y=0) = 0 \\ V_z(y=H) = V_{bz} \end{cases} \qquad \begin{cases} T(x=0) = T_s \\ T(x=W) = T_s \\ T(y=0) = T_s \\ T(y=H) = T_b \end{cases} \tag{15}$$

where V_{bx} and V_{bz} are barrel velocities in the x and z directions, respectively, T_s is screw temperature, T_b is barrel temperature, and H and W are the local depth and width of the screw channel, respectively.

The predictions produced by this approach were compared to those yielded by a 3D analysis using the Ansys Polyflow® software [36], in order to check if it was able to describe with sufficient accuracy the main flow features. The geometry consisted of a rectangular channel (24 mm wide, 5 mm deep and 1200 mm long), representing the unwound channel of a screw extruder, on top of which a flat surface moved at 0.0943 m/s (corresponding to a screw rotation speed of 60 rpm) making and angle of 17.6° with the down channel direction (equivalent to a square screw pitch). The 2D and 3D approaches used a Carreau-Yasuda law and a generalized Newtonian behavior, respectively (corresponding to the HDPE used in the experimental section below), and flow was taken as isothermal. As far as boundary conditions are concerned, equations 15 were applied. Figure 4 shows the calculated velocity profiles. In the simplified method (left), there is no velocity in the y direction and V_x is constant along the x-axis. Ansys Polyflow® predicts that V_y is nil in most of the channel and that V_x has a complex contour near to the screw flights. The discrepancy between the 2D and 3D velocity profiles (V_{2D} and V_{3D}, respectively) can be estimated from the difference between their double integral:

$$\varepsilon = \left| \frac{\iint_S V_{2D} - \iint_S V_{3D}}{\iint_S V_{3D}} \right| \tag{16}$$

The average differences associated with V_x, V_y and V_z are 10.4%, 2.9% and 6.5% respectively, thus encouraging the use of the simplified approach to achieve considerable savings in computational time.

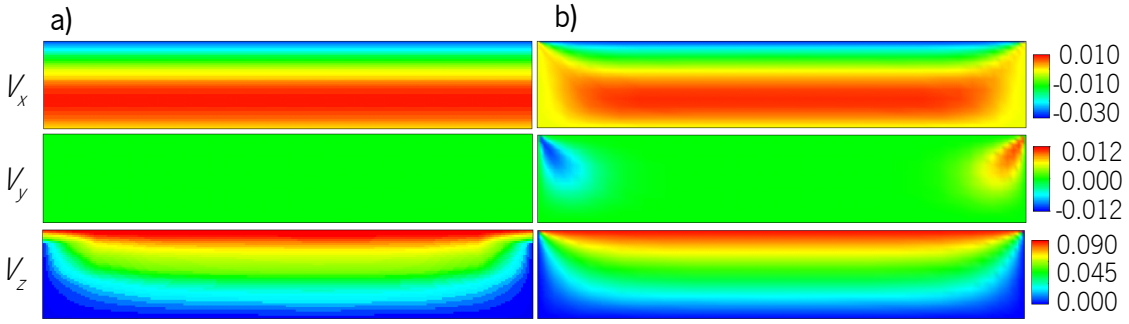

Figure 4: *x, y, z* - velocity profiles (m/s) computed using: **a)** 2D approach with finite differences and **b)** Polyflow.

4 Results and Discussion

4.1 Experimental Data

An assessment of the validity of the predictions would require their direct comparison with sufficient and appropriate equivalent experimental data. However, the latter is not easy to obtain, as one must:

i) interrupt the operation of the extruder after reaching steady state;

ii) gain fast access to the screw channel, collect samples and freeze them before any significant changes in morphology take place;

iii) observe and quantify eventual changes in drop size and shape.

The experimental data generated in this work had the exclusive intention of providing guidance to the computational modeling. The trials were performed on a prototype laboratorial (diameter D = 30 mm, changeable L/D) modular single screw extruder, fitted with a hydraulic screw extractor. Once the rotation of the screw was interrupted, it took circa 60 seconds to fully extract the screw (this involved switching-off the heaters, removing the die and pushing the screw while cooling the material with compressed air). The main

dimensions of the machine and the screw profile selected for this study (assembled from a number of available screw elements) are presented in Figure 5 and Table 1 – screw A).

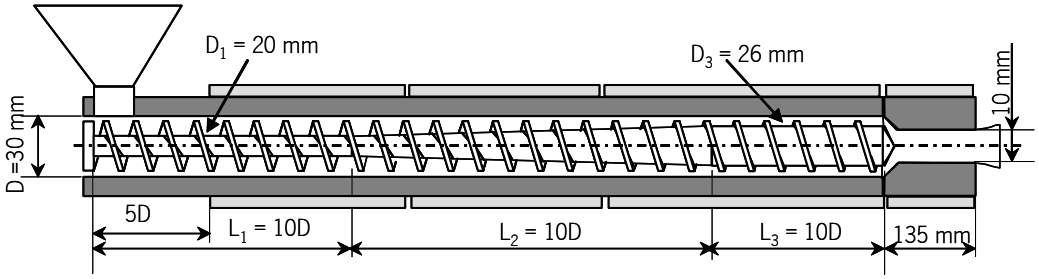

Figure 5: Extruder geometry.

Table 1: Screw geometries tested.

Screw		A	B	C	
Barrel Diameter	D		30		mm
Extruder Length	L_1	10D	10D	10D	
	L_2	10D	10D	10D	
	L_3	10D	**20D**	10D	
Channel Depth	H_1	5	5	5	mm
	H_2	2	2	**1.43**	mm
Compression ratio		2.5	2.5	**3.5**	

The material system consisted of an immiscible blend of High Density Polyethylene, HDPE (Repsol ALCUDIA TR-135) and Polypropylene, PP (Repsol ISPLEN PP 030 G1E) (90/10 w/w). A Perkin Elmer DSC 7 was used to determine the specific heat, the melting heat and the melting temperature. The remaining properties were taken from the literature. The viscous flow properties were determined at two different temperatures (180 and 200 °C) in a Rosand RH8 Dual Capillary Rheometer, considering both the Bagley and Rabinowistch corrections. The Carreau-Yasuda parameters were obtained and are presented in Table 2, together with the other relevant physical and thermal data. For a shear rate of $100s^{-1}$, which is typical of extrusion, the viscosity ratio is 0.67, thus favoring the occurrence of dispersion [22].

Table 2: Properties of the HDPE and PP selected.

			HDPE (ALCUDIA TR-135)	PP (ISPLEN PP 030 G1E)	
Density	Solids	ρ_s	560.00	690.90	$kg.m^{-3}$
	Melt	ρ	854.40	902.00	
Thermal Conductivity	Solids	k_s	0.19	0.21	$W.m^{-1}.°C^{-1}$
	Melt	k_m	0.10	0.18	
Specific Heat	Solids	C_s	2600.00	1881.92	$J.kg^{-1}$
	Melt	C_m	2000.00	1974.55	
Melting	Heat	H	$190.00x10^3$	$89.49x10^3$	$J.kg^{-1}$
	Temperature	T_m	118.0	169.11	°C
Carreau-Yasuda viscosity law		η_0	18000.00	3041.48	Pa.s
		E/R	10000.00	4023.29	K
		$\hat{\lambda}$	0.70	0.17	s
		a	1.70	1.82	
		n	0.30	0.35	
		T_0	463.15	493.15	K

Two trials were performed at two different screw speeds (20 and 60 rpm), with a set flat barrel temperature of 200 °C. The pre-mixed blend components were fed into the hopper, extrusion was allowed to reach steady state and then interrupted; the die was removed, the screw was extracted and the material helix was collected for subsequent analysis. Visual identification of the solids, melting and melt conveying stages showed that the latter started approximately at screw turn number 20 (starting from the hopper). Therefore, with the aim of obtaining data to serve as reference for the theoretical predictions, cross-sections 10 μm thick were obtained at regular intervals between screw turns 20 and 30 and were subsequently analyzed by optical microscopy under contrast phase, in order to assess the size evolution of the dispersed PP particles.

Figure 6 shows the cross-sections at screw turns 20 and 30 for 20 and 60 rpm. Depending on screw speed, PP drops or PP drops and threads were initially suspended in the melt, giving rise to two parallel evolutions: in the first case, drop break-up took place, especially in the first part of melt conveying, whereas in the second case threads became progressively thinner and shorter, while smaller drops were also forming.

One would assume that in the first situation threads formed and broke into drops during the melting stage, while in the latter the rate of morphology evolution is lower. These morphological evolutions were generally in agreement with previous reports [5, 7].

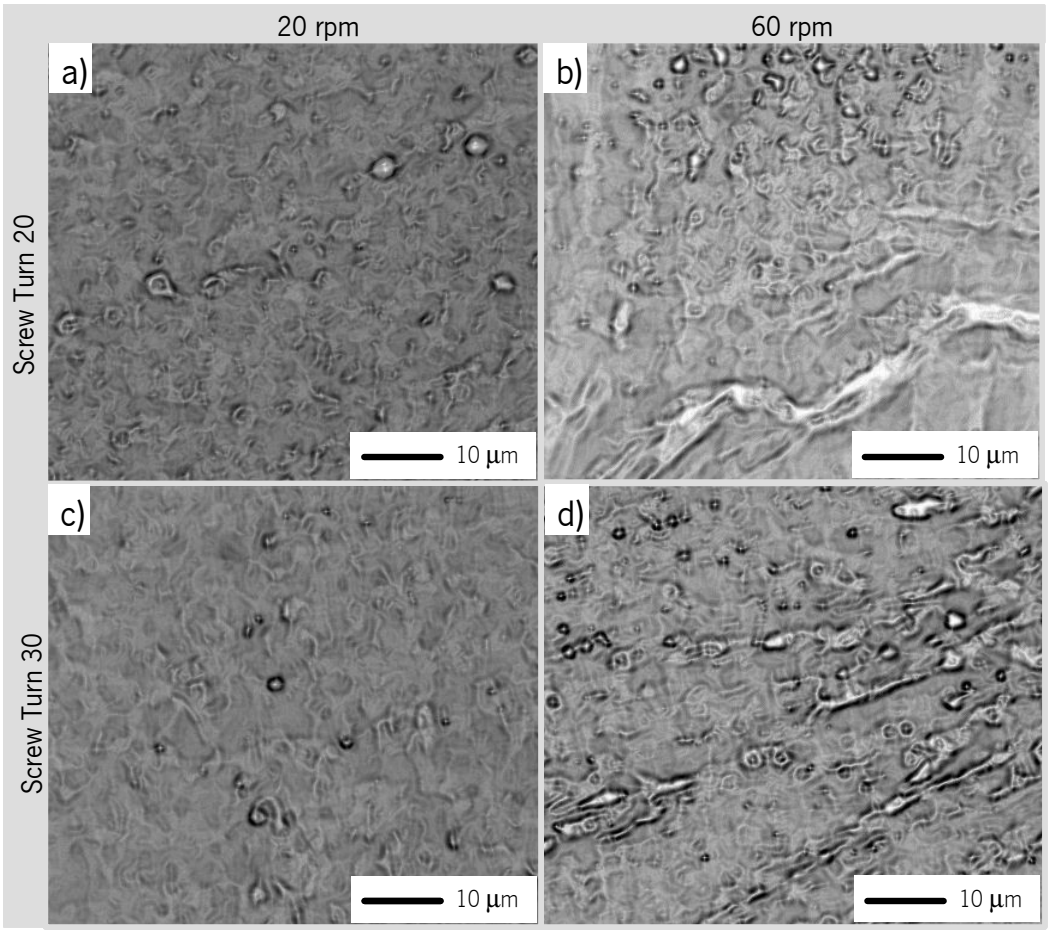

Figure 6: Melt cross-sections at the beginning (a) and b)) and end (c) and d)) of melt conveying, for 20 **(left)** and 60 **(right)** rpm.

The average drop size (equivalent diameter) was computed from an analysis of at least 40 particles. The points in Figure 7 correspond to the evolution measured along the metering zone. Although the size of the dispersed phase is the same at the beginning of the melt conveying zone (approximately 2.7 μm) , the lowest screw speed induced the highest dispersion. This should result from the balance between the effects of residence time (low screw speeds imply higher residence times, favoring dispersion) and average shear rate (high screw speeds generate higher shear rates, hence higher dispersion). In both cases, the rate of dispersion seems to decay along the screw channel, until a plateau is reached.

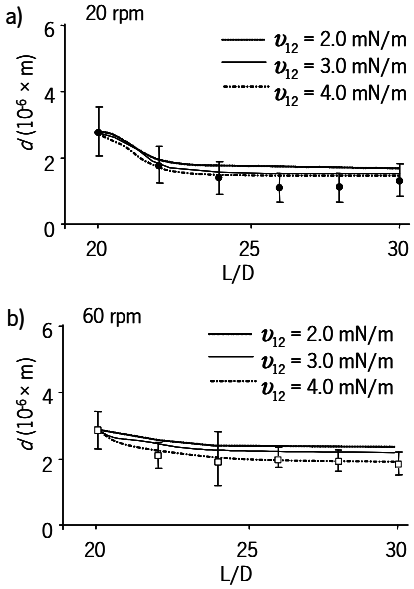

Figure 7: Evolution of drop size along melt conveying for two different screw speeds (**a)** 20rpm and **b)** 60 rpm) and different values of the interfacial tension.

An equivalent computational prediction was produced using the model and algorithms presented above. For the purposes of assessing morphology, a mesh with 10125 elements was created at each cross section, adjacent down-channel cross-sections being roughly 15 mm apart. The interfacial tension (υ_{12}) between the drops and the matrix was taken as 2.0, 3.0 and 4.0 mN/m, (as the literature proposes values between 1.53 and 3.68 mN/m [37]) and their initial sizes were made to coincide with the values measured (approximately 2.7 μm), so that the starting morphology is roughly the same. The results correspond to the lines in Figure 7.

The predictions overestimate somewhat the levels of dispersion, but the trends are correct and the effect of screw speed is accurately predicted. As expected, the correct determination of the value of the interfacial tension is mandatory. In this case, the best predictions were obtained for υ_{12}= 4 mN/m. These results were considered as encouraging, particularly when taking into consideration the various possible sources of error involved in this exercise. As a matter of fact, from the experimental point of view, different levels of coalescence of the dispersed phase could have taken place along the screw prior to sample collection. In turn, modeling:

i) assumed initial drops of uniform size, not the distribution observed;

ii) adopted a simplified cross-section flow leading to longer flow paths;

iii) used a number of values for properties that were taken from the literature for similar, but not the same, materials.

4.2 Computational case studies

A few case studies were selected with the aim of evaluating the sensitivity of the computational methodology proposed above to changes in the material properties, operating conditions and screw geometry. Table 1 presents three screw configurations compatible with the extruder represented in Figure 5. Screws A and B differ in terms of the length of the metering section, while screws A and C have different compression ratios (distinct channel depths in the metering zone). As reference conditions, a viscosity ratio of 1, an interfacial tension of 4.5 mN/m, a screw speed of 150 rpm and a uniform barrel temperature set at 200 °C were considered.

As explained above, as the polymer that will form the matrix melts, a proportional number of drops (corresponding to a total concentration of circa 10%), having a diameter of 20 μm, is inserted as uniformly distributed in the freshly generated melt. The value of 20 μm is assumed because since the computations cover the process from hopper to die, and values of a few micrometers were measured at screw turn 20, a bigger initial size should be considered. The evolution of the drop dimensions is monitored along the remaining of the screw length.

Effect of Material properties

Viscosity Ratio

As demonstrated by Grace [22], the viscosity ratio between the components of a liquid-liquid system plays a major role on the evolution of the morphology. Generally, as p decreases, drop break-up occurs under higher shear rates, but the time for drop break-up decreases and dispersion becomes more effective. This is confirmed in Figure 8 for values of p of 1 and 10^{-2}. The graph on top represents the evolution of the average drop size, d, together with the corresponding standard deviation, and average drop length, L, along the screw. Melting extends approximately from L/D = 7 to L/D = 18. Thus, it has a major contribution to the global morphology evolution.

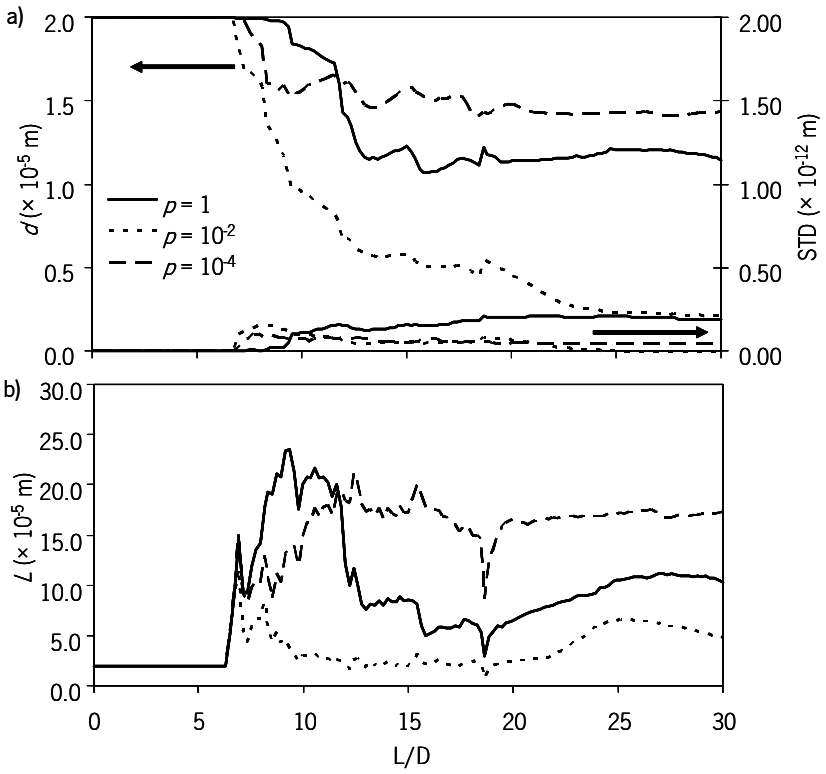

Figure 8: Effect of the viscosity ratio on average drop diameter **(a)** and drop length **(b)**.

If the viscosity ratio turns out to be much lower than 1 (e.g., $p = 10^{-4}$), the time for drop break-up tends to zero. However, dispersion becomes less important, since it requires higher shear rates than those attained under these operating conditions. It is also interesting to note that, under these conditions, the average drop length (*L*, in Figure 8 bottom) remains important along the remaining screw length. Although the morphology model used here assumes the existence of drops suspended in a melt, these predictions seem to indicate the subsistence of a thread-like morphology, possibly not too different from that shown in Figure 6 (60 rpm, turn 20).

Interfacial tension

The interfacial tension being another important material parameter, Figure 9 shows the evolution of the dimensions of the drops (*d* and *L*) for two different values of υ_{12}. Higher interfacial stresses decrease the value of *Ca* (equation 2), thus opposing dispersion, but the time for drop break-up decreases (equation 3). For the highest interfacial tension value, the figure shows fast dispersion during melting, followed by a plateau during melt conveying; conversely, a lower υ_{12} causes a more gradual dispersion, but yielding smaller drops. Also,

when υ_{12}= 2.0 mN/m, the drops become significantly extended during melting, relaxing thereafter (Figure 9 bottom). Again, this seems coherent with the cross-sections presented in Figure 6 for the highest screw speed (and similar values of υ_{12}).

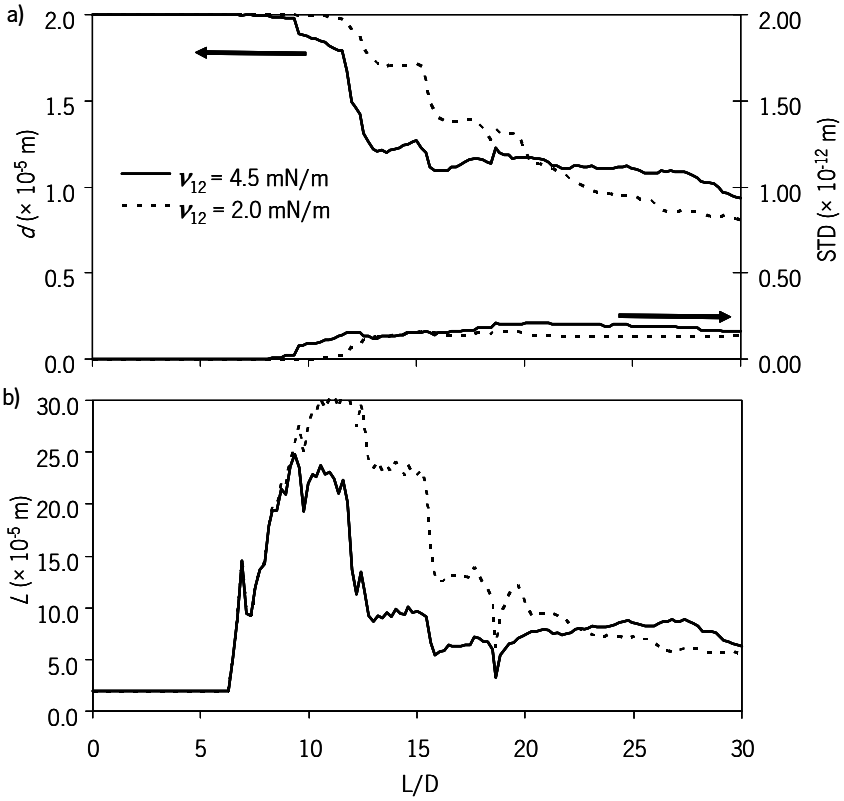

Figure 9: Effect of the interfacial tension on average **a)** drop diameter and **b)** drop length.

Effect of Operating Conditions

Screw Speed

As expected, when screw speed increases so does mass output (see Table 3). However, as shown in Figure 10, melting starts a little earlier and is significantly more efficient for lower screw speeds (for these materials, heat conduction is predominant over heat dissipation). As a result, the residence time of the flow of molten material (total residence time minus the residence time in the solids conveying zone) is higher for lower screw speeds, as it can be observed in Table 3. It should be also noted that, during melting, the expected down-channel decrease in drop size is attenuated by the continuous insertion/formation of drops in the freshly generated melt.

The consequences in terms of drop dimensions are shown in figure 11. When the screw speed increases from 50 to 150 rpm, the dispersion process is compromised, mainly due to a decrease of the residence time for flow. When the screw speed is further raised to 250 rpm, the resulting increase in average shear rate balances the additional reduction of the residence time.

Barrel Temperature

Changes in barrel temperature (keeping screw speed at 150 rpm) have little effect on drop dimensions – see Figure 12. As barrel temperature increases, completion of melting is achieved earlier in the screw. This results in increasing residence times for the molten material, particularly in the melt conveying zone. Also, the time required for drop break-up decreases, these effects being perceived in the early melting stages.

Table 3: Influence of screw speed on mass output and residence time of melted material (i.e., melting and melt conveying zones).

Screw Speed (rpm)	Mass Output (kg/h)	Residence Time (s)
50	4.7	245
150	14.8	65
250	25.0	30

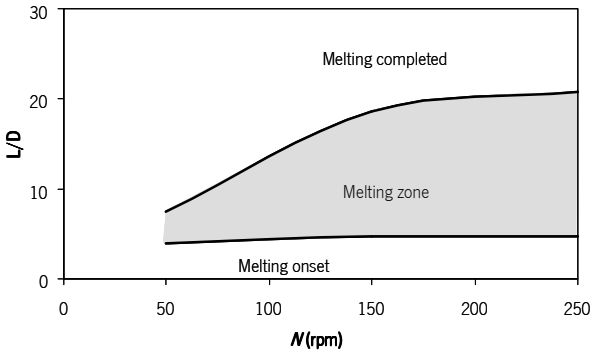

Figure 10: Effect of screw speed on melting.

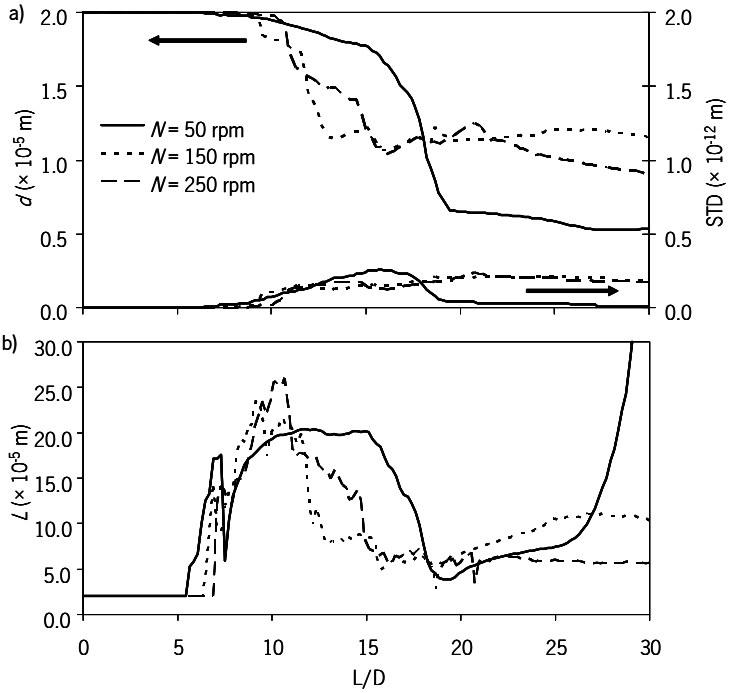

Figure 11: Effect of screw speed on **a)** drop diameter and **b)** drop length.

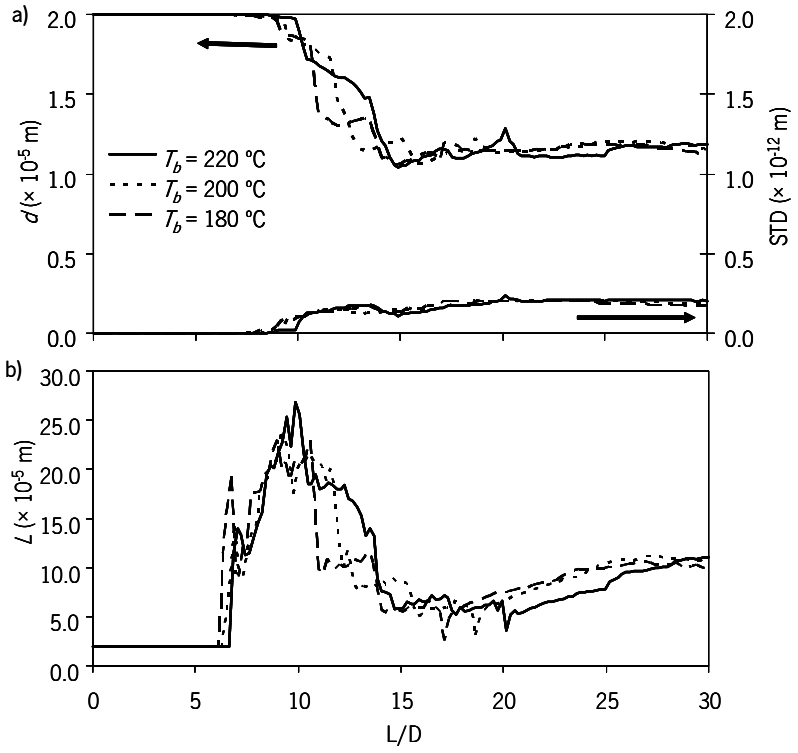

Figure 12: Effect of barrel temperature on **a)** drop diameter and **b)** drop length.

Effect of Screw Geometry

Screw geometry influences velocity and temperature profiles, hence it affects the melting pace, the residence time and the average shear rate and, consequently, flow morphology. In order to illustrate this, the effects on drop dimensions of the length of the metering zone and compression ratio were investigated.

Length of metering zone

As shown in Table 1, screw B has a longer metering zone than screw A. For that reason, under identical operating conditions, the mass output produced by Screw B is lower than that by screw A (see table 4), the residence time of molten material is also higher for Screw B and, as expected, the drop dimensions (Figure 13) are smaller for screw B.

Compression Ratio

In table 1, two screws (A and C) with different compression ratios (CR) were defined by changing the channel depth in the metering section from 2 to 1.43 mm. Thus, CR of 2.5 and 3.5 were obtained, respectively.

Figure 14 compares the evolution of the drop dimensions for these two screws. As expected, screw C causes more efficient melting (see Figure 15) hence creates higher residence times for melt flow. Moreover, shear rate levels should be higher. Therefore, it is not surprising that dispersion levels are also superior.

Table 4: Influence of screw speed and length of metering zone on mass output and residence time of the melted material (i.e., melting and melt conveying zones).

Screw Speed (rpm)	Mass Output (kg/h)			Residence Time (s)		
	Screw A	Screw B	Screw C	Screw A	Screw B	Screw C
50	4.7	4.2	4.3	245	301	233
150	14.8	13.7	14.7	65	87	59
250	25.0	21.2	24.5	30	49	24

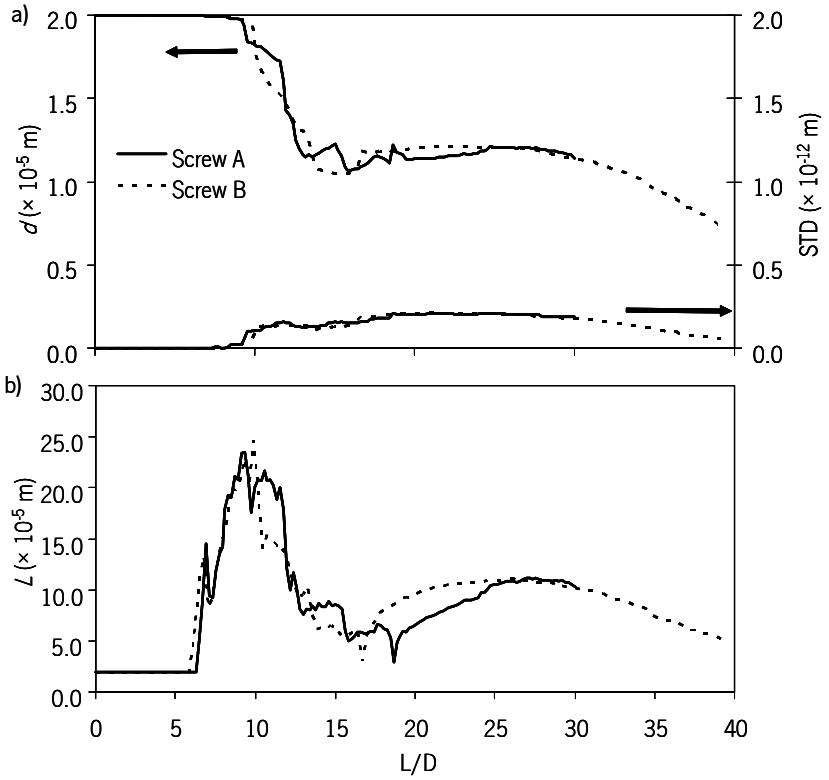

Figure 13: Effect of length of metering zone on average drop diameter **(a)** and drop length **(b)**.

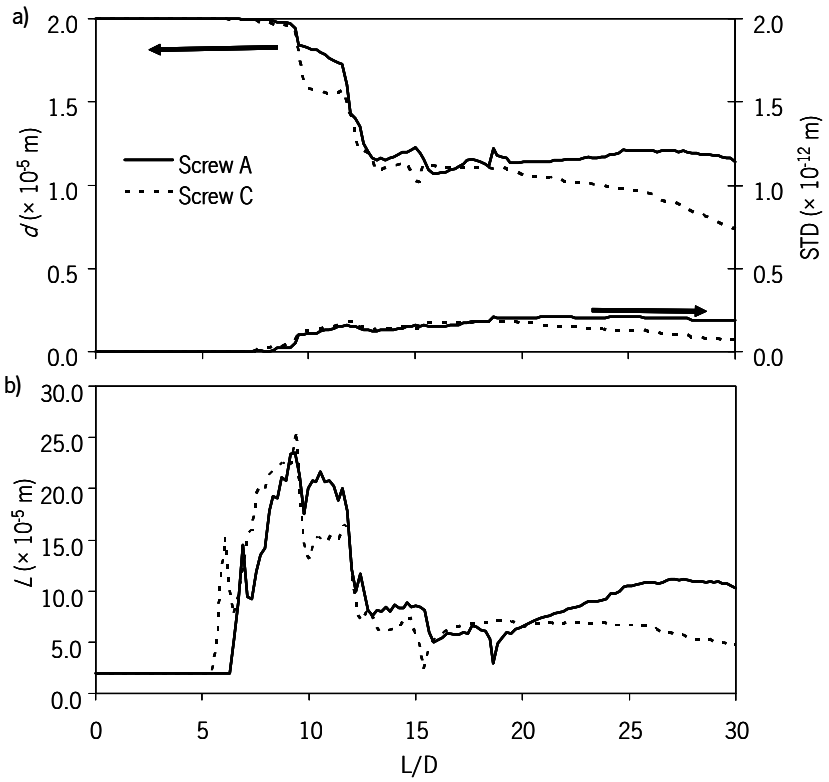

Figure 14: Effect on the compression ratio on average drop diameter **(a)** and drop length **(b)**.

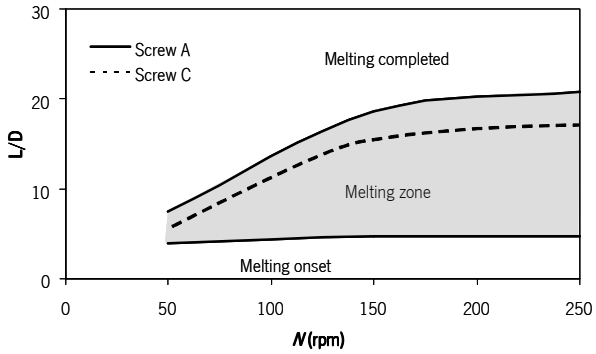

Figure 15: Effect of compression ratio on melting.

5 Conclusions

The evolution of the morphology of liquid-liquid systems along the axis of a single screw extruder is predicted, from the onset of melting until the die outlet. The possibilities of stretching, break-up and coalescence and taken into consideration. Melt flow was assumed as 2D (which is computationally advantageous), a simplified cross-channel helical pattern being adopted, after comparison with the results produced by a full 3D analysis showed little difference in the results.

Experimental observations of morphology development seemed to be generally in line with the corresponding computational predictions, especially if one considers the difficulties associated with such an exercise (comprehensive material characterization, collection of meaningful samplesl from within the extruder...).

The method was used to investigate the effects of material properties (viscosity ratio, interfacial tension), operating conditions (screw speed, barrel temperature) and screw geometry (length of metering zone, compression ratio) on the morphology development along the screw channel. In all cases, the results were sensitive to changes of the values of the parameters under study, and a plausible explanation of the end results could be put forward.

References

1. L.A. Utracki, *Polymer Alloys and Blends – Thermodynamics and Rheology*, Hanser Publishers, Munich (1989).

2. Y. Suetsugu, *The effect of mixing on some properties of compounds and composites*, In Mixing and Compounding of Polymers, Manas-Zloczower, I., Tadmor, Z. (Eds), Hanser Publishers, Munich, 521 (1994).

3. N. Domingues, M. Camesasca, M. Kaufman, I. Manas-Zloczower, A. Gaspar-Cunha and J.A. Covas, *Modeling Agglomerate Dispersion in Single Screw Extruders*, ANTEC-2006, Charlotte, NC, 2006.

4. J.T. Lindt and A.K. Ghosh, *Polym. Eng. Sci.*, **32**, 1802 (1992).

5. S. Tyagi and A.K. Gosh, *Polym. Eng. Sci.*, **42**, 1309 (2002).

6. J.M.H. Janssen and H. E. H. Meijer, *Polym. Eng. Sci.*, **35**, 1766 (1995).

7. H.-X. Huang, Y.-F. Huang and X.-J. Li, *Polym. Testing*, **26**, 770 (2007).

8. H. S. Jun, W. R. Hwang and T. H. Kwon, *Int. Polym. Proc.*, **19**, 218 (2004).

9. T.-M. Yeh, C.-S. Tuan, C.-Y. Chen, H.-H. Wang and M.-S. Lee, *J. Polym. Research*, **2**, 225 (1995).

10. H.-X. Huang, Y.-F. Huang and S.-L. Yang, *Polym. Int.*, **54**, 65 (2005).

11. L.A. Utracki and Z.H. Shi, *Polym. Eng. Sci.*, **32**, 1824 (1992).

12. M.A. Huneault, Z.H. Shi and L.A. Utracki, *Polym. Eng. Sci.*, **35**, 115 (1995).

13. A.K. Chesters, *Chem. Eng. Research & Design*, **69**, 259 (1991).

14. L. Delamare and B. Vergnes, *Polym. Eng. Sci.*, **36**, 1685 (1996).

15. D.Y. Moon and O.O. Park, *Adv. Polym. Techn.*, **17**, 203 (1998).

16. H. Potente, M. Bastian, K. Bergemann, M. Senge, G. Scheel and T. Winkelmann, *Polym. Eng. Sci.*, **41**, 222 (2001).

17. K. Wilczynski, A. Tyszkiewicz and Z. Szymaniak, *J. Mat. Proc. Techn.*, **109**, 320 (2001).

18. K. Wilczynski, Z. Szymaniak and A. Nastaj, *Development of Morphology in Single-Screw Extrusion of Polyblends*, Annual Meeting of Polym. Proc. Soc., PPS-18, Guimarães, Portugal (2003).

19. P. DeRoussel, D.V. Khakhar and J.M. Ottino, *Chem. Eng. Sci.*, **56**, 5511 (2001).

20. R. Chella and J.M. Ottino, *Ind. Eng. Chem. Fundam.*, **24**, 170 (1985).

21. H.E.H. Meijer and J.M.H. Janssen, *Mixing of Immiscible Liquids, in Mixing and Compounding of Polymers*, In Mixing and Compounding of Polymers; I. Manas-Zloczower, Z. Tadmor (eds), Hanser Publishers, Munich, 85 (1994).

22. H.P. Grace, *Chem. Eng. Commun.*, **14**, 225 (1982).

23. Y.M. Stegeman, *Time Dependent Behavior of Droplets in Elongational Flows*, PhD Thesis, Tech. Univ. Eindhoven, The Netherlands (2002).

24. Y. Renardy, V. Cristini and J. Li, *Int. J. of Multiphase Flow*, **28**, 1125 (2002).

25. J.J. Elmendorp and A.K. Van der Vegt, *Polym. Eng. Sci.*, **26**, 1332 (1986).

26. J.M. Ottino, *The Kinematics of Mixing: Stretching, Chaos and Transport*, Cambridge University Press, U.K. (1989).

27. A. Gaspar-Cunha and J.A. Covas, *Int. Polym. Proc.*, **16**, 229 (2001).

28. L.A. Utracki, *J. Rheol.*, **35**, 1615, (1991).

29. E. Broyer and Z. Tadmor, *Polym. Eng. Sci.*, **12**, 12 (1972).

30. L. Kacir and Z. Tadmor, *Polym. Eng. Sci.*, **12**, 387 (1972).

31. A. Gaspar-Cunha, *Modelling and Optimisation of Single Screw Extrusion*, PhD Thesis, Universidade do Minho, Guimarães (1999).

32. J.T. Lindt and B. Elbirli, *Polym. Eng. Sci.*, **25**, 412 (1985).

33. J.T. Lindt, *Polym. Eng. Sci.*, **25**, 585 (1985).

34. G. Pinto and Z. Tadmor, *Polym. Eng. Sci.*, **10**, 279 (1970).

35. P.J. Carreau, D.C.R. De Kee and R.P. Chhabra, *Rheology of Polymeric Systems: Principles and Applications*, Hanser Gardner Publications, New York (1997).

36. ANSYS FLUENT Manual (2009).

37. A.M.C. Souza and N.R. Demarquette, *Polymer*, **43**, 1313 (2002).

III

Modeling of Agglomerate Dispersion in Single Screw Extruders [2]

[2] Article published at International Polymer Processing, volume 25, pages 251-257, March 2010
Authores: N. Domingues, M. Camesasca, M. Kaufman, I. Manas-Zloczower, A. Gaspar-Cunha, J. A. Covas

1 Introduction

Single screw extruders are applied in many polymers processing operations, but their mixing capability is still subject to investigation. Mixing of solid additives into a polymeric matrix entails both a dispersive component (the reduction in size of filler agglomerates) and a distributive component (changing the spatial distribution of filler in the system) (Manas-Zloczower, 2009). Mixing in single screw extruders has been the focus of numerous publications (Janes and Winch, 1993; Gale, 2009; Rauwendaal, 1996; Ottino, 1989; Meijer and Janssen, 1994; Tyagi and Ghosh, 2002; Elemans and Wunnik, 2001). Solid additives are usually clustered into agglomerates. Agglomerate breakup occurs when hydrodynamic forces exerted in the flow exceed the cohesive forces holding the particle together. Agglomerate break-up involves two different mechanisms: erosion and rupture. Erosion is the detachment of particles from the surface of the agglomerate (Shiga and Furuta, 1985), whereas rupture involves breakage of the parent agglomerate, into a few large size fragments (Rwei et al., 1990).

Bolen and Colwell (1958) were the first to propose that agglomerate breakup occurs when internal stresses induced by viscous drag on the agglomerates exceed a certain threshold value. Other authors extended the analysis of agglomerate rupture and developed several models for solid cluster dispersion (McKelvey, 1962; Dizon et al., 1975; Tadmor, 1976; Manas-Zloczower et al., 1982; Scurati et al., 2005; Utracki, 2002; Seyvet and Navard, 2001). A comprehensive review on the subject of solid agglomerate dispersion was recently published (Manas-Zloczower and Feke, 2009).

One example of applying a model of agglomerate dispersion in modeling mixing in a single screw extruder is the work by Alemaskin et al. (2004). The authors developed an index reflecting both dispersion and distribution of cohesive solid agglomerates in the single screw extruder. In this work we propose to use a model for agglomerate breakup in conjunction with numerical flow simulations in the metering zone of a single screw extruder to characterize both dispersive and distributive mixing.

2 Model of Agglomerate Breakup

The solid additives used in the plastics and rubber industry are usual colloidal in nature and consist of agglomerates with a hierarchical structure. Generally, the agglomerates are clusters of aggregates and, in turn, these comprise primary particles that are fused together. Cohesive forces hold these structures together. Consequently, rupture of these entities requires that the hydrodynamic stress induced by the flow, σ_h

overcomes the cohesive strength of the agglomerate, σ_c. The hydrodynamic stress considered in this model is the maximum of the shear stress components at the location of the agglomerate in the flow field:

$$\sigma_h = \max\left(|\sigma_{xy}|, |\sigma_{yz}|, |\sigma_{xz}|\right) \quad (1)$$

The cohesive strength will obviously depend on the specific agglomerate structure and properties. Rwei et al. (1990) studied the mechanisms of carbon black agglomerates breakup in a range of different porosities due to the application of a simple shear flow field, while Scurati et al. (2005) performed dispersion experiments using silica agglomerates of various densities and liquid low molecular weight polymers of different viscosities. The authors found that the critical stress for erosion is smaller than that for rupture, and that once erosion starts, it continues for very long times. Making use of the fragmentation number concept, *Fa* (σ_h/σ_c) they showed that erosion takes place when $2 \leq Fa < 5$. By contrast, rupture occurs shortly after reaching a critical stress (i.e., $Fa \geq 5$) and concludes abruptly. These values of the fragmentation number delineating the occurrence of various dispersion mechanisms will be adopted also in the present work. Nevertheless, even at high *Fa* values, one should assume that there is a finite probability associated with the break-up of agglomerates, which can be defined as:

$$P_{break} = \lambda_N . \Delta t \quad (2)$$

The probability per unit time, λ, is proportional to the surface of the agglomerate. Assuming a compact geometry:

$$\lambda \propto \left(\frac{N_{cur}}{N_{ini}}\right)^{2/3} \quad (3)$$

where N_{cur} and N_{ini} denote the current and initial number of particles clustered in the agglomerate, respectively. The time interval is always chosen such that $\lambda \Delta t << 1$. In the particular case of melt extrusion, it is convenient to initially set each time interval, Δt, as a function of screw speed (N) and extruder geometry:

$$\Delta t = \frac{k\,\mathrm{H}}{\pi N D_b} \quad (4)$$

where k is a constant, H is the channel depth and D_b is the internal barrel diameter. Following a Monte Carlo scheme, at each Δt, a random number, $\delta \in$ [0, 1], is generated and associated to each agglomerate/particle. If $\delta > P_{break}$ the dispersion mechanism is not activated, whereas if $\delta \leq P_{break}$, the

agglomerate either erodes or ruptures, depending on the value of the fragmentation number. The probability of agglomerate dispersion increases with increasing residence time.

3 Distributive Mixing Characterization

The Shannon entropy (S) will be used as an entropic measure to characterize particle distribution (Camesasca et al., 2005, 2006):

$$S = -\sum_{j=1}^{M} p_j \log p_j \tag{5}$$

where M represents the total number of sub-regions of equal volume/area in which the system is divided (in other words, M defines the scale of observation) and p_j is the probability of finding a particle in sub-region j. The lowest entropy ($S = 0$) corresponds to a system where all the existing particles are located in one sub-region. Conversely, the maximum entropy ($S=S_{max}$) is reached when the probability of finding a particle in each sub-region is uniform ($p_j = 1/M$), *i.e.*, $S_{max} = \log M$. Therefore, a normalized Shannon entropy can be defined as:

$$S_{norm} = \frac{-\sum_{j=1}^{M} p_j \log p_j}{\log(M)} \tag{6}$$

The normalized entropy will be used as an index for distributive mixing characterization.

4 Numerical Procedure

In this work, the agglomerate dispersion model is applied to the 3D flow in a rectangular channel (unwound screw), to emulate the flow in the melt conveying zone of a single screw extruder (Tadmor and Klein, 1970). A flat surface on the top of the channel (the barrel) moves at constant speed in a direction making an angle (equivalent to the screw helix angle) with the down-channel axis (see Figure 1). The channel width, W, height, H and length, L, are 0.024m, 0.005m 1.20m, respectively.

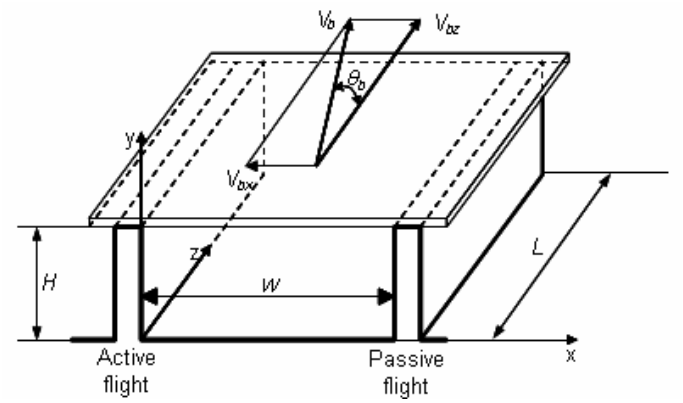

Figure 1: Flow configuration studied.

The implementation of the dispersion model requires the calculation of the residence time of each particle in the system as well as the hydrodynamic stresses experienced. Velocity and temperature profiles can be determined implicitly by solving numerically the governing equations (mass and momentum, respectively):

$$div(\vec{v}) = 0 \tag{7}$$

$$\nabla p = div(\eta \nabla \vec{v}) \tag{8}$$

where p is the pressure, $\vec{v} = (V_x, V_y, V_z)$ is the velocity vector and η is the viscosity. The concentration of the agglomerates is as low as 1.2% (to minimize the effect of filler on melt viscosity) and these clusters will be assumed mass-less, not affecting the flow field and not interacting with each other. Their cohesive strength (σ_c) is set at 1000 Pa. In this work we solved for the 3D isothermal flow of a Newtonian fluid with boundary conditions:

$$\begin{cases} V_x = -V_{bx} \\ V_y = 0 \\ V_z = V_{bz} \end{cases}, \qquad \text{for} \quad y = \mathrm{H} \tag{9a}$$

$$V_x = V_y = V_z = 0, \qquad \text{for} \quad x \in \{0, \mathrm{W}\} \quad \text{and} \quad y = 0 \tag{9b}$$

where V_{bx} and V_{bz} are the moving surface velocities in the x and z directions, respectively. The commercial software FIDAP (**ANSYS FLUENT web page: http://www.ansys.com**) was employed in the numerical simulations.

One thousand agglomerates of equal size (100 μm), each comprising 100 primary particles of size 1-4 μm , are positioned at the entrance of the rectangular channel, near the upper wall. As they progress

along the channel, they are replaced by new ones, thus ensuring continuous feeding. The solids flow patterns are determined by applying a particle tracking algorithm based on the 4th order Runge-Kutta Method, with an adaptive time step, on the velocity field. In each time interval determined from equation 4 (making $k = 0.17$), we evaluate the break-up probability. Fragmentation numbers are computed for those agglomerates that can potentially break. Depending on the resulting *Fa* value, they will either remain intact, erode (one individual particle will detach), or break (split in two aggregates of equal size, or in two aggregates where one will contain an extra primary particle, if necessary to guarantee primary particle indivisibility). The scheme is repeated for the remaining time steps, until reaching the channel outlet. The corresponding flow chart is presented in Figure 2.

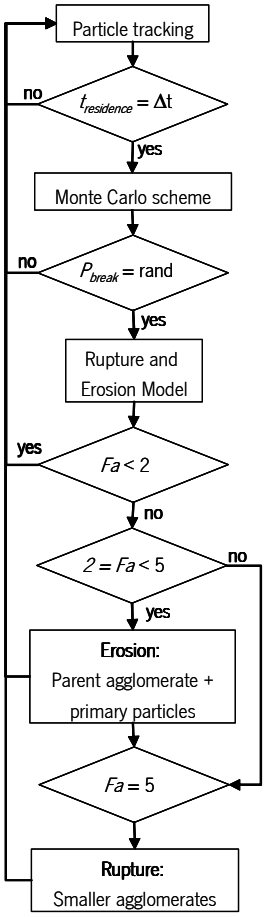

Figure 2: Flow chart for the dispersion model

5 Results & Discussion

We use a commercial High Density Polyethylene extrusion grade (HDPE ALCUDIA TR-135, from Repsol YPF) – see Table 1 - in the flow simulations. V_{bx} and V_{bz} (transversal and down-channel components of the velocity of the top plate) in equation 10 were made equal to 0.024 m/s and 0.091 m/s, respectively (this

corresponding to an equivalent screw rotating at 60 rpm) and to 0.008 m/s and 0.030 m/s, respectively (corresponding to the screw rotating at 20 rpm). The velocity components at a typical channel cross-section are illustrated in Figure 3, for a screw speed of 60 rpm.

Table 1 – Properties of HDPE ALCUDIA TR-135 (Repsol YPF, Spain)

Property	Value
Melt density	854 kg.m^{-3}
Viscosity	3800 Pa.s.

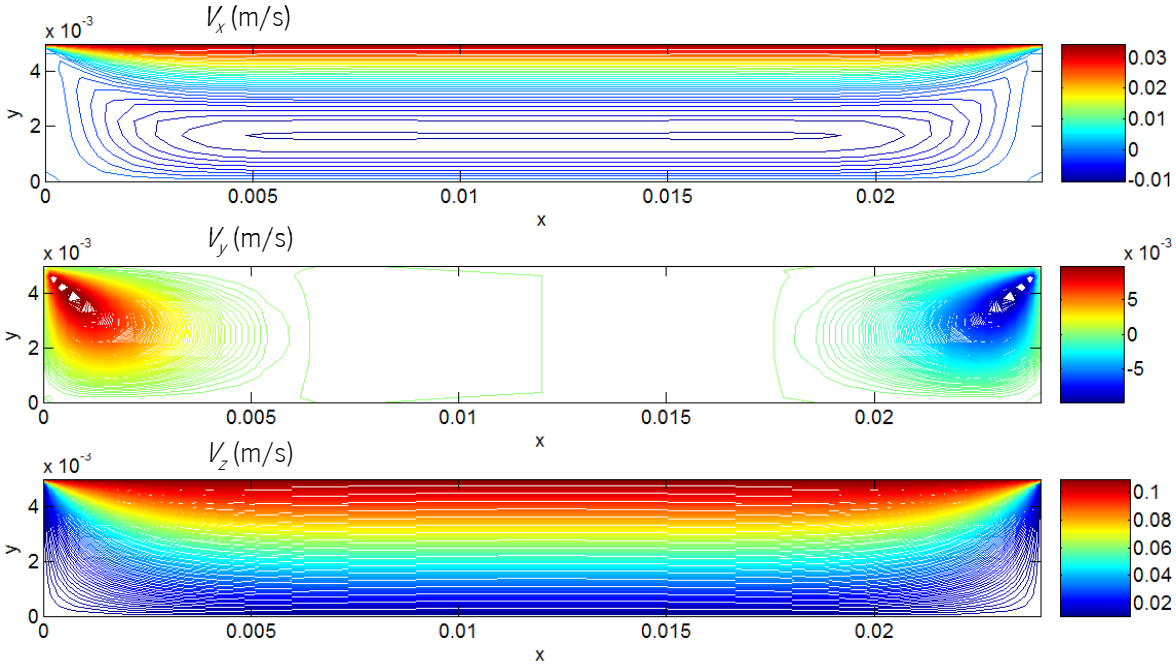

Figure 3: 3D velocity components in a channel cross-section (60 rpm).

Figure 4 shows the dynamics of distributive mixing along the channel, under isothermal flow conditions at 190 °C, screw rotating at 60 rpm and open discharge. The helical flow patterns can be clearly observed, solid particles being progressively distributed across the entire cross-section. The dynamics of agglomerate size distribution indicates the occurrence of rupture and erosion phenomena.

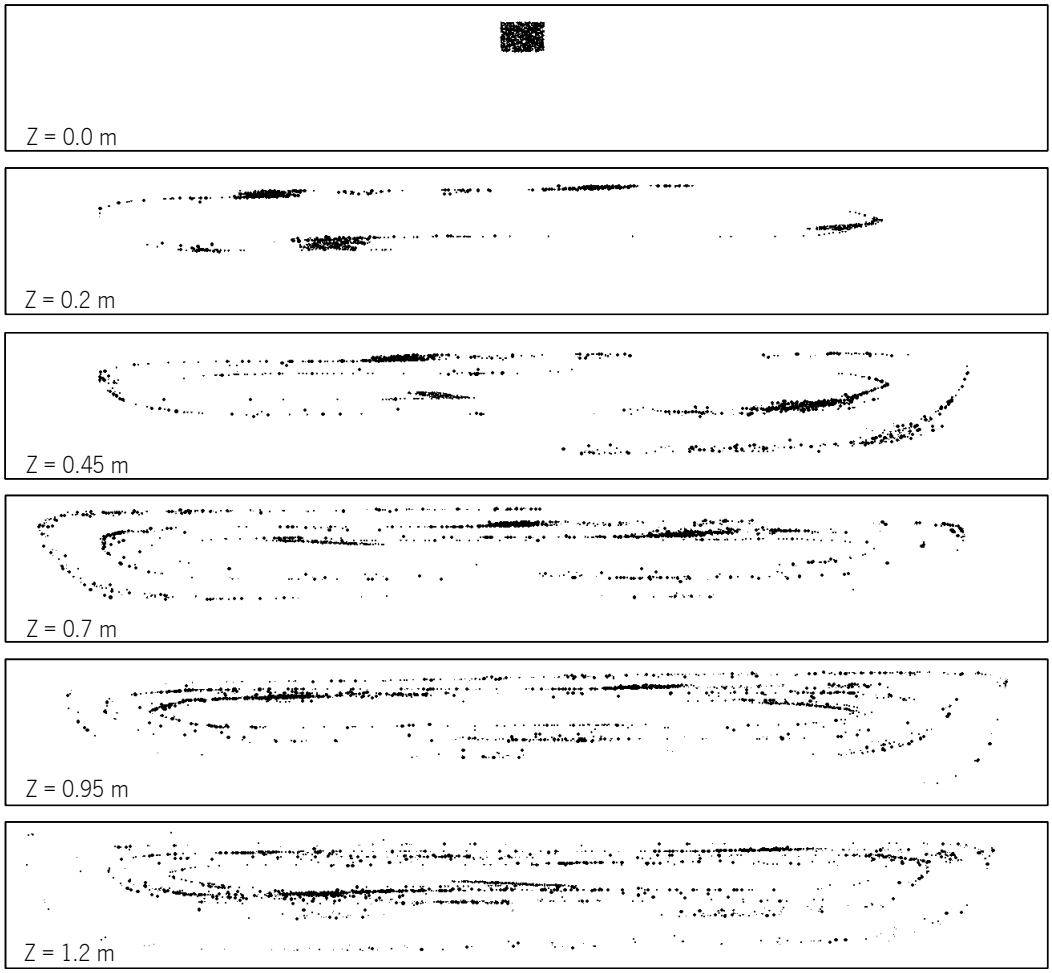

Figure 4: Dynamics of flow and mixing along the channel.

Figure 5 shows the locations where these two phenomena occur along the entire screw length, whereas Figure 6 provides a more detailed analysis of the behavior. Apparently, most of the erosion takes place where flow reorientation occurs, close to the lateral channel walls. Rupture seems to happen mainly after this reorientation is completed and flow along the x direction develops. Figure 6 (top) shows the regions of the channel cross-section where the various shear stresses are typically prevalent. As per equation 1, at each location, one of these stresses will be σ_h. Figure 6 (middle) quantifies σ_h for a specific cross-section. Stresses increase from the center to the channel walls. However, as seen in Figure 6 (bottom), most of the dispersion phenomena occur at a distance from the walls, because of the distribution of the particles in the channel, as shown in Figure 4.

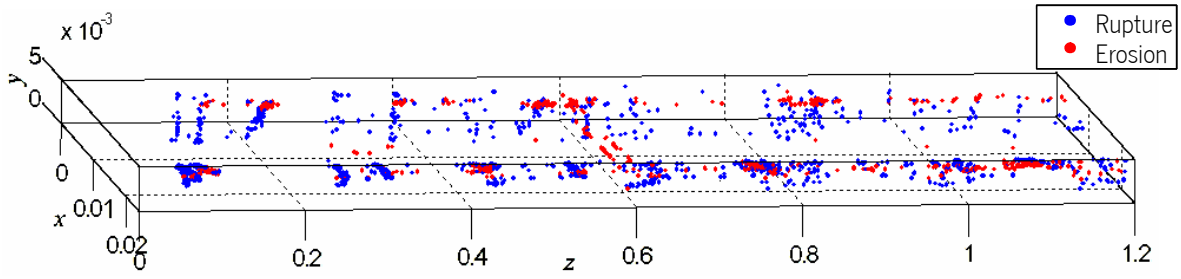

Figure 5: Agglomerate rupture/erosion events along the rectangular channel.

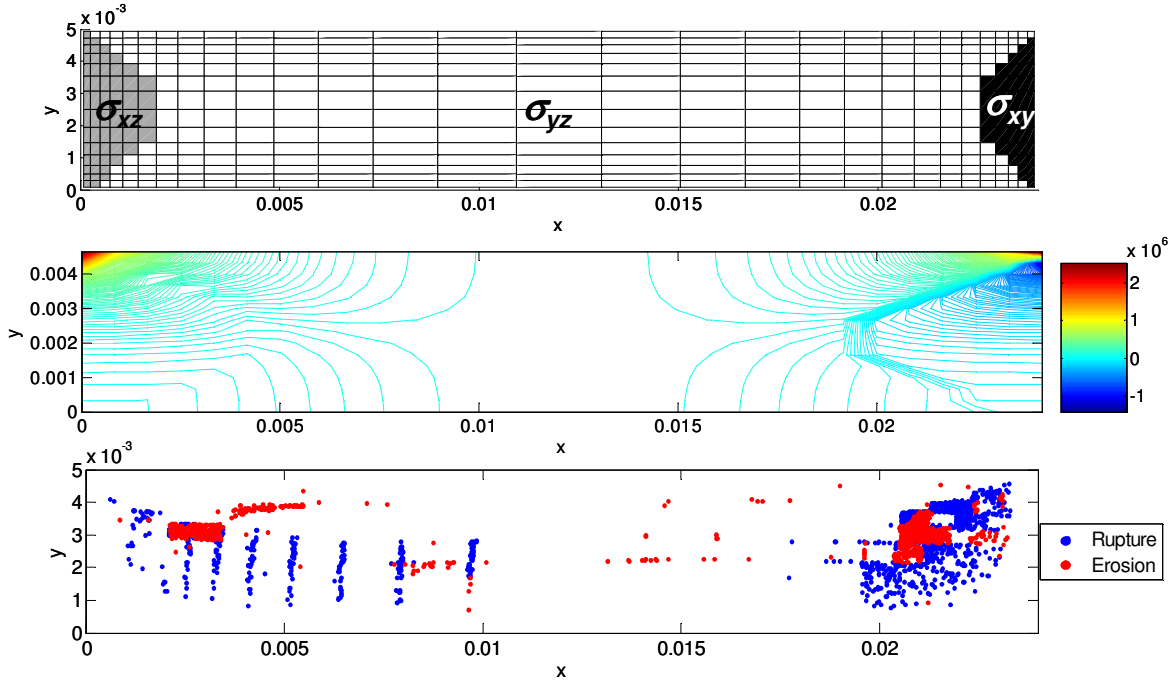

Figure 6: Hydrodynamic stresses and dispersion in a rectangular channel. Top: Locations where the different shear stresses are predominant; Middle: map contour of σ_n. Bottom: rupture and erosion phenomena.

The actual evolution of the solids dimensions at four different times is given in Figure 7. The progressive conversion of the initial agglomerates into aggregates and primary particles is obvious, but it is also clear (especially at short residence times) that primary particles are formed from the erosion of both agglomerates and fragments. Figure 8 quantifies the evolution of the solids size distribution at different cross sections along the channel. As stated above, at the beginning of the channel 1000 agglomerates of equal size (100 μm) are present. Under the simulated flow conditions, at the extruder outlet less than 20% of the initial agglomerates survive, and a range of particles and aggregates of different dimensions are present. A closer look at the

Figure also reveals that the range of particle sizes present at the outlet is also present at around half the channel length. From there onwards dispersion proceeds at a slower rate, with the continuous rupture of agglomerates and of aggregates of half that size (around 50 μm) yielding smaller aggregates (around 10 μm) and small particles (1-4 μm). This constant decrease in dispersion rate is also revealed in Figure 9 for the parent agglomerates. This behavior is to be expected, since the larger the number of smaller species, the lower the probability for break-up (equation 2).

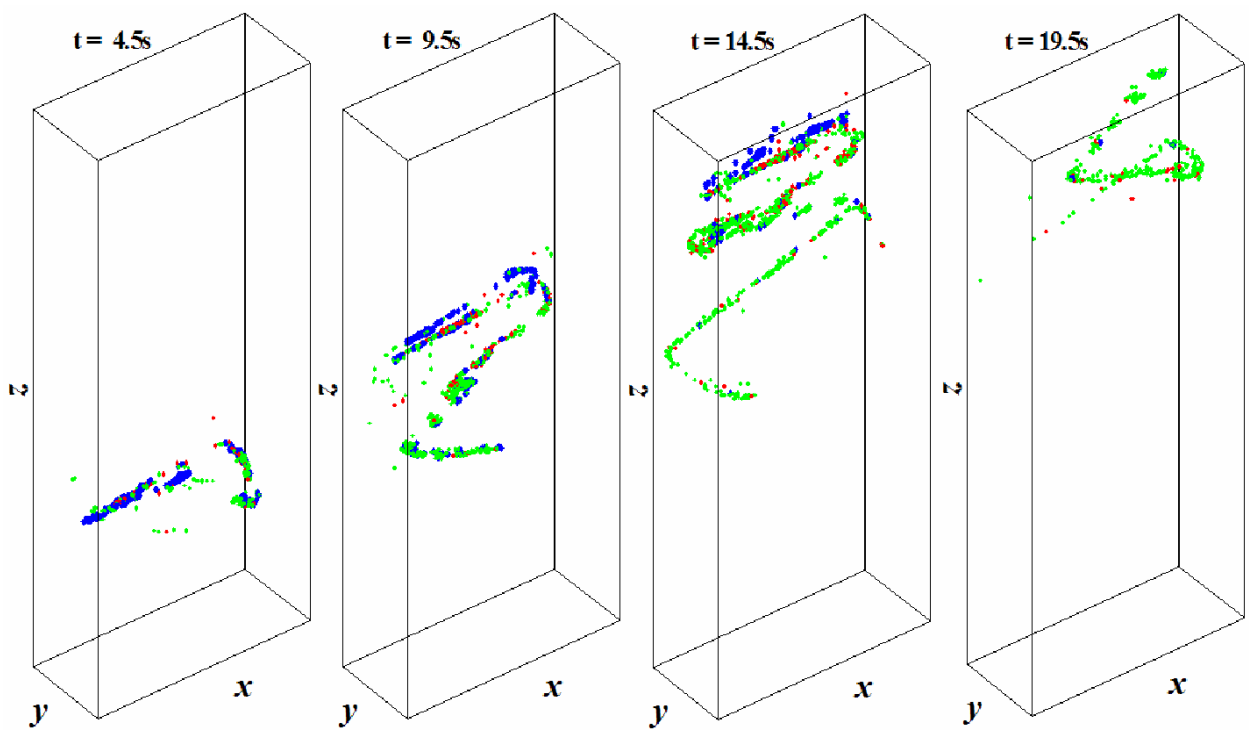

Figure 7: Dynamics of the evolution of parent agglomerates (blue), aggregates (green) and primary particles (red).

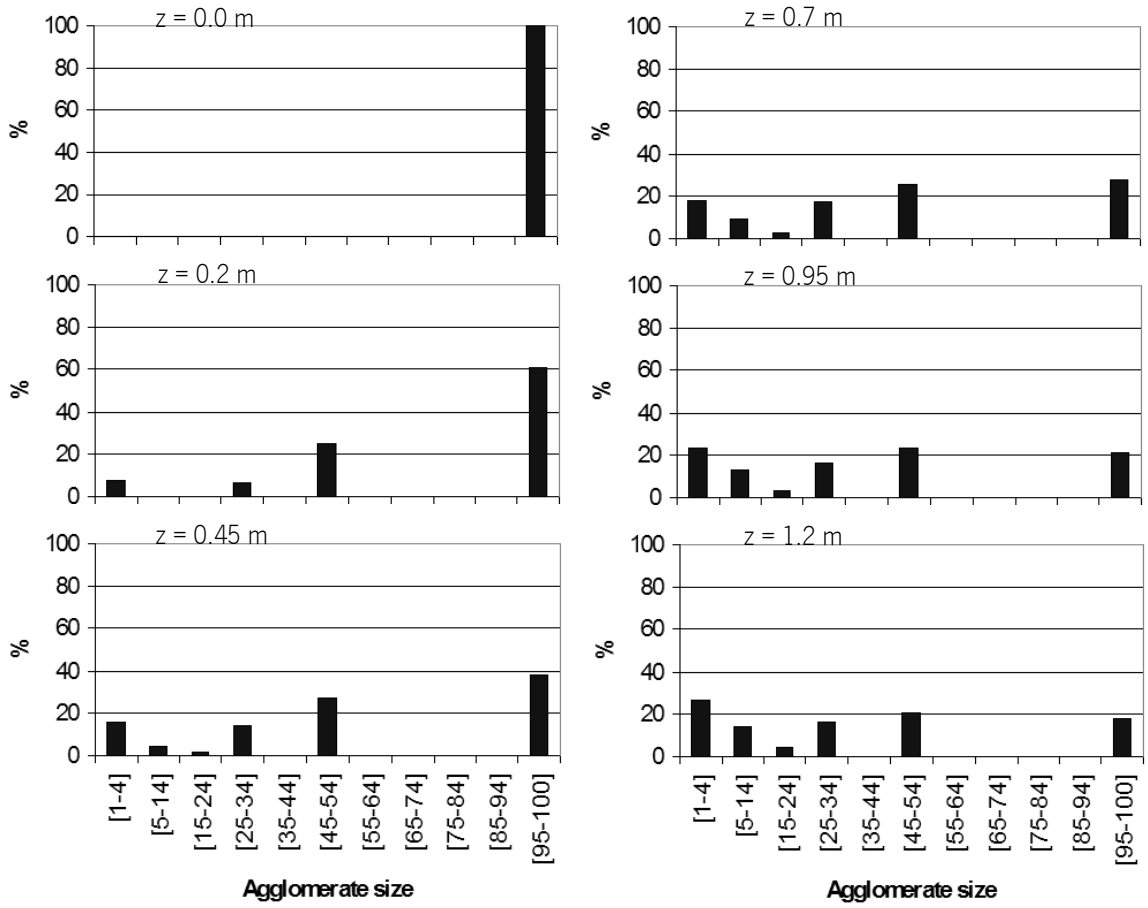

Figure 8: Particle size distribution along the flow channel.

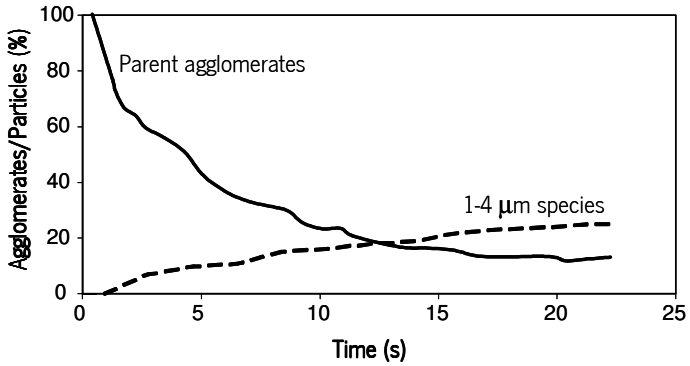

Figure 9: Dynamics of parent agglomerates and 1-4 μm species.

The spatial distribution of the solid species in the system is assessed using an entropic measure based on the Shannon entropy. As per equation 6, S_{norm} is computed by dividing each section in a number of sub-

regions, or bins. The Shannon entropy was computed by analyzing cross-sections (divided into 225 × 190 sub-regions) at constant down-channel increments. Figure 10 shows the dynamics of distributive mixing at different scales of observation. As expected, the Shannon entropy decreases as the scale of observation decreases, i.e., with an increase in the number of bins. Above 1625 bins the results become relatively similar and consistently show that the entropy increases as the solids become better distributed along the extruder channel. At the outlet the system is globally well distributed, but due to the large number of big clusters (initial agglomerates and large size fragments) present in the system, the entropy levels are lower than those that could eventually be attained for better dispersed systems (smaller numbers of initial agglomerates and large size fragments).

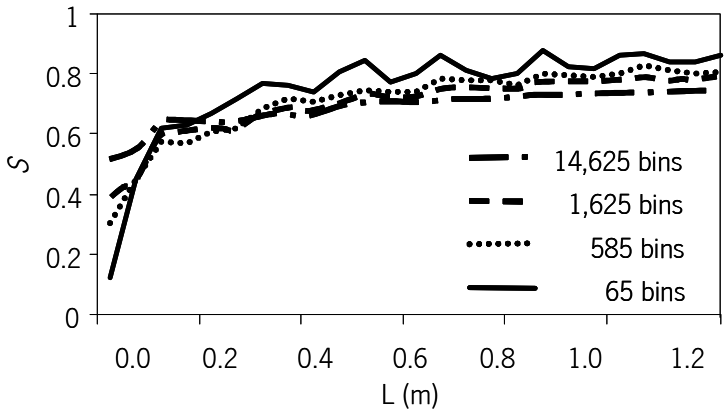

Figure 10: Evolution of Shannon entropy along the channel as a function of the number of bins (the population used is always identical, 1000 × 100 particles).

Figure 11 shows the effect of screw speed on agglomerate dispersion and distribution. The number of surviving initial agglomerates (Figure 11a) decays exponentially with time (or, equivalently, with down-channel distance). This decay increases as the screw speed increases from 20 to 60 rpm, since this generates higher hydrodynamic forces. Figure 11b provides evidence that the decrease in average particle size arising from changes in screw speed results primarily from the increasing number of primary particles that were released from the erosion of fragments/aggregates.

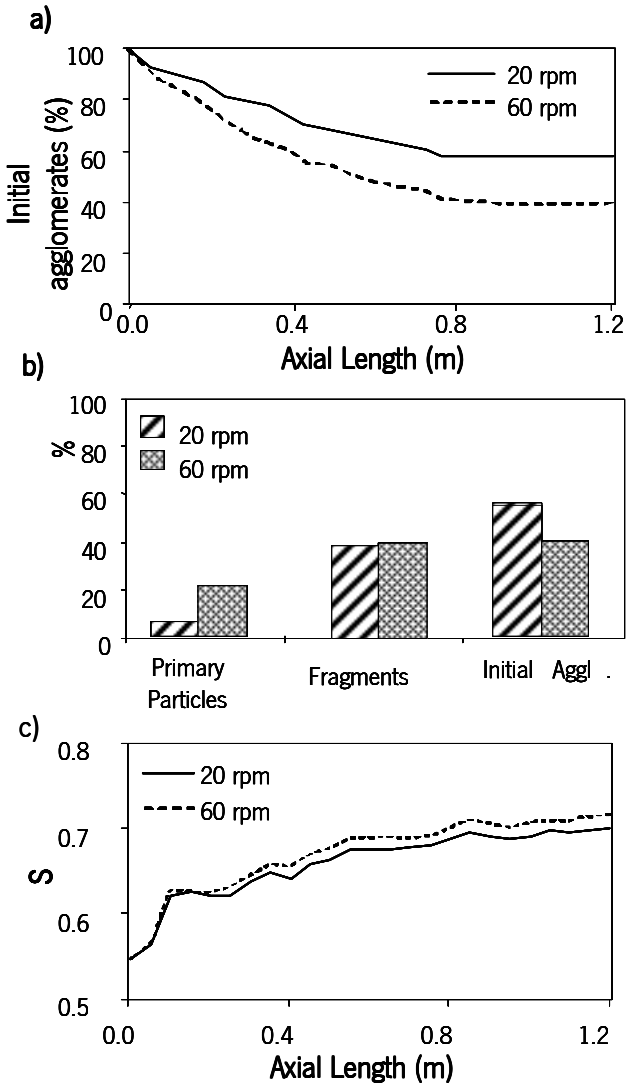

Figure 11: Effect of screw speed on dispersion and distribution: a) evolution of the number of initial agglomerates; b) particle size distribution at the outlet; c) Shannon entropy along the channel.

Distributive mixing (Figure 11c) improves along the screw channel and with increasing screw rotational speed, reflecting not only better particle spatial distribution, but also the increasing number of primary particles suspended in the melt, as a result of enhanced dispersive mixing.

6 Conclusions

A mixing model for agglomerate dispersion and distribution was applied to the melt conveying section of a single screw extruder. The model is based on the determination of the flow patterns in the screw channel using Computational Fluid Dynamics (CFD) and the calculation of the particle trajectories by employing a tracking routine with an adaptive time step. A Monte Carlo algorithm is used to model erosion and rupture using the dispersion probability which is postulated to depend on the size of the agglomerate and on the shear stress. We quantify mixing by using the Shannon entropy.

The mixing model developed in this work provides a detailed description of the system mixing dynamics along the flow channel and is sensitive to changes in screw speed. The approach described here is general and can be adapted for different polymer/additive systems and for different processing equipment.

References

Alemaskin, K., Manas-Zloczower, I., Kaufman, M., "Index for simultaneous dispersive and distributive mixing characterization in processing equipment", International Polymer Processing, **19**, 327-334 (2004)

Bolen, W.R., Colwell, R.E., Intensive mixing", Soc. Plast. Engng, J., **14**, 24 (1958)

Camesasca, M., Manas-Zloczower, I., Kaufman, M., "Entropic characterization of mixing in microchannels", J. Micromech. Microengin. **15**, 2038-2044 (2005)

Camesasca, M., Kaufman, M., Manas-Zloczower, I., "Quantifying Fluid Mixing with Shannon Entropy", Macromolecular Theory and Simulations, **15**, 595-607 (2006)

Dizon, E.S., "Processing in an Internal Mixer as Affected by Carbon Black Properties", Rubber Chemistry & Technology, **49**, 12-27 (1976)

Elemans, P.H.M., van Wunnik, J.M., "The Effect of Feeding Mode on Dispersive Mixing Efficiency in Single-Screw Extrusion", Polym. Eng. Sci., **41**, 1099-1106 (2001)

Gale, M., Mixing in Single Screw Extruders, Chemetech Publishing (2009)

Janes, R.I., Winch, P.J., "Mixing and shear predictions for a single-screw extruder, using computational simulation", IMA Journal of Management Mathematics, **5**, 399-415 (1993)

Kim, S.J., Kwon, T.H., "Measures of mixing for extrusion by averaging concepts", Polymer Engineering and Science, **36**, 1466–1476 (1996)

Manas-Zloczower, I., Nir, A., Tadmor, Z., "Dispersive Mixing in Internal Mixers - A Theoretical-Model Based on Agglomerate Rupture", Rubber Chem. Technol., **55**, 1250-1285 (1982)

Manas-Zloczower, I (editor.), Mixing and Compounding of Polymers, Hanser, Munich (2009)

Manas-Zloczower, I., Feke, D.L., "Dispersive Mixing of Solids Additives", in Mixing and Compounding of Polymers: Theory and Practice, Ica Manas-Zloczower Editor, Hanser Verlag, 2009

McKelvey, J.M., Polymer Processing, Wiley-Interscience, New York (1962)

Meijer, H.E.H., Janssen, J.M.H., "Mixing of Immiscible Liquids, in Mixing and Compounding of Polymers", in Mixing and Compounding of Polymers: Theory and Practice, Manas-Zloczower, I., Tadmor, Z. (eds), Hanser Publishers, Munich (1994)

Ottino, J.M., The Kinematics of Mixing: stretching, chaos and transport Cambridge, Cambridge University Press (1989)

Rauwendaal, C., Mixing in Polymer Processing, Marcel Dekker Inc., New York (1991)

Rwei, S.P., Manas-Zloczower, I., Feke, D.L., "Observation of Carbon Black Agglomerate Dispersion in Simple Shear Flows", Polym. Eng. Sci., **30**, 701-706 (1990)

Scurati, A., Feke, D.L., Manas-Zloczower, I., "Analysis of the Kinetics of Agglomerate Erosion in Simples Shear Flows", Chem. Eng. Sci., 60, 6564-6573 (2005)

Seyvet, O., Navard, P., "In situ study of the dynamics of erosion of carbon black agglomerates", J. Applied Polym Sci., **80**, 1627-1629 (2001)

Shiga, S., Furuta, M., "Processability of Electron-Paramagnetic-Res in an Internal Mixer .2. Morphological-Changes of Carbon-Black Agglomerates During Mixing", Rubber Chem. Technol., **58**, 1-22 (1985).

Tadmor, Z., Klein, I., Engineering Principles of Plasticating Extrusion, Van Nostrand Reinhold, New York (1970)

Tadmor, Z., "Forces in Dispersive Mixing", Ind. Eng. Chem. Fundam., **15**, 346-348 (1976)

Tyagi, S., Ghosh, A.K., Morphology Development during Blending of Immiscible Polymers in Screw Extruders, Polym. Eng. Sci, **42**, 1309-1321 (2002)

Utracki, L.A., Polymer blends handbook, Kluwer Academic Publs (2002)

IV

Dynamics of Filler Size and Spatial Distribution in a Plasticating Single Screw Extruder - Modeling and Experimental Observations [3]

[3] Article published at International Polymer Processing, volume, 25, pages 188-198, March 2010
Authores: N. Domingues, A. Gaspar-Cunha, J. A. Covas, M. Camesasca, M. Kaufman, I. Manas-Zlockzower

1 Introduction

Although much of the available scientific know how on plasticating single screw extrusion was obtained via theoretical and/or experimental studies using single resins (Tadmor and Klein, 1970; Rauwendaal, 1986), current industrial practice involves the extrusion of more complex material systems (known as compounds), which generally comprise one or more polymers and a number of additives. Many of the latter consist of solid agglomerates with a hierarchical structure comprised of aggregates which in turn are made of primary particles. Typical examples are pigments and fillers, such as carbon black, titanium dioxide, calcium carbonate and silica. Organoclays and carbon nanotubes (or fibers) are more recent examples of solid additives. The level of dispersion and the quality of the distribution of such additives into the matrix determine the compound performance under service conditions. Therefore, it is of utmost scientific and practical importance to correlate the characteristics of flow and heat transfer in the extruder, as determined by screw geometry, material characteristics and processing conditions with the dispersive and distributive mixing levels achieved for the compounds.

Despite of its importance, this subject is seldom studied in the open literature. Manas-Zloczower and co-authors (Wang and Manas-Zloczower, 2004; Camesasca et al., 2005, 2006; Scurati et al., 2005; Alemaskin et al., 2003) have been addressing the important topic of characterizing dispersive and distributive mixing of solids-liquid systems. Any such analysis requires data on particle size, particle size distribution and particle spatial distribution, as well as on its evolution along the flow channel. These authors have developed a model for the kinetics of erosion of solid agglomerates in simple shear flow (denoted here as kinetic dispersion model) making use of the concept of the fragmentation number, defined as the ratio between the hydrodynamic stresses induced by the flow and the cohesive stresses of the agglomerates (Scurati et al., 2005). Agglomerate dispersion and distribution in the matrix was determined by employing a particle tracking algorithm (Alemaskin et al., 2003) in conjunction with the kinetic model of dispersion. Dispersive mixing was characterized by the solid phase size distribution in the system and its evolution along the extruder line, whereas distributive mixing was analyzed using entropic measures (Alemaskin et al., 2003; Camesasca et al., 2006). Later, the kinetic dispersion model was extended to incorporate both rupture and erosion phenomena (Domingues et al. 2006, 2009a).

In this paper we present the results of using the kinetic dispersion model described above to predict mixing in a plasticating single screw extruder. We focus our attention on the melting and melt conveying zones of the extruder. A numerical model of the plasticating extruder is coupled with the agglomerate dispersion model. As melting occurs, a number of solid agglomerates in direct proportion with the pace of melting are

injected into the freshly molten material. Agglomerates are assumed to be uniformly distributed in the melt at their injection point. At the end of the melting zone, the number of agglomerates present in the system corresponds to the prescribed filler concentration in the system. The dynamics of particle size distribution and filler spatial distribution is calculated for the remaining of the screw channel.

2 Agglomerate Dispersion and Distribution

Solid additives used in plastics and rubber industry are colloidal in nature and exhibit a hierarchical structure. Primary particles are fused together into aggregates which in turn cluster under the influence of surface forces into agglomerates. The present model (detailed elsewhere, Domingues et al., 2009a) considers that these multi-scale entities may be progressively broken down into smaller size entities, denoted fragments, by either a rupture mechanism (fragments produced are of the same size scale as the original agglomerates) or an erosion mechanism (small fragments are detached from the outer surface of the agglomerate). Particle break-down requires that the hydrodynamic stress induced by the flow (σ_h) is higher than the cohesive strength of the agglomerate (σ_c). A local fragmentation number can be defined as (Scurati et al., 2005):

$$Fa = \frac{\sigma_h}{\sigma_c}. \tag{1}$$

In turn, the hydrodynamic stress considered in this model is the maximum of the shear stress components at the location of the agglomerate in the flow field:

$$\sigma_h = \max\left(\left|\sigma_{xy}\right|,\left|\sigma_{yz}\right|,\left|\sigma_{xz}\right|\right). \tag{2}$$

Agglomerate cohesive strength depends on the specific agglomerate structure and properties. The presence of structural heterogeneities within the agglomerate is mostly significant and consequently it would seem appropriate to define an average value and a range for the agglomerate cohesivity. Experimental observations point out that erosion occurs when hydrodynamic stresses are only slightly higher than the cohesive ones, whereas rupture occurs at much higher applied stresses (Rwei, 1990). This translates into a lower limit for the fragmentation number (labeled in this work as α) below which no dispersion occurs and an upper limit for the fragmentation number (labeled as β) for which the mechanism of dispersion changes from erosion to rupture. For example, for a silica/polydimethyl siloxane system, it was experimentally determined that for fragmentation numbers bellow $Fa < 2$, dispersion does not occur, for $2 \leq Fa < 5$ the

agglomerates will erode, whereas for $Fa \geq 5$ rupture becomes the predominant breakup mechanism (Scurati et al., 2005). Nevertheless, even for sufficiently high fragmentation numbers, there is a finite probability associated to the break-up of agglomerates, which is given by (Domingues et al., 2009a):

$$P_{break} = \lambda_N . \Delta t \tag{3}$$

Here λ is proportional to the fractional change in the agglomerate surface area with respect to the initial surface area (Domingues et al., 2009a) and the time interval, Δt, is set as a function of screw speed (N) and extruder geometry (Rauwendaal, 1987):

$$\Delta t = \frac{kH}{\pi N D_b} \tag{4}$$

where k is a constant, H is the extruder channel depth, D_b is the internal barrel diameter and N is the screw rotational frequency. This time interval is related to a characteristic time scale for the shearing process in the extruder and is always chosen such that $\lambda \Delta t << 1$. Following a Monte Carlo procedure, we generate, at each Δt, a random number, δ, in the interval [0, 1], to be associated to each agglomerate/particle. If $\delta > P_{break}$, the dispersion mechanism in not activated. If $\delta \leq P_{break}$, the agglomerate either erodes or ruptures, depending on the value of the fragmentation number, as pointed out above. This numerical procedure determines a Poisson process provided $\lambda \Delta t << 1$. The probability of agglomerate dispersion will increase with increasing residence time.

To quantify agglomerate distribution in the system we use an entropic measure based on the Shannon entropy (Shannon and Weaver, 1948; Khinchin, 1957). The entropy can be correctly calculated only if:

1. all the particles present in the system are in one or more of the bins used;
2. the bins have the same size;
3. the same binning procedure is used at different times.

Therefore, the normalized Shannon entropy is given by:

$$S_{norm} = \frac{-\sum_{j=1}^{M} p_j \log p_j}{\log(M)} \tag{5}$$

where M represents the total number of sub-regions of equal volume/area in which the system was divided (M determines the scale of observation) and p_j is the probability of finding a particle in sub-region j, i.e., the density of the particles in bin j. The lowest entropy ($S = 0$) corresponds to a system where all the existing particles are located in one sub-region. The maximum entropy is reached when the probability of finding a particle in each sub-region is the same ($p_j = 1/M$), *i.e.*, $S_{norm} = 1$.

3 Computer Modeling

The implementation of the above model requires the calculation of the residence time of each particle in the system and the level of stresses experienced during this time. Implicitly, velocity and temperature profiles in the extruder need to be numerically determined by solving the field equations:

$$div(\vec{v}) = 0 \tag{6}$$

$$\nabla p = div(\eta \nabla \vec{v}) \tag{7}$$

$$\rho C_m \frac{DT}{Dt} = k\nabla^2 T + \eta\dot{\gamma}^2 \tag{8}$$

where p is the pressure, $\vec{v} = (V_x, V_y, V_z)$ is the velocity vector, η is the viscosity, ρ is the density, C_m is the specific heat, k is the thermal conductivity, T is the melt temperature and $\dot{\gamma}$ is the shear rate.

Computation of the corresponding flow patterns would require a constitutive model (viscosity function) that would take into account the effect of particle size and concentration, in order to couple flow and morphology evolution. Not only such a constitutive rheological equation is not readily available, but the determination of its parameters would be prohibitive in terms of experimental effort. The following law correlates the viscosity of diluted suspensions of identical non-interacting rigid spherical particles in pure shear with that of the matrix, η_0 and the concentration of the spheres, ϕ (Roscoe, 1952):

$$\eta = \eta_0 (1 - \phi)^{-2.5} \quad (9)$$

If the solids concentration is lower than 4%, an increase of 10% in viscosity is predicted. In this work agglomerate concentration was kept at 1.2% and these were assumed to be mass-less entities, *i.e.*, not affecting the flow field and not interacting with each other. Based on experimental observations for silica agglomerates of comparable packing densities, agglomerate average cohesive strength (σ_c) was set at 1000 Pa (Boyle, 2004).

Numerical modeling of the plasticating extruder involves a number of sequential steps (Tadmor and Klein, 1970; Rauwendaal, 1986):

i. Solids conveying in the hopper due to gravity; here, an analytical equation is used to compute the vertical pressure development.

ii. Frictional solids conveying in the initial turns of the screw; here it is assumed that the solid behaves like a plug and force and momentum balances are used to calculate the down-channel pressure generation. This is coupled with a non-isothermal analysis that enables computation of the temperature raise due to friction near the screw and barrel walls and to conduction from the barrel.

iii. Delay zone, which is sub-divided in two sequential steps: initially, a melt film develops adjacently to the inner barrel wall due to the combined effects of frictional heat generation and heat conduction from the barrel; later, the same mechanism creates melt films near the screw walls.

iv. Melting according to a Tadmor-type mechanism that considers the co-existence, at a given channel cross-section, of a solid plug, a melt pool and three melt films near the barrel, screw root and passive screw flank, respectively, as proposed by Elbirli *et al.* (1984). The model yields pressure, velocities, temperature and solids width evolution along the helical screw channel assuming the non-isothermal flow of a non-Newtonian fluid.

v. Melt conveying, modeled as a 2D non-isothermal incompressible flow of a non-Newtonian fluid and the melt flow is fully developed in the down and cross channel directions and the temperature field is fully developed in the cross channel and down-channel directions (i.e., $\partial T / \partial x = 0$ and $\partial T / \partial y = 0$) (Fenner, 1979). The boundary conditions are:

$$\begin{cases} V_x(y=0)=0 \\ V_x(y=H)=-V_{bx} \end{cases} \quad \begin{cases} V_z(x=0)=0 \\ V_z(x=W)=0 \\ V_z(y=0)=0 \\ V_z(y=H)=V_{bz} \end{cases} \quad \begin{cases} T(x=0)=T_s \\ T(x=W)=T_s \\ T(y=0)=T_s \\ T(y=H)=T_b \end{cases} \tag{10}$$

where V_{bx} and V_{bz} are barrel velocities in the x and z directions, respectively, T_s is screw temperature, T_b is barrel temperature, and H and W are the local depth and width of the screw channel, respectively.

The program computes velocity and temperature profiles for channel cross sections at Δz intervals in the down-channel direction, after detecting which of the above steps is valid (Gaspar-Cunha and Covas, 2001). This is done on the basis of the values of the temperature of the material at certain cross-channel locations (for example, the delay will start when the temperature of the polymer adjacent to the inner barrel wall attains its melting temperature). Within each functional zone, the distinction between solids and melt is simply done on the basis of the local material temperature. Agglomerate dispersion model was applied at the melting and melt conveying zones.

Figure 1 illustrates the corresponding algorithm. As soon as melting starts, a number of agglomerates (proportional to the width of the melt pool) are inserted at the specific cross-section and they are uniformly distributed. This procedure is repeated for the various cross-sections along the melting zone, until melting is completed. Therefore, at all cross-sections selected, except for the initial one, the melt pool contains freshly introduced new agglomerates and a number of solid particles, of different sizes, that were inserted upstream as agglomerates. The total number of agglomerates introduced in the melting zone corresponds to the prescribed filler concentration in the system.

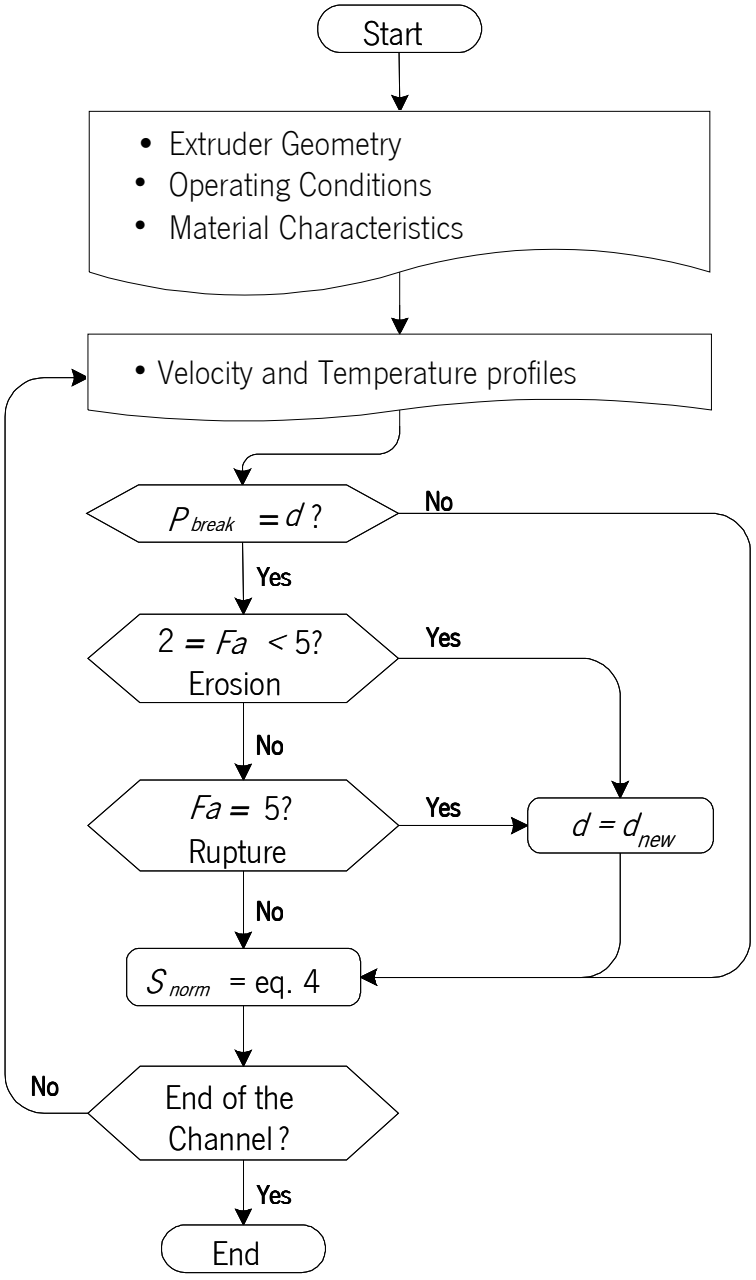

Figure 1: Algorithm for dispersion and distribution of solid additives in a plasticating extruder.

At each time interval (determined from equation 4 with $k = 0.17$), the Monte Carlo method referred above is applied to evaluate the break-up probability. At each cross-section along the extruder channel the Shannon entropy is computed. The process is repeated for the remaining time steps, until the channel outlet is reached.

4 Equipment and material

Figure 2 shows the layout and the main dimensions of the extruder used in this work. This prototype of modular construction is fitted with a hydraulic screw extractor, to enable performing rapidly Maddock-type experiments, i.e., interrupting steady-state operation and extracting the screw for subsequent analysis of the helical material carcass. Table 1 presents the various screw profiles considered in the computational experiments.

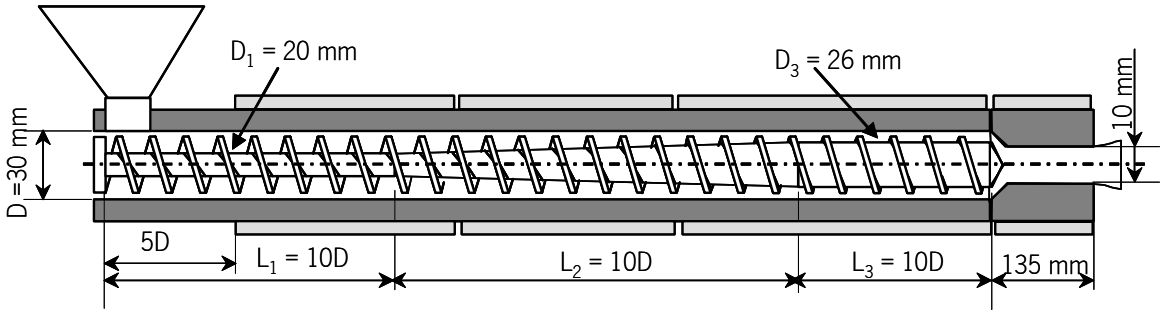

Figure 2: Layout of the single screw extruder.

Table 1: Screw geometry used in the computations

Screw		A	B	C	
Extruder Length	L_1	10D	10D	10D	
	L_2	10D	10D	10D	
	L_3	10D	20D	10D	
Internal Diameter	D	30	30	30	mm
	D_1	20	20	20	mm
	D_2	26	26	27	mm
Compression ratio		2.5	2.5	3.5	

An extrusion grade of High Density Polyethylene (HDPE ALCUDIA TR-135, from Repsol YPF) was selected as matrix. The main properties are presented in Table 2. Specific heat, heat of fusion and melting temperature values were obtained from DSC tests. Rheological data were obtained in a Rosand RH8 (dual bore) capillary rheometer, at 190°C and 210°C employing Bagley and Rabinowitsch corrections. The data was fitted to the Carreau-Yasuda viscosity equation used by the modeling routine:

$$\eta = \eta_0 e^{\frac{E}{R}\left(\frac{1}{T}-\frac{1}{T_0}\right)}\left[1+\left[\lambda\dot{\gamma}e^{\frac{E}{R}\left(\frac{1}{T}-\frac{1}{T_0}\right)}\right]^a\right]^{\frac{n-1}{a}} \quad (11)$$

where η_0, E/R, λ, n and a are material constants and T_0 is the reference temperature. The remaining properties were obtained from the literature. An antiblocking masterbatch of HDPE/Silica (CFLD-0033/2 from Ferro), containing 40% of micronized silica (equivalent to a volume fraction of 16%), was used as the second component.

Table 2: Properties of HDPE ALCUDIA TR-135 (Repsol YPF, Spain).

Density	Solids	ρ_s	560.00	kg.m^{-3}
	Melt	ρ	854.40	
Thermal Conductivity	Solids	k_s	0.19	W.m^{-1}.°C^{-1}
	Melt	k_m	0.10	
Friction coefficients	Polymer-Barrel		0.45	
	Polymer-Screw		0.25	
Specific Heat	Solids	C_s	2600.00	J.kg^{-1}
	Melt	C_m	2000.00	
Heat of fusion		H	190.00x10^3	J.kg^{-1}
Melting Temperature		T_m	118.0	°C
Carreau-Yasuda equation		η_0	18000	Pa.s
		E/R	10000	K
		$\hat{\lambda}$	0.70	s
		A	1.70	
		N	0.30	
		T_0	463.15	K

5 Results and discussion

5.1 Experimental data on the dispersion in the single screw extruder

Despite the inherent practical difficulties, an attempt was made to generate experimental data that could provide guidance to the computational modeling. The exercise involved four stages:

1. Process a pre-mixed 98/02 w/w recipe of HDPE and silica masterbatch (to yield a volume concentration of 1.2%) under steady state conditions (using screw configuration A in Table 1, uniform barrel temperature of 190 °C, screw speeds of 20 and 60 rpm) followed by a Maddock-type experiment, *i.e.*, stop the rotation of the screw and switch-off the heaters, remove the die and extract the screw (while cooling it and the polymer helix with compressed air). This sequence of operations took approximately one minute.

2. Identify the extension of the solids conveying, melting and melt conveying zones in the helix of material encircling the screw. In both experiments, melting started at the 10th screw turn if numbered from the hopper side. Obtain three 10 μm thick cross-sections of the helix at regular down-channel intervals between screw turns 10 and 30.

3. For each sample, identify the number of particles and their sizes, using image analysis software. Since it was not possible to analyze cross-sections from the entire channel under the optical microscope (operating in bright field mode), selected areas were chosen for the study. Each image was divided into 500 × 200 sub-regions. Figure 3 exemplifies the images analyzed, in this example, cross-sections at screw turns 10 and 30, when the screw rotated at 60 rpm. For the melting zone, the correct fraction of solids present in each image was taken into account when calculating the Shannon entropy.

4. Generate numerical predictions. Since at the beginning of the melting zone the average particle size was measured as 8.9 μm and 7.5 μm, for screw speeds of 20 rpm and 60 rpm, respectively, these values were taken as input for the computational predictions.

5. Compare the experimental results with the corresponding numerical predictions.

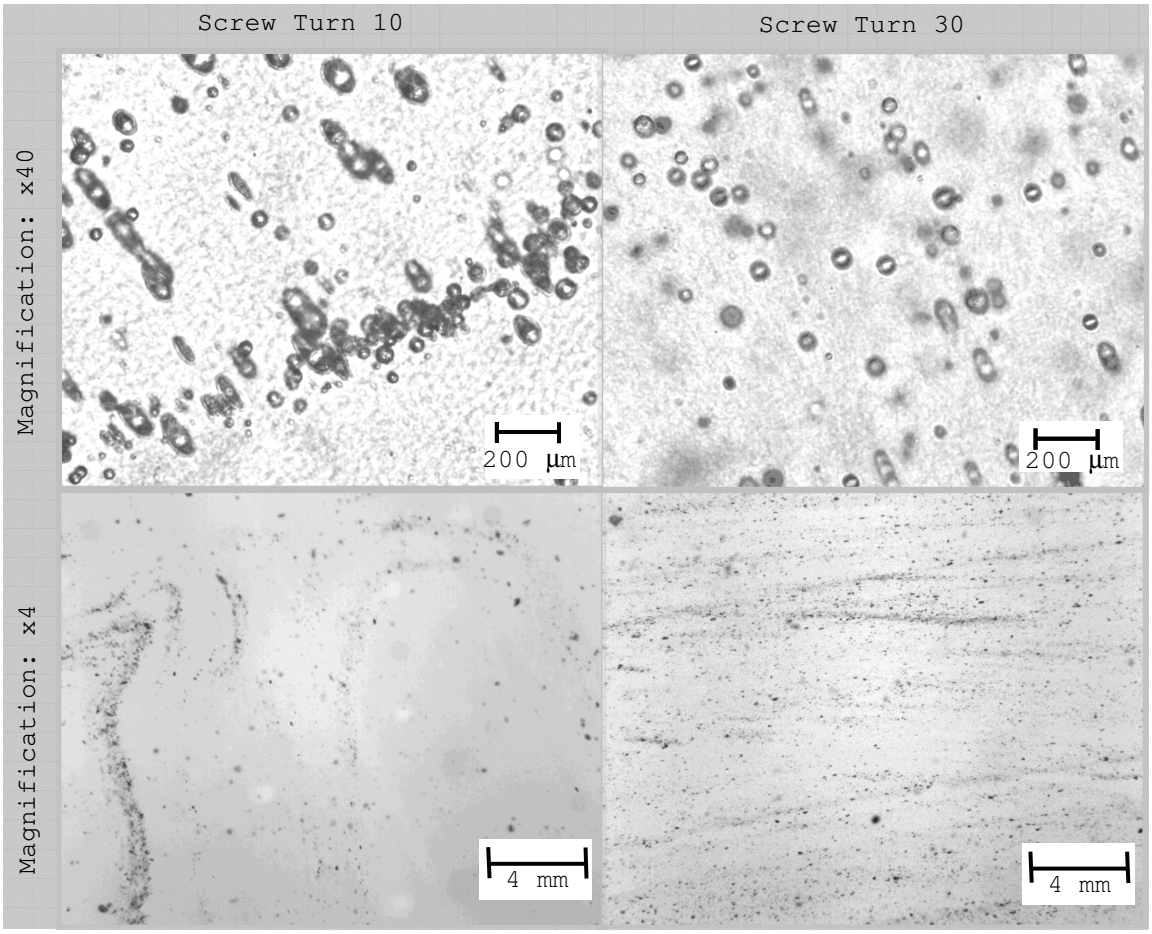

Figure 3: Material cross-sections at the beginning (left) and end (right) of the melting zone (screw speed of 60 rpm).

There are several potential sources of error associated with the methodology described above, some deserving a specific comment:

a. Due to the low thermal diffusivity of polymers, when carrying out Maddock-type experiments, instantaneous freezing of the polymer helix surrounding the screw was not possible. It has been shown that in the case of multiphase systems this may have consequences in terms of preserving the morphology (Domingues et al. 2009b). In this case, the solid particles suspended in the melt could change their positions or even re-aggregate before the solidification of the helix.

b. As discussed above, identifying for each cross-section the number of particles and their sizes requires a number of frame analyses by optical microscopy. Potential overlapping or, conversely, lack of analysis of some areas is possible.

c. As Figure 3 (top left) clearly shows, there is a size distribution associated to the solid particles suspended in the melt at the beginning of the melting zone. This is ignored in the computer implementation. Instead an average value is assumed as input.

d. The properties of the solid particles were taken from the literature, since data is very scarce and difficult to generate (Alemaskin et al., 2003). Thus, not only the average cohesive strength, but also the limiting values for the fragmentation number defining the dispersion mechanisms are most likely material/system dependent and therefore the numbers used in the simulation might not necessarily be accurate.

As shown in Figure 4a, the average agglomerate size reduces along the screw. Figure 4b presents the results for particle size distribution at the extruder outlet. Dispersion involves mostly rupture of the initial agglomerates into fragments, total dispersion (i.e., obtaining primary particles) being rarely achieved. Melting/compression play an important role in the dispersion process, the rate of dispersion decreasing along the screw, until a plateau seems to be reached. Dispersion levels increase with screw speed. Shannon entropy increases along the extruder and with screw speed.

Figure 5 discriminates between the size reductions taking place in the melting and melt conveying zones. Most of the dispersion occurs in the melting zone, most likely due to the development of a melt film being sheared between the inner barrel wall and the solid bed.

Figures 6 and 7 compare the particle sizes and Shannon entropy along the screw and at the exit from the extruder measured experimentally and predicted computationally. The calculations were performed considering that the average cohesive strength could range between 1 and 3 kPa - Figure 6, or that the limiting values of the fragmentation number, *Fa* (denoted as α and β) could change between 2 and 6 for α and between 5 and 9 for β – see Figure 7. As explained above, the presence of solid particles suspended in the melt was assumed from screw turn number 10 onwards, the insertion rate of new agglomerates matching the melting rate. The model shows sensitivity to changes in the filler characteristics. As expected, when the cohesive strength increases, there is little change in the dispersion rate, but the final levels of dispersion reached are lower. More initial agglomerates survive and less primary particles are obtained, regardless of the screw speed. Changes in the lower threshold value (α) of the fragmentation number causes variations of the same order of magnitude as those generated by the cohesive strength. As expected, higher α values hinder dispersion (Figure 7), whereas β does not seem to affect the predictions (not shown in the Figure 7).

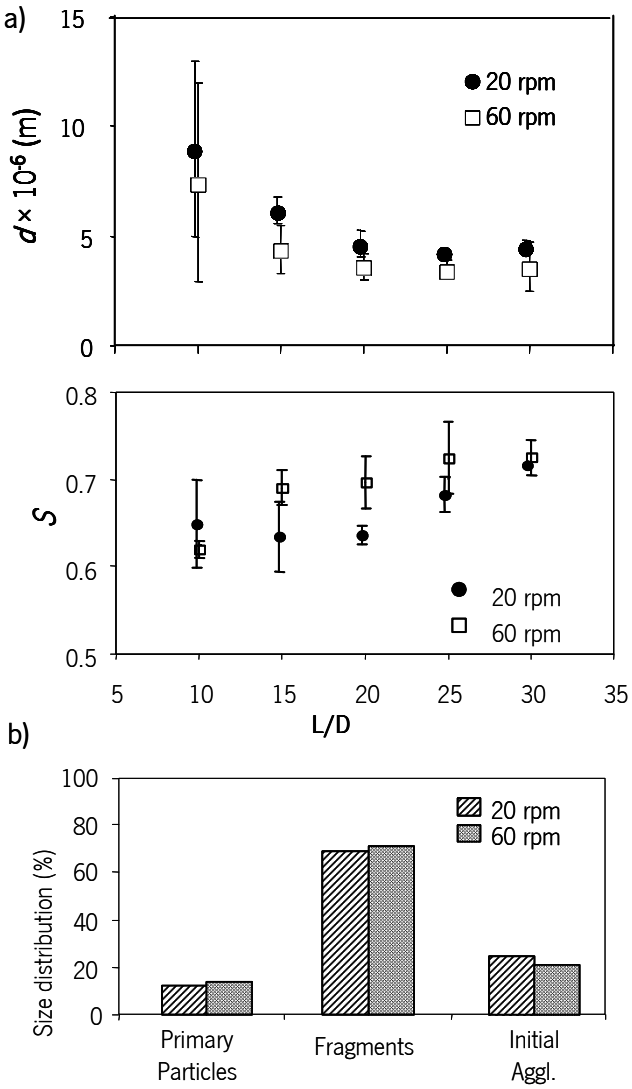

Figure 4: Experimental results for two screw speeds (20 and 60 rpm): **a)** evolution of the number of initial agglomerates and Shannon entropy along the channel; **b)** particle size distribution at the outlet – **Note:** "fragments" comprise a distribution of sizes on the scale of half the size of the initial fragments.

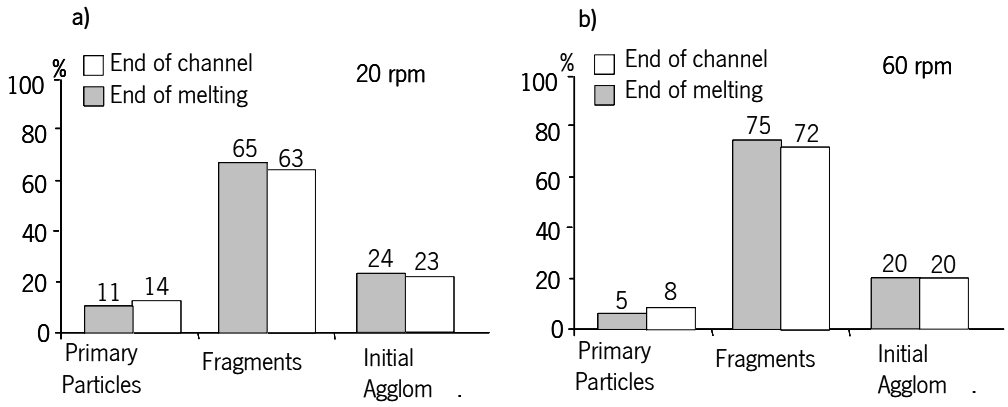

Figure 5: Effect of screw speed on the scale of particle sizes at the end of the melting zone and at the end of the channel.

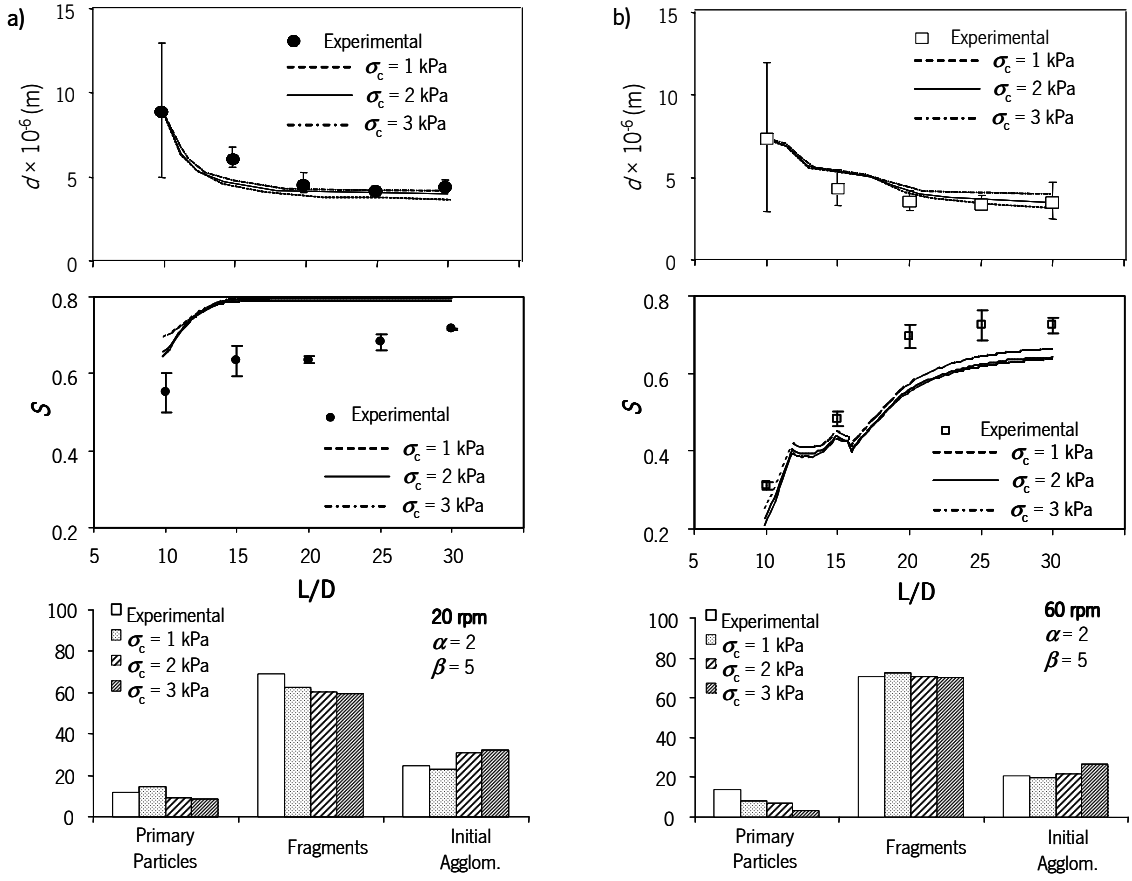

Figure 6: Experimental and numerical data for the evolution of particle size and Shannon entropy, for different values of cohesive strength; a) screw rotating at 20 rpm and b) screw rotating at 60 rpm.

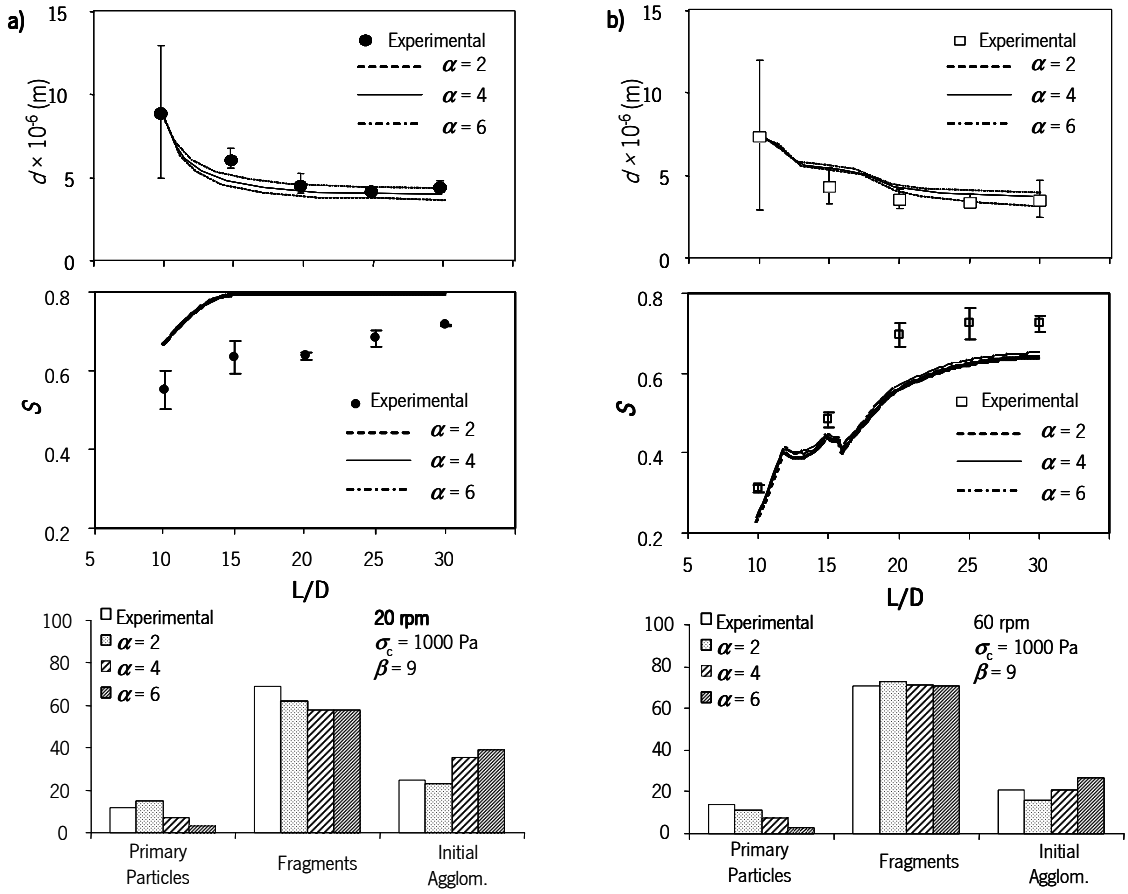

Figure 7: Experimental and numerical data for the evolution of particle size and Shannon entropy, for different limiting values α and β of the fragmentation number; a) screw rotating at 20 rpm and b) screw rotating at 60 rpm.

Although the limited experimental data used in this study do not render a formal validation of the predictions, there seems to be a good qualitative agreement between experimental and computational results. The best fit seems to be obtained for an average cohesive strength of 2 kPa and for the lower limit of the fragmentation number allowing dispersion, α = 4 and the upper limit delineating a change of mechanism from erosion to rupture β = 9. Differences in terms of particle size along the extruder are higher in the melting zone, which is not surprising given the associated potential sources of error of the software/model, particularly:

i. the modeling software may not be sufficiently able to describe accurately the melting sequence;

ii. the methodology for the progressive insertion of agglomerates in the melt may be far-off from reality;

iii. the melt and melt-filled rheologies are not accurately described.

As for the distributive mixing assessment, qualitative agreement and the correct effect of screw speed on the normalized Shannon entropy are obtained. The numerical curves are somewhat shifted in relation to the experimental data, which may indicate that the initial assumption of uniform distribution of the agglomerates in the newly formed melt pool at turn number 10 of the extruder might be an oversimplification.

5.2 Effect of material and process parameters

This section investigates whether the numerical simulation proposed above is sensitive to the effects of material properties, operating conditions and screw geometry on the dispersion of solid agglomerates in polymeric melts in a single screw extruder, and whether the predictions seem to bear the correct physical meaning.

The following reference values were used for the simulations: screw speed of 150 rpm, constant flat barrel temperature of 200 °C, insertion of a total of 10 125 agglomerates with a cohesive strength of 1000 Pa at the same rate as the melting rate (this is equivalent to a total concentration of around 1.2% in the polymeric matrix). The agglomerates have a diameter of 10 μm, and comprise 10 000 primary particles, each with a diameter of 0.25 μm.

Material Properties

Melt Viscosity

In order to assess the effect of viscosity on dispersion, computations were performed for the HDPE characterized in Table 2, and for a less viscous version (denoted as HDPE-*l*), with the following Carreau-Yasuda parameters: η_o = 3041.48 Pa.s, E/R = 4023.29 K, $\hat{\lambda}$ = 0.17 s, a = 1.82, n = 0.35, T_o = 533.15 K. Figure 8a shows the shear viscosity curves at 190°C for both materials.

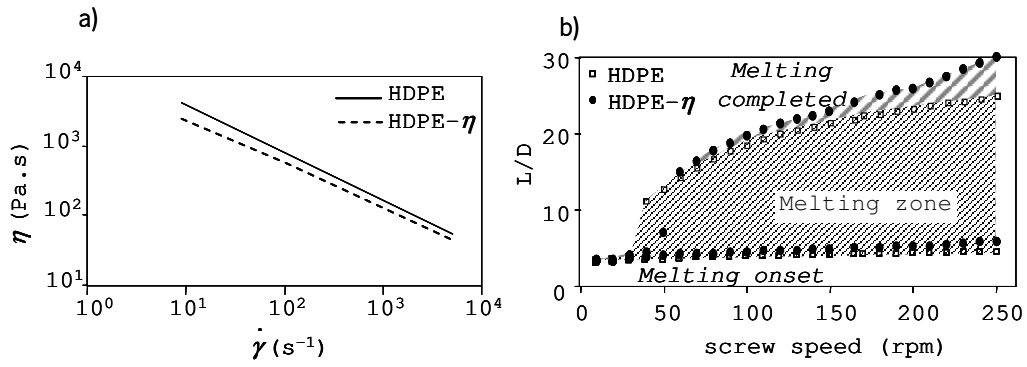

Figure 8: **a)** Viscosity curves of HDPE (Table 2) and modified version (HDPE-η); **b)** Melting behavior of these materials as a function of screw speed.

As expected and shown in Table 3, the higher viscosity system generates higher values of the average hydrodynamic stresses, as well as slightly higher residence times of molten material in the extruder, which in turn provides for better dispersive and distributive mixing. This results directly from the relative melting efficiency, as depicted in Figure 8b, which shows the calculated effect of screw speed on melting onset and completion: the higher polymer melt viscosity system shows an earlier melting onset and an earlier melting completion in the screw (given that all other properties were maintained constant), with the magnitude of the effect increasing with screw speed. Consequently, the higher polymer melt viscosity system should enhance dispersion and distribution of the solid phase, as depicted in Figure 9. Figure 9a shows that the average particle size increases downstream, which may be unexpected. In fact, this results from a balance of two conflicting processes developing as melting proceeds:

i. the progressive dispersion of particles suspended in the melt, versus

ii. the insertion in the newly formed melt of particles with the original size.

If the rate of the latter is higher than the dispersion, the above referred increase is observed.

Table 3: Influence of melt viscosity on the average hydrodynamic stresses and melt residence times (computational data)

Screw Speed (rpm)	Hydrodynamic Stresses (MPa)		Residence Time (s)	
	HDPE	HDPE-//	HDPE	HDPE-//
50	80.90	33.67	256	253
150	102.50	51.92	52	45
250	110.37	84.38	22	10

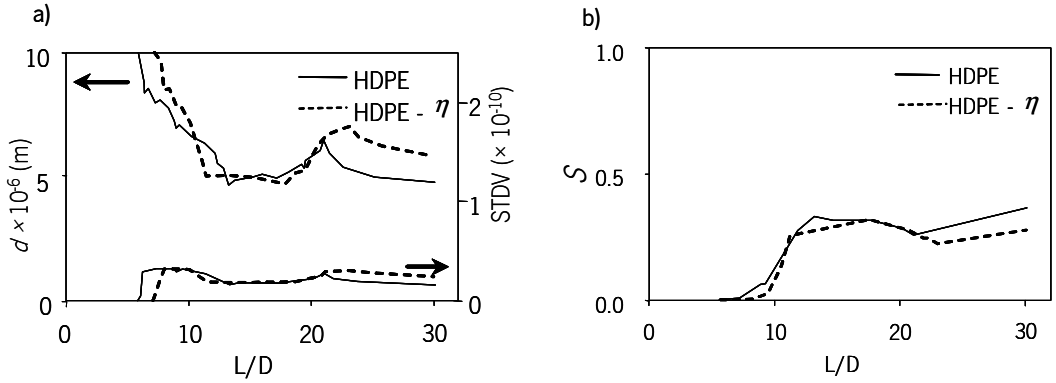

Figure 9: Effect of polymer melt viscosity on the evolution along the screw of: **a)** average particle size (*d*) and standard deviation (STDV) and **b)** Shannon entropy.

Cohesive Strength of the Dispersed Phase

As discussed above (Figure 8), for the HDPE and extruder geometry selected for this work, the numerical simulations predict that when the cohesive strength increases, the dispersion rate is hardly affected, but the final levels of dispersion are lower.

Operating Conditions

Screw Speed

As shown in Table 3 for HDPE, the residence time for mixing (total residence time minus the residence corresponding to solids conveying where no mixing takes place) decreases steadily with increasing screw speed from 50 to 150 rpm. Consequently, the length of screw required for melting increases (see also Figure 10b, for HDPE) and in spite of the higher hydrodynamic forces associated with higher screw speeds, lower screw speeds favor both agglomerate dispersion and distribution (Figure 10). However, for rotational speeds below a certain limit, decreasing the rpm is no longer beneficial primarily due to diminished dispersion efficiency (see also Figure 4 for additional results at 20rpm).

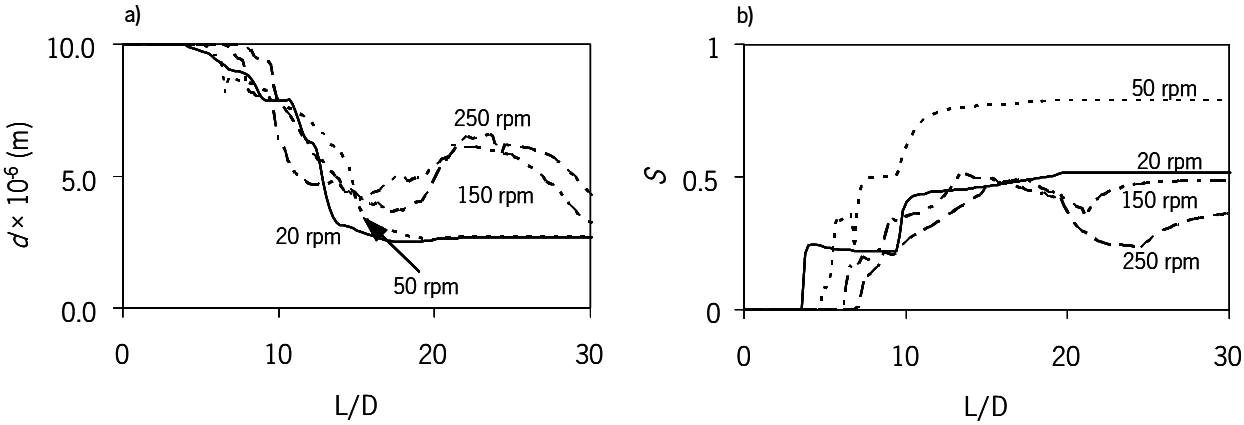

Figure 10: Effect of screw speed on **a)** agglomerates size and **b)** Shannon entropy.

Barrel Temperature

Increasing barrel temperature enables completion of melting earlier in the screw, i.e., offers higher residence times for mixing but, simultaneously, reduces the intensity of the hydrodynamic forces. As can be seen from the results represented in Figure 11, in the present case study, the global consequence of these two opposite effects is an increase of dispersion with increasing barrel set temperature.

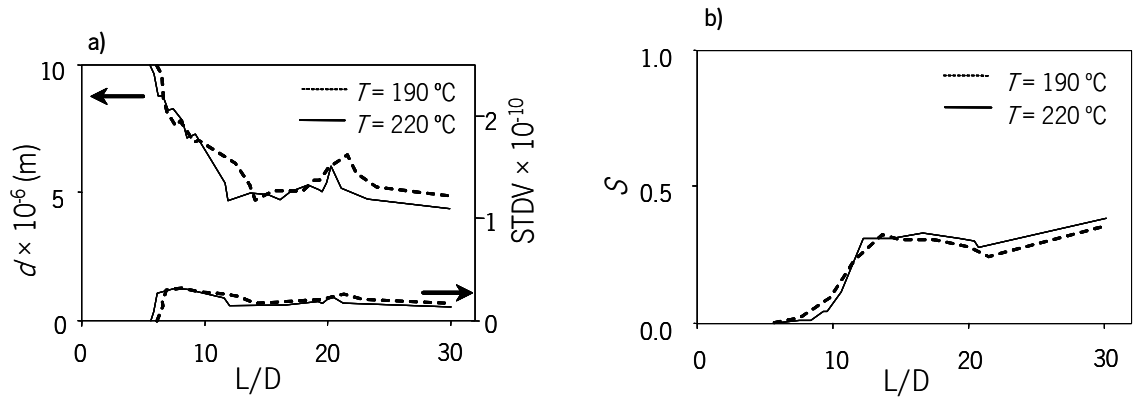

Figure 11: Effect of barrel temperature on the evolution along the screw of: **a)** average particle size (*d*) and standard deviation (STDV) and **b)** Shannon entropy.

Screw Geometry

Length of metering zone

Screws A and B in Table 1 differ in terms of the length of their metering zone - screw B has a longer metering zone. Therefore, the overall residence time is higher for screw B (together with a slightly lower output), resulting in higher agglomerate dispersion, as observed in Figure 12a. Shannon entropy increases steadily along the metering zone, therefore, the longer the screw, the higher the entropy (Figure 12b).

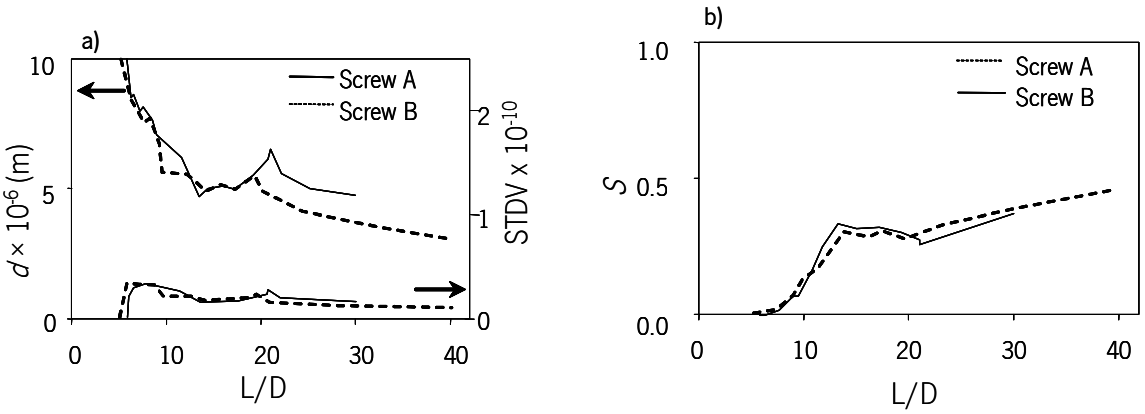

Figure 12: Effect of the length of the metering zone on the evolution along the screw of: **a)** average particle size (*d*) and standard deviation (STDV) and **b)** Shannon entropy.

Compression Ratio

Screws A and C in Table 1 differ in terms of their compression ratio (CR), as they have distinct channel depths in the metering section. Since higher compression ratios enhance melting efficiency, these bring about higher residence times for melt flow and higher average shear rates, but lower mass output, as presented in Table 4. Consequently, it is not surprising that numerical simulations show that both that dispersion and Shannon entropy increase significantly with increasing CR, as demonstrated in Figure 13.

Table 4: Influence of compression ratio on residence time, average shear rate and mass output.

Screw Speed	Residence Time		Shear Rate		Mass Output	
(rpm)	(s)		(s^{-1})		(Kg/h)	
	Screw A	Screw C	Screw A	Screw C	Screw A	Screw C
50	256	285	56	80	5.35	3.92
150	52	73	200	255	17.54	12.18
250	22	39	411	442	32.59	20.78

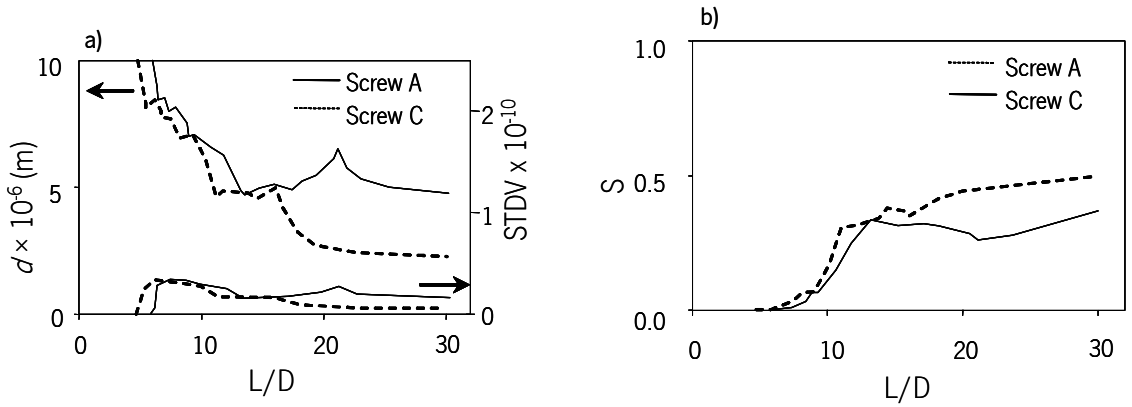

Figure 13: Effect of compression ratio on the evolution along the screw of: **a)** average particle size (*d*) and standard deviation (STDV) and **b)** Shannon entropy.

6 Conclusions

This work presents a model of agglomerate dispersion and distribution along a single screw extruder from the onset of melting to the exit from the extruder taking into consideration relevant material properties of the polymer and of the agglomerates, as well as the extruder/die geometry and the operating conditions. This involved coupling a description of flow and heat transfer in a plasticating extruder with a model for agglomerate break-up. Dispersion levels can be readily characterized via average particle sizes, whereas the spatial distribution of the particles (distributive component) can be evaluated via the Shannon entropy.

Results of a limited number of experiments provided good guidance to the computational modeling. Using this methodology to investigate (computationally) the effect of material properties (melt viscosity, agglomerate cohesive strength), operating conditions (screw speed, barrel temperature) and screw geometry (length of metering zone, compression ratio) on agglomerate dispersion and distribution evidenced that the observed behavior is primarily affected by the residence time available for melt flow and the intensity of the hydrodynamic stresses developed in the system. These effects however might be influenced in opposite ways by the various design and processing conditions.

References

Alemaskin, K., Manas-Zloczower, I., Kaufman, M., "Index for simultaneous dispersive and distributive mixing characterization in processing equipment", International Polymer Processing, **19**, 327-334 (2004)

Boyle, J., Manas-Zloczower, I., Feke, D.L., "Influence of Powder Morphology and Flow Conditions on the Dispersion Behavior of Fumed Silica in Silicone Polymers", Particle and Particle Systems Characterization, **21**, 205-212, (2004).

Camesasca, M., Manas-Zloczower, I., Kaufman, M., "Influence of the Extruder Geometry on Laminar Mixing: Entropic Analysis", Plastics, Rubber & Composites: Macromolecular Engineering, **33**(9/10), 372-376 (2004)

Camesasca, M., Kaufman, M., Manas-Zloczower, I., "Quantifying Fluid Mixing with Shannon Entropy", Macromolecular Theory and Simulations, **15**, p. 595-607 (2006)

Domingues, N., Camesasca, M., Kaufman, M., Manas-Zloczower, I., Gaspar-Cunha, C., Covas, J.A., "Modeling Agglomerate Dispersion in Single Screw Extruders, SPE ANTEC Tech. Papers, p. 942-946 (2006)

Domingues, N., Camesasca, M., Kaufman, M., Manas-Zloczower, I., Gaspar-Cunha, A., Covas, J.A., "Modelling Agglomerate Dispersion in Single Screw Extruders", Int. Polym. Process., In press (2009)

Domingues, N., Gaspar-Cunha, A., Covas, J.A., "Morphology Analysis of Liquid-Liquid Systems in Single Screw Extruders", Polym. Eng. Sci., In press (2009b)

Elbirli, B., Lindt, J.T., Gottgetreu, S.R., Baba, S.M., "Mathematical Modelling of Melting of Polymers in a Single-Screw Extruder", Polym. Eng. Sci., **24**, pp. 988- 999 (1984)

Fenner, R.T., Principles of Polymer Processing, McMillan, London (1979)

Gaspar-Cunha, A., Covas, J.A., "The Design of Extrusion Screws: an Optimization Approach", Int. Polym. Process., **16**, pp. 229-240 (2001)

Khinchin, A.I., Mathematical Foundations of Information Theory, Dover, New York (1957)

Rauwendaal, C., Polymer Extrusion, Hanser Publishers, Munich (1986)

Rauwendaal, C., "Scale-up of Single Screw Extruders", Polym. Eng. Sci., **27**, pp. 1059-1068 (1987)

Roscoe, R., "The Viscosity of Suspensions of Rigid Spheres", British J. of Appl. Physics, **3**, pp. 267-269 (1952)

Rwei, S.P., Manas-Zloczower, I., Feke, D.L., "Observation of Carbon Black Agglomerate Dispersion in Simple Shear Flows", Polym. Eng. Sci., **30**, pp. 701-706 (1990)

Shannon, C.E., Weaver, W., The Mathematical Theory of Communication, Urbana, University of Illinois Press (1948)

Scurati, A., Feke, D.L., Manas-Zloczower, I., "Analysis of the Kinetics of Agglomerate Erosion in Simples Shear Flows", Chem. Eng. Sci., **60**, p. 6564-6573 (2005)

Tadmor, Z., Klein, I., Engineering Principles of Plasticating Extrusion, Van Nostrand Reinhold, New York (1970)

Wang, W., Manas-Zloczower, I., "Temporal Distributions: A New Tool for the development of Mixing Indices for Scale-up of Polymer Processing Equipment", Polym. Eng. Sci., **41**, 1068-1077 (2001)

V

A Quantitative Approach to Assess the Mixing Ability of Single Screw Extruders for Polymer Extrusion [4]

[4] Article submitted at Journal of Polymer Engineering
Authores: N. Domingues, A. Gaspar-Cunha, J. A. Covas

1 Introduction

Single-screw extruders are extensively used in polymer extrusion and as plasticating units in other technologies, such as injection molding and blow molding. In extrusion, the screw rotates at a fixed speed inside a heated barrel and conveys, melts, mixes, pressurizes and pumps the polymeric compound through a shaping die. The compound may include a polymer or a polymer blend and a number of additives, such as colorants, stabilizers, lubricants, fillers, etc. Thus, mixing, *i.e.*, the reduction of spatial composition non-uniformity, is an important process prerequisite. From a design point of view, mixing in screw extruders can be enhanced by the insertion of periodic obstacles in the channel, such as pins, barriers and vanes, which cause repeated flow reorientation and/or increased hydrodynamic forces [1]. Design concepts attempting to improve mixing via chaotic flow have also been proposed [2]. The mixing performance levels that can be currently attained in single screw extrusion make this technology viable for several compounding operations [3], rather than exclusively for processing.

The reduction of composition non-uniformity can be achieved through two routes. The spatial arrangement of the formulation components can be improved by imposing a certain shear deformation history, this being known as distributive mixing. The extent of mixing depends on the interfacial area generated, which is proportional to the applied strain, as shown by Spencer and Wiley [4]. It is well known that in single screw extruders individual fluid particles experience different shear rate histories during distinct residence times, *i.e.*, they attain total different strains. Accordingly, Pinto and Tadmor [5] computed the degree of distributive mixing during melt conveying using a weighted-average total strain (WATS), assuming isothermal Newtonian flow between parallel plates. Bigg *et al.* [6, 7] extended this analysis to a two-dimensional non-Newtonian isothermal flow and predicted residence times and strain distributions. Composition uniformity can also be improved by decreasing the size of at least one of the components of the formulation (*i.e.*, droplets of the minor phase for an immiscible polymer blend, solid agglomerates in the case of a filled system). Particles are progressively broken down (or de-agglomerate) by the hydrodynamic stress levels generated if a certain stress threshold is attained over a certain time [8]. Simultaneously, droplets may collide with each other and coalesce into larger drops, which may in turn break again. The breakup and coalescence processes compete against each other and it is the overall result of this competition that determines the final drop size distribution [9, 10]. DeRussel *et al.* [11] suggested strategies to calculate local variations in drop size distribution due to changes in material and process parameters, to be used in conjunction with a fluid mechanics flow model.

Consequently, the complete description of the state of a given mixture in a single screw extruder requires the identification of the size, shape, orientation, and spatial location of every particle or droplet of the minor component along the flow channel. This is very difficult to obtain, a qualitative or semi qualitative estimation being often searched instead [12]. From an experimental point of view, the evolution of mixing in a single screw extruder is usually investigated by performing Maddock-type experiments where steady-state operation is halted and the screw is extracted from the barrel, representative material samples being then obtained from known locations on the helical channel. Subsequently, concentrations of the minor component (or tracer) are measured and the mixing levels are generally characterized in terms of normalized variances of the concentration [12-15]. More recently, Wong and Lam [16] obtained similar data from dynamic measurements using an extruder fitted with glass windows, while Amin *et al.* [17] used Magnetic Resonance Imaging to follow *in situ* the mixing of two streams of 1% aqueous sodium carboxymethylcellulose with different MnCl2 concentrations. According to Benkreira *et al.* [18] mixing in a conventional screw primarily occurs during the melting phase and improves little thereafter. Numerical simulations provide an opportunity to study the mechanisms of flow and mixing in the extruder without the need to perform experiments. Wang *et al.* [19] reviewed the work devoted to assess the mixing efficiency of screws with different mixing devices, whereas Heniche and Tanguy [20] analyzed the efforts to model chaotic single phase viscous mixing.

The evaluation of the global degree of mixing of a polymer system processed under specific conditions has great practical significance, as it would be very useful for scaling, comparison and optimization purposes. Wang *et al.* [19] and Connely and Kokini [21] reviewed the approaches previously adopted by various research groups, that ranged from the classical intensity of segregation, scale of segregation and striation thickness, to the use of residence time distributions, the utilization of the length stretch or stretch rate of the interface, the computation of a cluster distribution index, the tracking of the motion of passive tracers, the construction of Poincaré sections and the use of Lyapunov exponents [22], or the development of mapping methods (where the flow is divided into a large number of sub-domains, whose boundaries are tracked for a given period of time or space [23]). Manas-Zloczower and co-workers [24] explored the idea of using Renyi entropies to measure the degree of distributive mixing, a well-distributed multi-component system having a high entropy. Also, by means of the concept of Shannon entropy, the same team [25] defined an index of color homogeneity to study the mixing of two colored particle populations along the metering section of a conventional single screw extruder. A particle tracking technique was employed to describe the actual dynamics of the mixing process.

The present work builds on the above ideas to compute general mixing indices quantifying the degree of distributive and dispersive mixing in liquid-liquid and solids-liquid systems in single screw extruders. They can be obtained by coupling a description of the flow in the screw from hopper to die to models of morphology evolution (which compute the dimensions of the dispersed phase, taking into account stretching, break-up and coalescence phenomena) or of agglomerate dispersion [26-28], and compare the characteristics of the morphology at the location of interest with the initial morphology. The aim is to provide a simple tool readily available to, *e.g.*, directly assess the mixing ability of a given screw for a specific polymer system, to scale-up for mixing, or to predict the mixing performance of a set of different screws. In order to illustrate the usefulness of the work, the mixing indices are used to optimize the operating conditions and the screw geometry the yield the highest mixing efficiency.

2 Mixing Indices

Mixing of an additive with a molten polymeric matrix may involve dispersion and/or distribution phenomena, depending on the characteristics of the two components and on the level and duration of local shear and/or extensional stresses. Liquid-liquid and solids-liquid systems will be analyzed separately.

2.1 Liquid-Liquid System

The liquid-liquid system considered in this analysis consists of many single drops suspended in the melt. Upon flow, the local viscous forces deform each drop and, if they are sufficiently high and act during enough time, will force the drop to break into smaller droplets [29]. The event of drop break-up is defined by the value of the capillary number (*Ca*), which balances the relative intensity of the viscous forces (η_c is matrix viscosity, $\dot{\gamma}$ is shear rate and *r* is drop radius) with the interfacial tension (υ_{12}) acting across the interface between two immiscible liquids:

$$Ca = \frac{\eta_c \dot{\gamma} r}{\upsilon_{12}} \tag{1}$$

Break-up occurs when a critical capillary number is exceeded and acts during sufficient time (break-up time) [29, 30]. While υ_{12} can be determined experimentally using well defined methods, the break-up time also requires information on the dominant growth rate of interfacial disturbances, which may be estimated graphically [30]. In addition, the competing coalescence phenomenon must be taken in account when evaluating the resulting droplet size [30]. The morphological model as well as the algorithm to predict the

evolution of the morphology along the axis of a single screw extruder, from the onset of melting until the die outlet, have been presented in detail elsewhere [26]. The process modeling routine yields the location and length of solids conveying, melting and melt conveying, as well as down-channel velocity and temperature profiles. As melting develops, drops of a given size are inserted as uniformly distributed in the melt pool at the rate of melting. Therefore, if no changes in morphology would take place during melting, the amount of suspended drops in the melt would vary from zero at the melting onset to a number equivalent to the concentration of the minor phase as melting is completed. Changes in morphology will cause break up and/or coalescence of these drops. Thus, at any channel cross-section during melting, the system is tested for break up and coalescence and new drops are inserted. If both the capillary number and the break-up time are sufficiently high, the initial drop is replaced by two equal droplets and a third smaller drop. The coalescence probability is also tested locally; if higher than 0.5, larger drops are generated. Similar calculations are performed along the melt conveying zone, except that no new drops are inserted.

The degree of distributive mixing can be estimated using the concept of striation thickness (S) [1]. It has been shown that during the affine deformation of a droplet its width (B) decreases as S decreases [29]. In a simple shear flow, stretching of the drop proceeds slowly, its width decreasing in accordance with the following equation [29]:

$$B = \begin{cases} \left(1 + \frac{\gamma^2}{2} + \frac{\gamma}{2}\sqrt{4+\gamma^2}\right)^{-0.25} \cdot d & \text{if } \gamma < 5 \\ \gamma^{-0.5} \cdot d & \text{if } \gamma \geq 5 \end{cases} \tag{2}$$

where γ is shear deformation and d the initial drop diameter (which changes if the drop breaks). The size of the drops is weighted against the initial preset drop diameter (d_i). Since B/d_i represents the width reduction, the degree of distributive mixing (mix_{dist}) may be quantified by:

$$mix_{dist} = \frac{\sum_j^N \left[\left(\frac{d}{d_i}\right)_j \times \left(1 - \frac{B}{d_i}\right)_j\right]}{\sum_j^N \left(\frac{d}{d_i}\right)_j} \tag{3}$$

where $mix_{dist} \times 100\%$ is the percentage of width reduction, N is the total number of drops in the system and $(d/d_i)_j$ is a weight factor related to the drop dimension (in any given cross-section under examination bigger drops occupy more area, hence this fact should be considered when computing the average).

Similarly, the degree of dispersive mixing (mix_{disp}) can be quantified via the following equation:

$$mix_{disp} = \frac{\sum_{j}^{N}\left[\left(\frac{d}{d_i}\right)_j \times \left(1-\frac{d}{d_i}\right)_j\right]}{\sum_{j}^{N}\left(\frac{d}{d_i}\right)_j} \quad (4)$$

where d is the drop diameter after break-up. Since d/d_i represents the reduction in drop size, $mix_{disp} \times 100\%$ will be the percentage of average drop size reduction.

2.2 Solids-liquid System

The dispersive model followed here has been presented and validated in separate reports [27, 28]. Particle break-down arises when the maximum hydrodynamic shear stress (σ_H) the agglomerate is subjected to is higher than its cohesive strength (σ_c) [33].

$$F_a = \frac{\sigma_H}{\sigma_C} \quad (5)$$

The cohesive strength represents the mechanical resistance of an agglomerate to the external forces, which in turn depends on the number of bonds that must be severed to cause detachment of a fragment [33]. Scurati *et al.* [33] developed an experimental methodology using an oscillatory shear device to estimate the σ_c of compacts of precipitated silica powder suspended in Poly(dimethy l siloxane) of different viscosities. The authors also showed that depending on the relative magnitude of F_a (known as fragmentation number), different dispersion mechanisms may develop. As F_a increases progressively above 1, no dispersion, erosion and rupture will become gradually predominant [33]. However, even for high F_a, there is a finite probability associated to break-up, that can be defined as [27]:

$$P_{break} = \lambda \, \Delta t \quad (6)$$

where λ is proportional to the fractional change in the agglomerate surface area and Δt is the time interval. Their values should be chosen so that $\lambda\Delta << 1$. The probability of agglomerate dispersion increases with increasing flow time.

Distributive mixing can be measured using an entropic measure, such as the Shannon entropy [24]. Dividing the system in M equal sub-regions (denoted here as bins), Shannon entropy can be calculated from [31, 32]:

$$S = -\sum_{j=1}^{M} p_j \log p_j \quad (7)$$

where p_j is the probability of finding a particle in bin j. Shannon entropy is maximized (S_{max}) when the probability of finding a particle in each bin is the same, *i.e.*, $p_j = 1/M$ and is nil when all particles are located in a single bin [27]. Dividing S by $S_{max} = \log(M)$, a normalized Shannon entropy can be defined and used as a distributive mixing index:

$$mix_{dist} = \frac{-\sum_{j=1}^{M} p_j \log p_j}{\log(M)} \tag{8}$$

The global degree of dispersive mixing can be estimated from equation 4, where d now represents the diameter of the solid agglomerate.

3 Computer Implementation

The mixing models presented above were incorporated into a 2D plasticating extrusion modeling software [27, 34]. The program computes pressure, velocity and temperature profiles along the screw channel for a given extruder geometry, operating conditions and material characteristics (these will be presented in the case study below). The following sequence of individual process steps is assumed and made coherent via appropriate boundary conditions:

a. *solids conveying* in the hopper due to gravity, an analytical equation yielding the vertical pressure gradient;

b. *friction drag solids conveying* in the initial screw turns, taking the solids as a plug and performing force and momentum balances to determine the pressure generation; the temperature rise both due to friction near to the screw and barrel walls and to conduction from the hot barrel is also taken into consideration;

c. *delay in melting*, corresponding to the development of a melt film, initially adjoining the barrel wall and later encapsulating the solid plug, as a result of the local dissipated and conducted heat;

d. *melting*, involving the evolution of 5 individual zones identifiable in a representative channel cross-section, namely a solid plug, a melt pool and melt films adjacent to the barrel, the screw root and the screw trailing flight; the model developed by Elbirli *et al.* [35] was applied to compute the pressure, velocity, temperature and solid bed width progression along the extruder, for the non-isothermal flow of a non-Newtonian fluid;

e. *melt conveying*, described as a 2D non-isothermal flow of a non-Newtonian fluid.

Figures 1 and 2 show the flowcharts for assessing mixing for the liquid-liquid and solids-liquid systems, respectively. In the first case, the sequence of steps is the following:

i. Determine pressure, velocity and temperature profiles in the down-channel direction, once the various individual process steps are detected;

ii. Select a channel cross-channel upstream and apply a fine mesh;

iii. Compute the local viscous forces and compare the maximum with the interfacial tension of the minor component. If they are high enough, the time for break up is computed;

iv. The local residence time is determined. If this is higher than the break-up time, rupture occurs and the drop is replaced by smaller ones;

v. Test for coalescence probability. If it is likely, set the new drop dimensions;

vi. If the drop does not break nor coalesce, calculate its new width;

vii. Repeat the calculations in the remaining fractions of the same channel cross-section;

viii. Evaluate the mixing indices for the channel cross-section under consideration;

ix. Repeat the above steps for a cross-section at a Δz increment in the down-channel direction, until reaching the outlet.

In the case of solids-liquid systems, the algorithm consists of:

i. Determine pressure, velocity and temperature profiles in the down-channel direction, once the various individual process steps are detected;

ii. Select a channel cross-channel upstream and apply a fine mesh;

iii. Apply a Monte Carlo scheme to determine a break-up probability, which is then compared to a random number in the interval [0, 1]; if it is higher than this random number, break up can occur;

iv. Even if rupture can potentially occur from the previous step, this will only come about if the hydrodynamic forces computed from the velocity profiles exceed sufficiently the agglomerate cohesive forces. The dispersion mode is identified;

v. The new particle dimensions are estimated.

vi. Repeat the calculations in the remaining fractions of the same channel cross-section;

vii. Evaluate the mixing indices for the channel cross-section under consideration;

viii. Repeat the above steps for a cross-section at a Δz increment in the down-channel direction, until reaching the outlet.

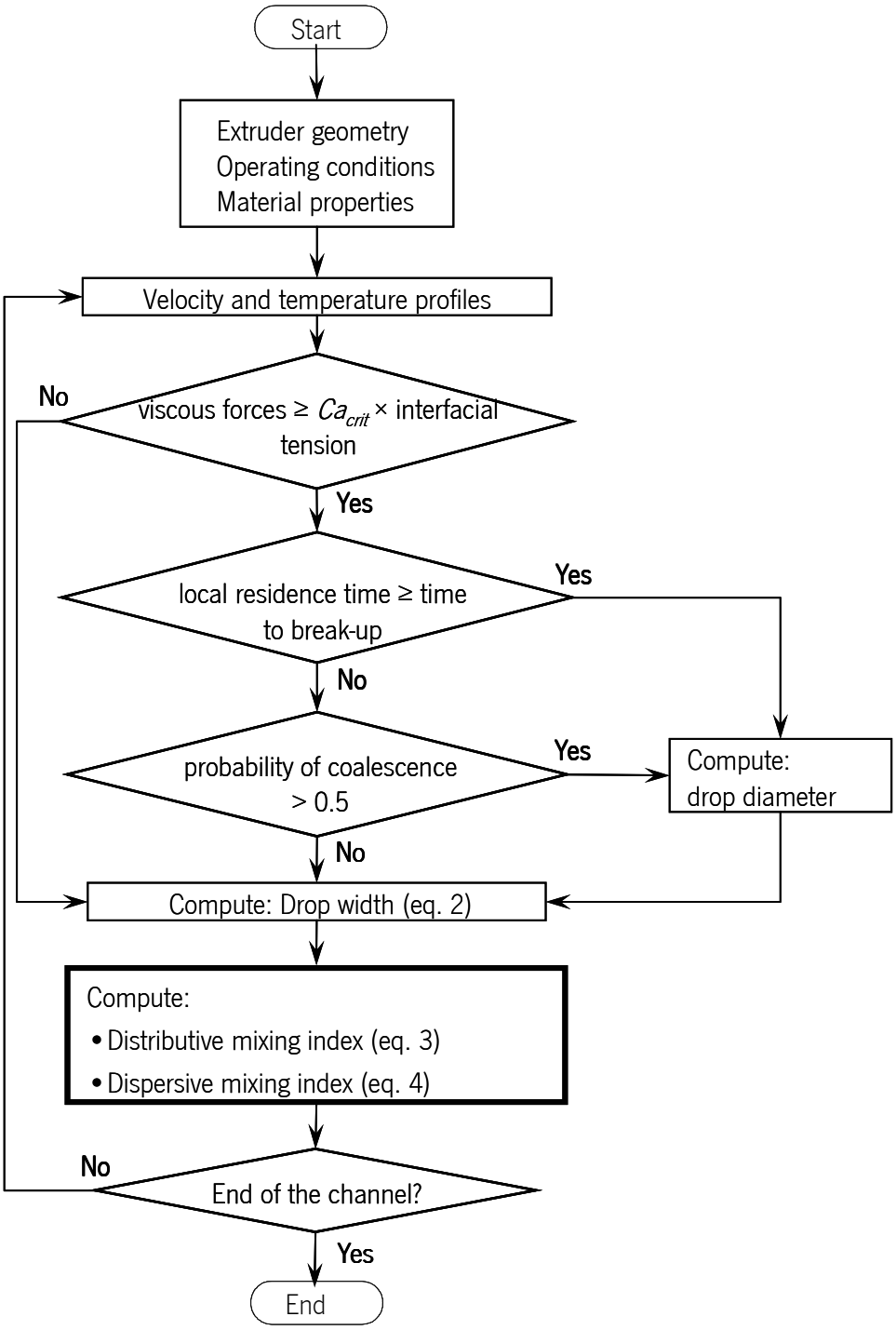

Figure 1: Flowchart for assessing mixing in liquid-liquid systems.

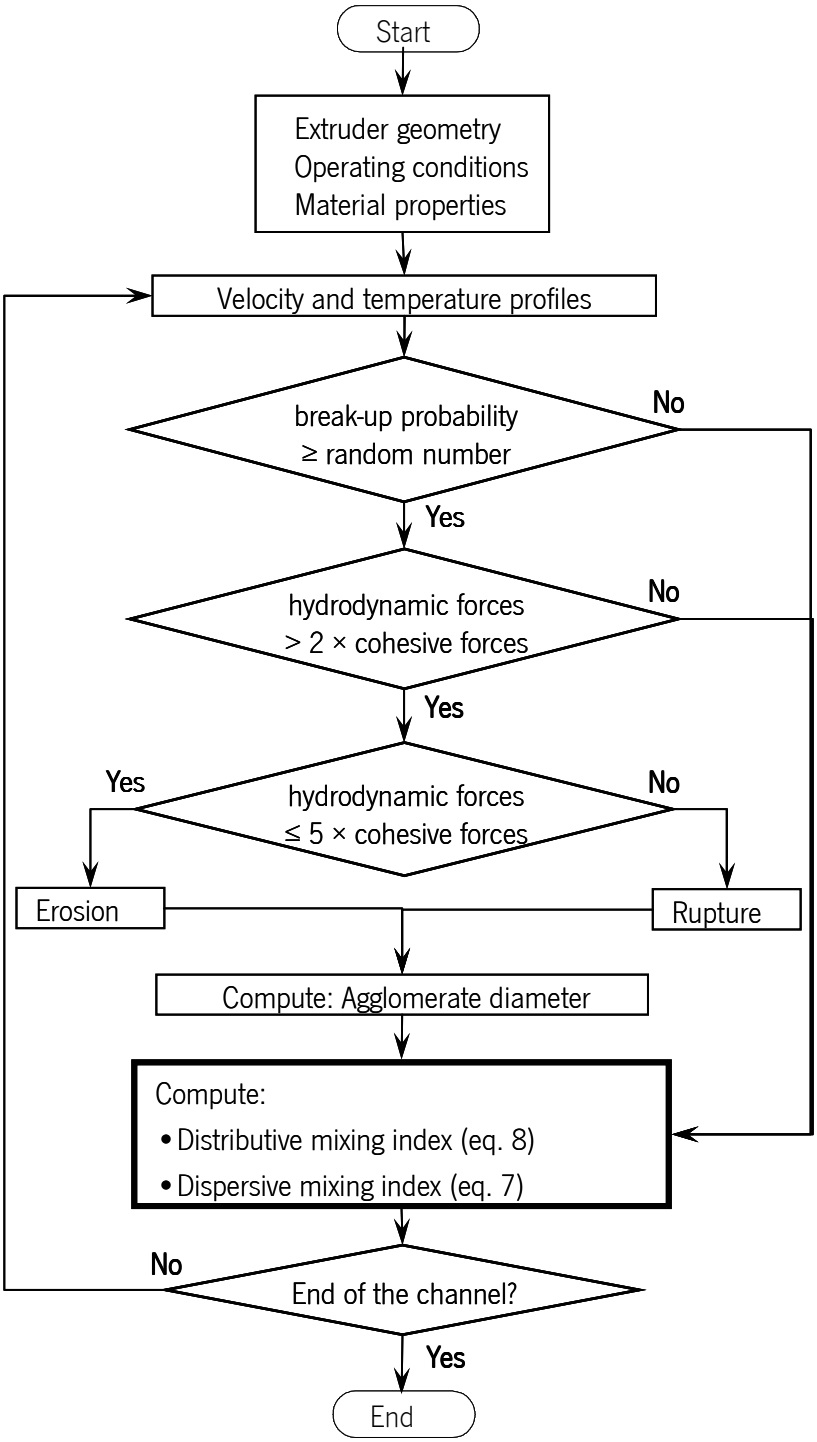

Figure 2: Flowchart for systems involving a solid-liquid system.

4 Results and Discussion

4.1 Case Studies

The results of a limited number of experiments performed with the two types of systems provided a good guidance to the computational modeling in terms of predicting the evolution of morphology or filler size [26-28]. Therefore, rather than focusing on a specific polymer system, this section sets a few computational case studies with the aim of providing a broader evaluation of the sensitivity of the mixing indices to changes in polymer properties, operating conditions and extruder (screw and die) geometry.

An HDPE (see identification and properties in Table 1) was selected as matrix for both the liquid-liquid and solids-liquid systems. The viscous flow properties were determined in a Rosand RH8 Dual Capillary Rheometer, considering both the Bagley and Rabinowistch corrections. From these, the Carreau-Yasuda equation parameters were obtained and are also presented in Table 1:

$$\eta = \eta_0 e^{\frac{E}{R}\left(\frac{1}{T}-\frac{1}{T_0}\right)}\left[1+\left[\lambda\dot{\gamma}\, e^{\frac{E}{R}\left(\frac{1}{T}-\frac{1}{T_0}\right)}\right]^a\right]^{\frac{n-1}{a}} \quad (9)$$

where η_0, E/R, λ, n and a are material constants and T_0 is the reference temperature. A Perkin Elmer DSC 7 was used to determine the specific heat, the melting heat and the melting temperature. The remaining properties were taken from the literature.

As a reference, it will be assumed that the liquid-liquid system has a viscosity ratio of 1 and an interfacial tension of 4.5 mN/m. Accordingly, as the polymer melts, a proportional number of drops of the second immiscible component with a radius of 10 μm (corresponding to a total concentration of 10% w/w) will be inserted as uniformly distributed in the freshly generated melt. In the case of the solids-liquid system, when the matrix melts, a proportional number of solid clusters of 100.000 particles, each with a diameter of 0.25 μm (corresponding to a total concentration of around 1.2%) and a cohesive strength of 1000 Pa will be inserted as uniformly distributed in the freshly generated melt.

Table 1: Properties of the HDPE selected.

			HDPE (ALCUDIA TR-135)	
Density	Solids	ρ_s	560.00	kg.m^{-3}
	Melt	ρ	854.40	
Thermal Conductivity	Solids	k_s	0.19	W.m^{-1}.°C^{-1}
	Melt	k_m	0.10	
Specific Heat	Solids	C_s	2600.00	J.kg^{-1}
	Melt	C_m	2000.00	
Melting	Heat	H	190.00x10^3	J.kg^{-1}
	Temperature	T_m	118.0	°C
Viscosity Carreau-Yasuda law		η_0	18000.00	Pa.s
		E/R	10000.00	K
		$\hat{\lambda}$	0.70	s
		a	1.70	
		n	0.30	
		T_0	463.15	K

Table 2 presents the various screw configurations tested. Screws A and B differ in terms of the length of the metering section, while screws A and C have different compression ratios. Screws C and D have the same compression ratio, but differ in the internal screw diameter (equivalent to channel depth) at the feeding and metering sections. In each case study the computations were performed for screw speeds ranging between 10 rpm and 250 rpm, with increments of 10 rpm. As reference, a flat barrel/die temperature of 190 °C was used and the die had a circular channel with a diameter of 10 mm and a length of 135 mm.

Table 2: Geometry of the screws tested (L_1, L_2, L_3, lengths of the feed, compression and metering screw sections, respectively; D, screw diameter; D_1, D_2, internal diameter of the feed and metering zones, respectively)

Screw		A	B	C	D
Extruder Length (m)	L_1	0.3	0.3	0.3	0.3
	L_2	0.3	0.3	0.3	0.3
	L_3	0.3	**0.6**	0.3	0.3
Barrel Diameter (m)	D	0.030	0.030	0.030	0.030
	D_1	0.020	0.020	0.020	**0.016**
	D_2	0.026	0.026	**0.027**	0.026
Compression ratio		2.5	2.5	**3.5**	**3.5**

4.2 Evolution of Mixing along the Extruder

The evolution along the screw of the mixing indexes for two different screw speeds (50 rpm and 200 rpm) is shown in Figure 3. The significant contribution of the melting stage to the final mixing levels is obvious, which is in agreement with the observations of Benkreira *et al* [18]. This is not surprising, given the relatively high shearing levels developing in shallow melt conveying zones (*i.e.*, melt films and melt pool). As the screw speed increases, the melting zone occupies a greater screw fraction, thus further increasing its importance to mixing. Nevertheless, the Figure also shows that both distribution and dispersion continue along the melt conveying zone. Curiously, the relative magnitude of distribution and dispersion is inverted for the two material systems, as a result of their specific properties.

The relative instability of the curves in the melting stage, as well as the eventual decrease of the actual value of a given mixing index along the screw axis, is due to the insertion of new suspended material as the matrix melts. In fact, during melting the average size of the filler/droplets results from the balance between dispersion and number and size of the new entities injected in the system. Since these new entities are not deformed and are assumed as uniformly distributed in the melt, they also affect negatively the local distribution.

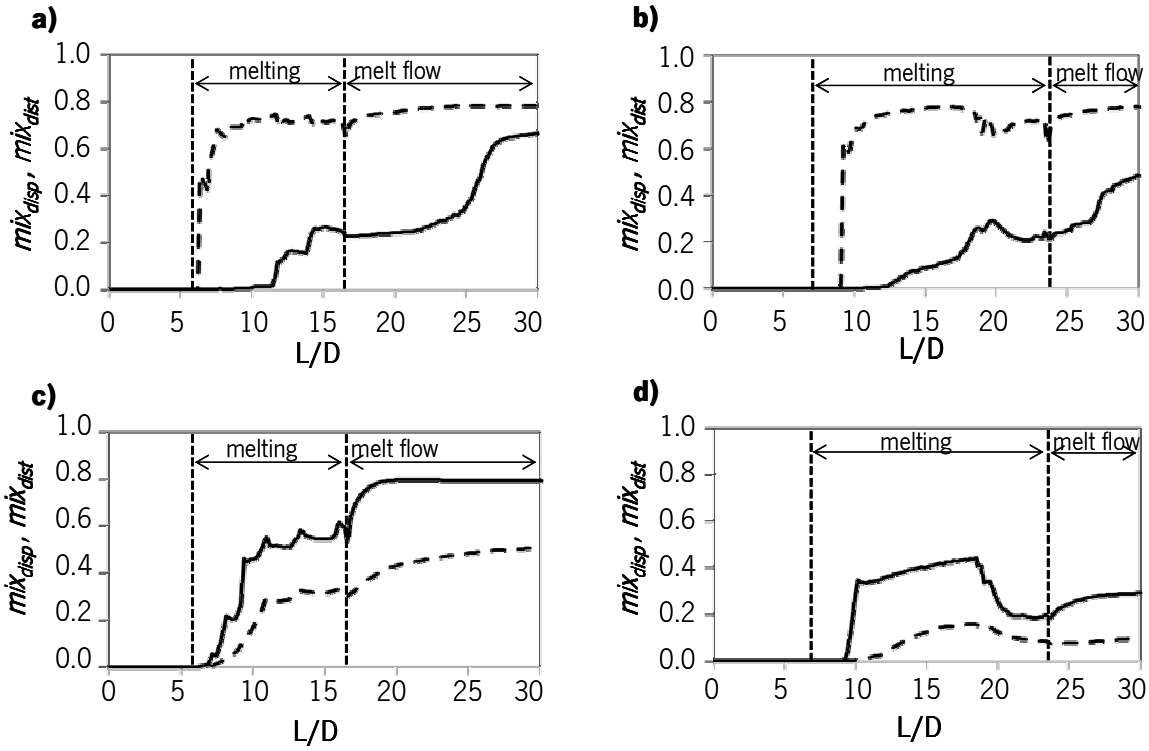

Figure 3: Evolution of the mixing indices along the extruder: **a)** liquid-liquid system, 50 rpm; **b)** liquid-liquid system, 200 rpm; **c)** solids-liquid system, 50 rpm; **c)** solids-liquid, 200 rpm (solid line: dispersive mixing; broken line: distributive mixing).

4.3 Effect of Material Properties

Interfacial Tension

Figure 4 shows the effect of the interfacial tension on the final level of mixing of the liquid-liquid system as a function of screw speed. Generally, lower interfacial tension causes lower dispersive mixing levels. Although a lower υ_{12} induces a higher capillary number (equation 1), it also requires higher times for break-up. In this case, the resulting balance is unfavorable to mixing. Increasing screw speeds reduce the residence time for mixing, further deteriorating mixing. Concurrently, distributive mixing is slightly favored for lower values of the interfacial tension at the higher screw speed range, since the corresponding higher hydrodynamic stresses together with less break-ups cause higher drop deformation.

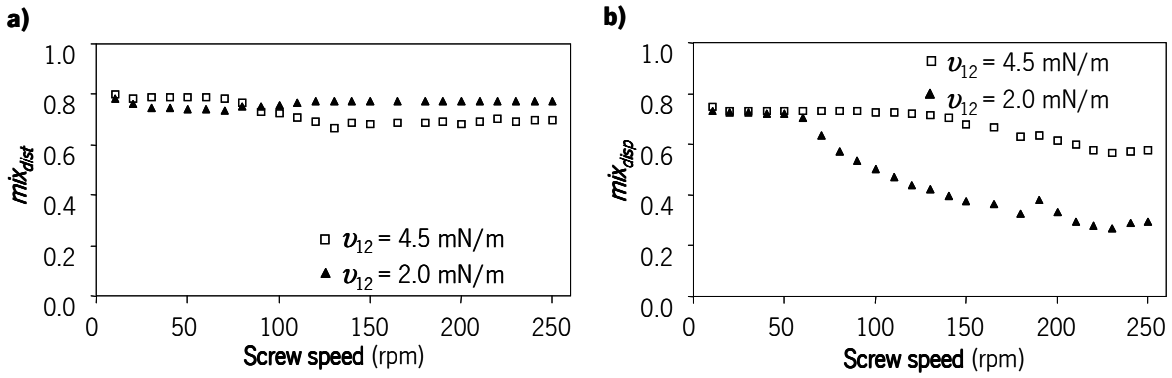

Figure 4: Effect of interfacial tension on the mixing of a liquid-liquid system: **a)** distributive and **b)** dispersive mixing indices.

Viscosity Ratio

The relative viscosity between the liquid additive and the matrix (viscosity ratio, p) is a major factor for dispersive mixing of liquid-liquid systems, as shown by Grace [37], who studied the deformation and break-up of single drops in shear and extensional flow fields. Grace postulated that droplets are stable when their capillary number is below a critical value, that they deform and break more easily when p ranges between 0.25 and 1 (in shear flow) and that break-up is again not possible when p is becomes larger than 4. For this reason, Figure 5 shows the effect on mixing when p equal to 10^{-4}, 10^{-2}, 1 and 4.

As expected, for values of the viscosity ratio in the limits of the range studied (10^{-4} and 4) lower dispersive mixing is attained. In particular, for p = 10^{-4} the viscous stresses required to cause drop break-up are extremely high. Actually, at low screw speeds coalescence is predicted. Upon decreasing p from 1 to 10^{-2} higher viscous hydrodynamic stresses are required for break-up, but at the same time the time for break-up decreases. As shown in the Figure, in this case dispersion is privileged. Distributive mixing is less influenced by the viscosity ratio. Coherently with the performance of dispersive mixing, higher distributive mixing indexes are obtained for the lowest and the highest p values, as less break-ups enable higher drop deformation.

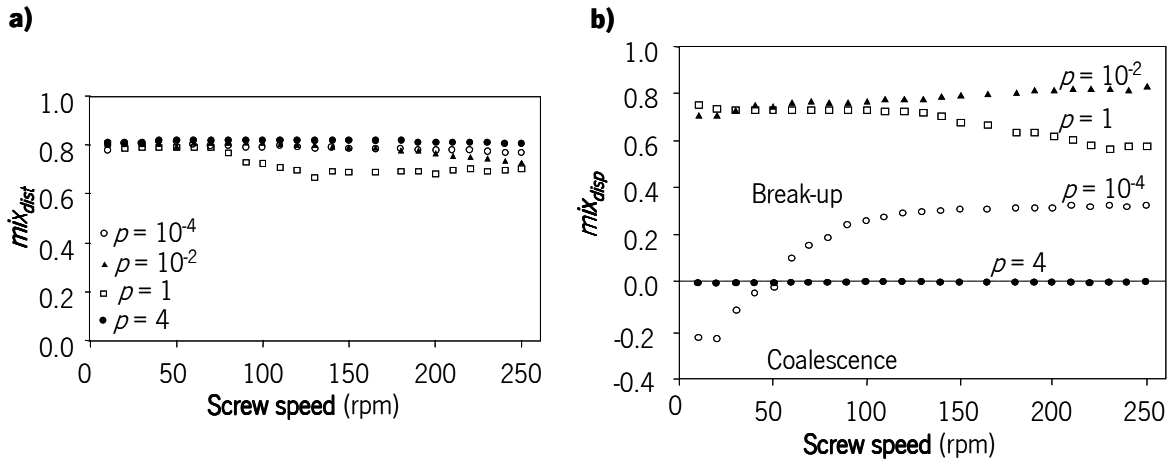

Figure 5: Effect of viscosity ratio on the mixing of a liquid-liquid system: a) distributive and b) dispersive mixing indices.

Matrix Viscosity

Figure 6 shows the influence of matrix viscosity on the mixing indices for the solids-liquid system. Computations with a 20% less viscous HDPE (denoted as HDPE2, while the HDPE of Table 1 is now denoted as HDPE1) were performed. Lower shear viscosities generate smaller hydrodynamic stresses and, consequently, less agglomerate dispersion. In turn, with less dispersion the total number of particles in the system decreases and as a consequence distributive mixing will decrease.

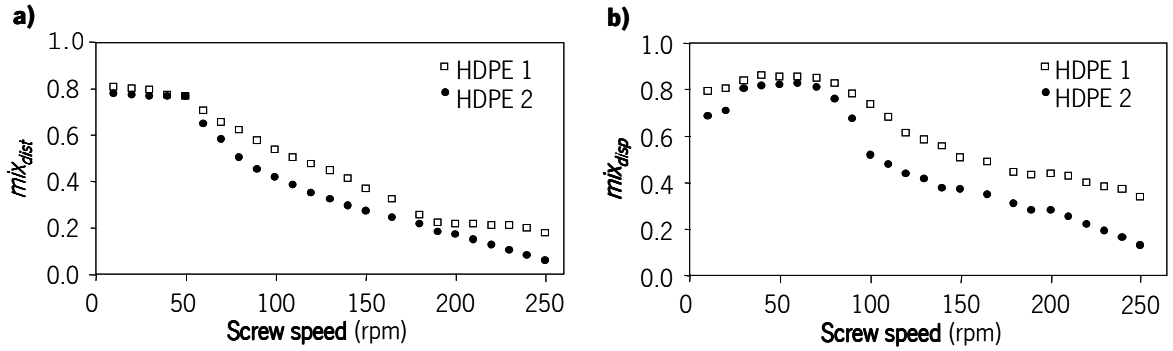

Figure 6: Effect of matrix viscosity on the mixing of a solids-liquid system: a) distributive and b) dispersive mixing indices

Cohesive Forces

In principle, the other parameters remaining constant, those agglomerates with stronger cohesiveness should be more difficult to break, as this requires the development of higher hydrodynamics stresses. Figure 7 confirms this expectation when σ_c is made to increase from 1.0 MPa to 1.5 MPa. It also shows a similar, albeit smaller, effect on distributive mixing (less particles in the system usually bring on less distributive mixing).

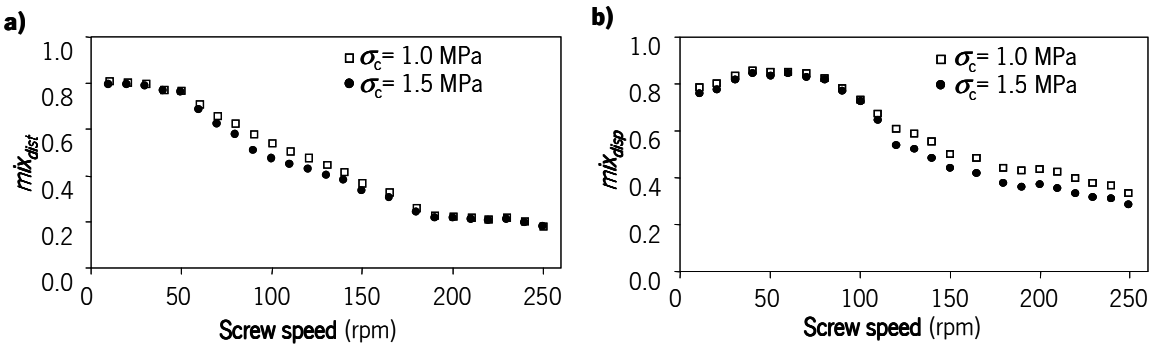

Figure 7: Effect of the agglomerate cohesiveness on the mixing of a solids-liquid system: a) distributive and b) dispersive mixing indices.

4.4 Effect of Operating Conditions

Screw Speed

The effects of changing the screw speed on mixing were already illustrated in Figures 4-7. Generally, the degree of mixing of liquid-liquid systems shows a tendency to decrease with increasing screw speed, as the effect of reducing the residence time for mixing (*i.e.*, the residence time in the melting and melt conveying zones) is not compensated by the raise of the shear rate/stress levels. Nonetheless, in some circumstances (to be discussed below) improvements in mixing are predicted at the upper screw speed range.

In the case of the solids-liquid system, distributive mixing generally decreases with increasing screw speed, reflecting predominantly the decrease in residence time. As for dispersive mixing, the balance between average shear rate (shear stress) and residence time for mixing induces dissimilar responses at low and high screw speeds. Below 60 rpm, the residence times are sufficiently high for agglomerate break-up to occur and an increase in shear rate brings about benefits to mixing (due to the progressively higher hydrodynamic

stresses). Above this rotating frequency, further increases in shear rate do not compensate for the losses in residence time.

Barrel Temperature

Changes in barrel temperature (at a constant screw speed) have little effect on mass output, hence on average shear rate as well and should decrease the hydrodynamic stress levels due to the associated low viscosities. However, as barrel temperature increases, completion of melting is achieved earlier in the screw, which results in increasing residence times for mixing. As shown in Figure 8 (for a constant screw speed of 60 rpm), in the case of the liquid-liquid system barrel temperatures have no visible effect on either distribution or dispersion. Although in the solids-liquid system the influence is also small, distributive mixing increases with increasing barrel temperatures.

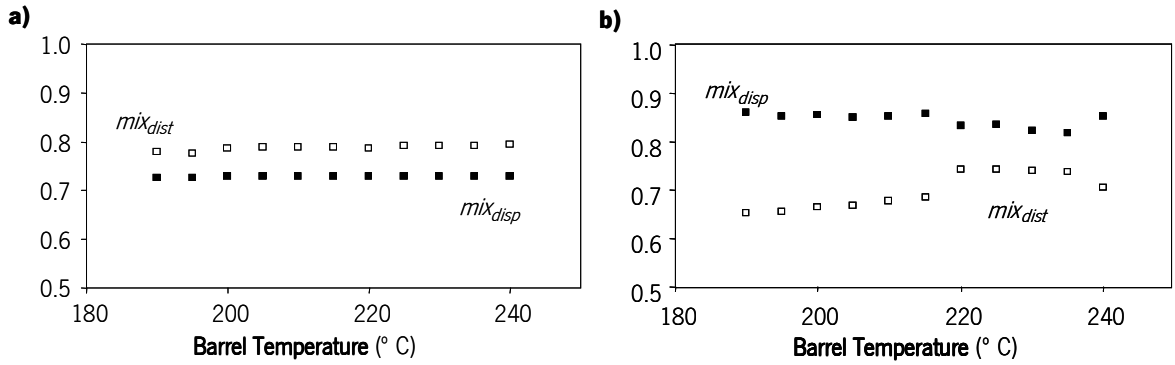

Figure 8: Effect of the barrel temperature on the mixing of: a) a liquid-liquid system, b) a solids-liquid system.

4.5 Effect of Screw Geometry

Screw geometry strongly influences the velocity and temperature profiles, as it affects the melting pace, the residence time for mixing, the average shear rate/stress and, consequently, the mixing effectiveness. The effects on mixing of the length of the metering zone and of the compression ratio are discussed.

Length of metering zone

As shown in Table 2, screw B has a longer metering zone than screw A. At the same screw rotation frequency, the mass output of screw B is lower than that of screw A (at 100 rpm, 10 kg/h versus 11.0 kg/h), hence the average shear rate of the latter is higher (120 s^{-1} versus 86 s^{-1}), but the residence time

for mixing is lower (94 s versus 134 s). As shown in Figures 9 and 10 for the liquid-liquid and solid-liquid systems, respectively, the mixing levels are higher for screws with a longer metering section, *i.e.*, the increase in residence time dominates over the decrease in shear rate.

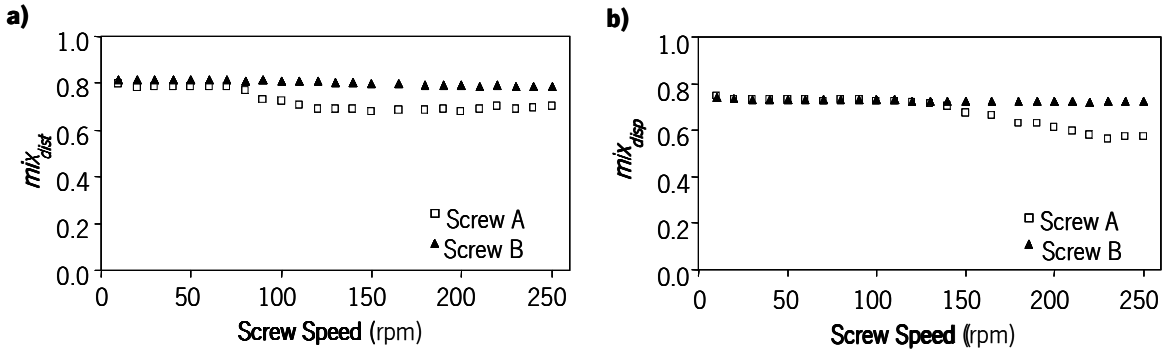

Figure 9: Effect of the length of the metering zone on the mixing of a liquid-liquid system: a) distributive and b) dispersive mixing indices.

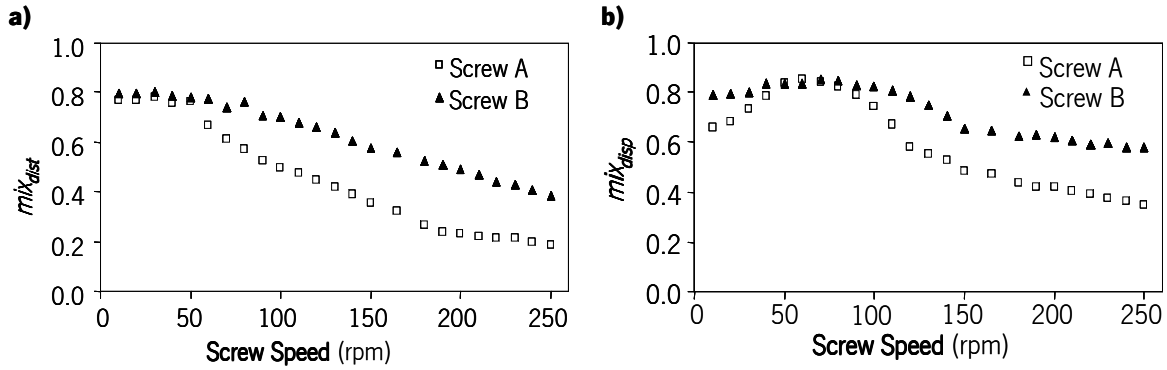

Figure 10: Effect of the length of the metering zone on the mixing of a solids-liquid system: a) distributive and b) dispersive mixing indices.

Compression Ratio

Screws A and C in Table 2 have different compression ratios (CR) as the channel depth in the metering section is 2 mm and 1.43 mm, corresponding to a CR of 2.5 and 3.5, respectively. Changing the CR yields the mixing indices presented in Figures 11 and 12. Particularly at the higher screw speed range, screws with higher compression ratio induce better mixing, as melting becomes more efficient and the residence time for mixing increases. At 200 rpm, by increasing CR from 2.5 to 3.5, gains of 15% in distributive mixing and 22% in dispersive mixing are attained.

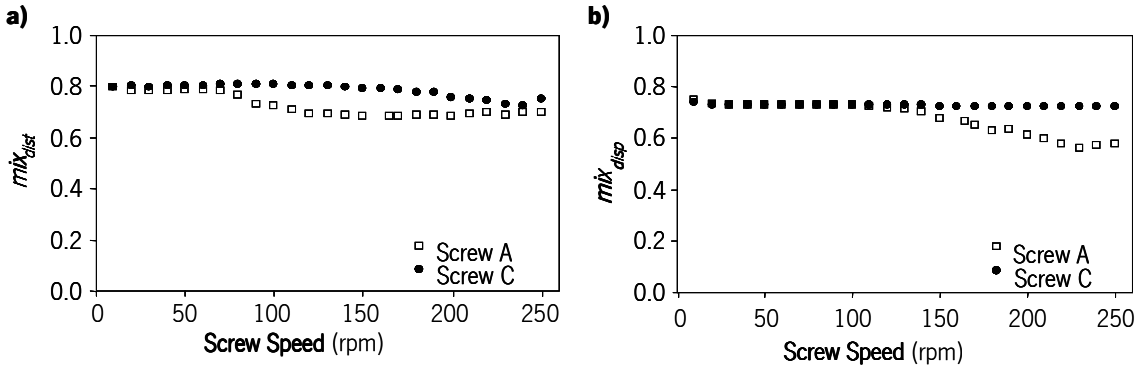

Figure 11: Effect of the compression ratio on the mixing of a liquid-liquid system: a) distributive and b) dispersive mixing indices.

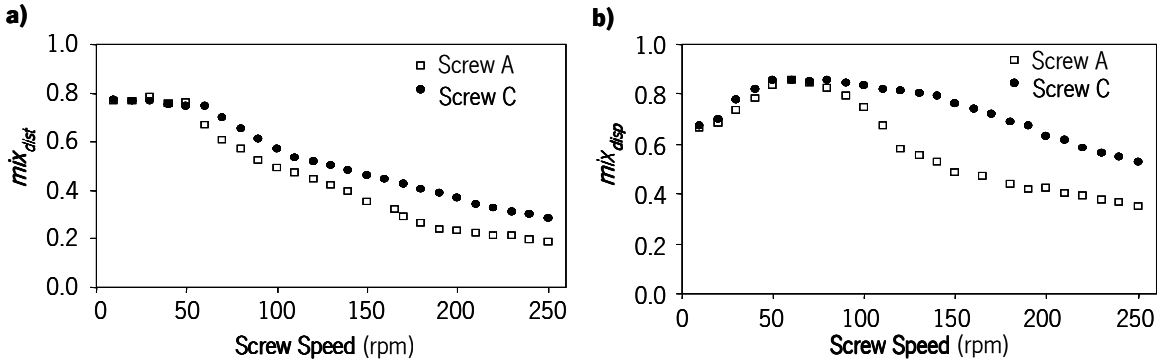

Figure 12: Effect of the compression ratio on the mixing of a solids-liquid system: a) distributive and b) dispersive mixing indices.

Channel depth

Screws C and D in Table 2 have the same geometrical profile and compression ratio (3.5), but screw C is shallower (lower channel depths). As can be observed in Figure 13, screw C melts the material more efficiently, which means that more screw length is available for mixing. Also, due to its shallower channels, the output capacity of screw C is smaller, hence the residence time is higher, but the average attained shear rates/stresses are higher. The resulting mixing indices are displayed in Figures 14 and 15, for the liquid-liquid and solids-liquid system, respectively. In both cases, the mixing ability of screw C is higher than that of screw D, especially between 100 rpm and 200 rpm, when the effect of the residence time becomes predominant over that of the hydrodynamic stresses.

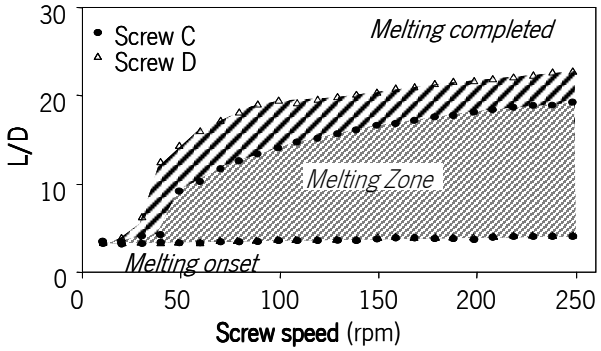

Figure 13: Effect of screw diameter on melting.

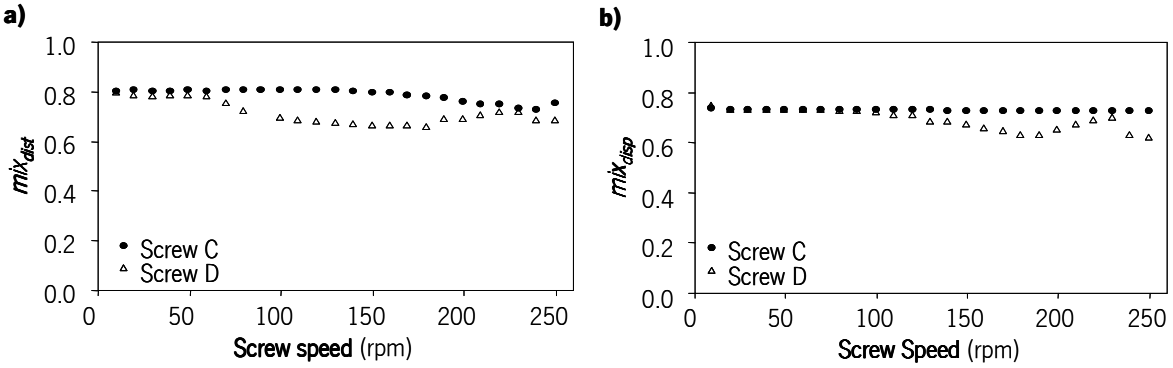

Figure 14: Effect of the channel depth on the mixing of a liquid-liquid system: **a)** distributive and **b)** dispersive mixing indices.

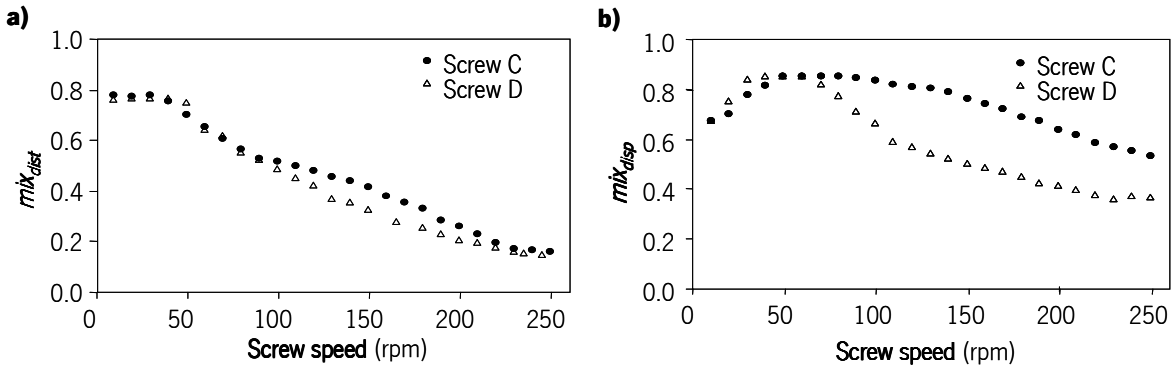

Figure 15: Effect of the channel depth on the mixing of a solids-liquid system: **a)** distributive and **b)** dispersive mixing indices.

Die restriction

A longer die land length will generate a higher back pressure, thus reducing the mass output and increasing the residence time for mixing. Therefore, it is not surprising that the global mixing levels tend to be higher for longer dies (Figures 16 and 17).

Another possibility of using the die to tune the mixing intensity is to impose a certain constant output independently of the screw speed, by varying the pressure via a regulator (which typically consists of an obstacle that can be made to protrude more or less into the flow channel depending on the back pressure level to be imposed). The process is illustrated in Figure 18, which shows the variation of mass output with screw speed and the resultant residence time for mixing (average residence time in the melting and melt conveying zones). The trend set by the open square symbols in Figure 18a corresponds to the conventional correlation between output and screw speed when using the reference die. As seen in Figure 18b, as the screw speed increases, the residence time for mixing decreases. The remaining responses resulted from adopting the following procedure: when a certain combination of mass output – screw speed was attained, the screw speed continued to be progressively increased, but the output was maintained constant by increasing the local back pressure as necessary. As a consequence, the residence time for mixing remained practically constant. Indeed, some minor changes occurred, because the onset and extent of the melting zone were slightly affected.

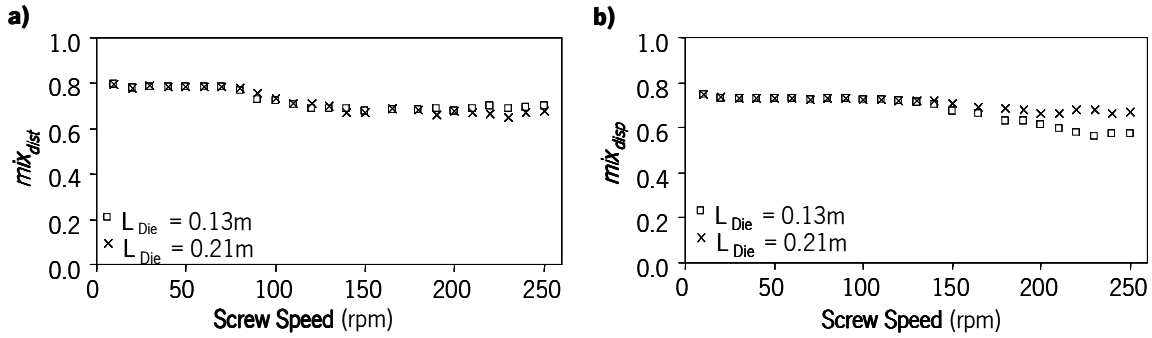

Figure 16: Effect of the die land length on the mixing of a liquid-liquid system: a) distributive and b) dispersive mixing indices.

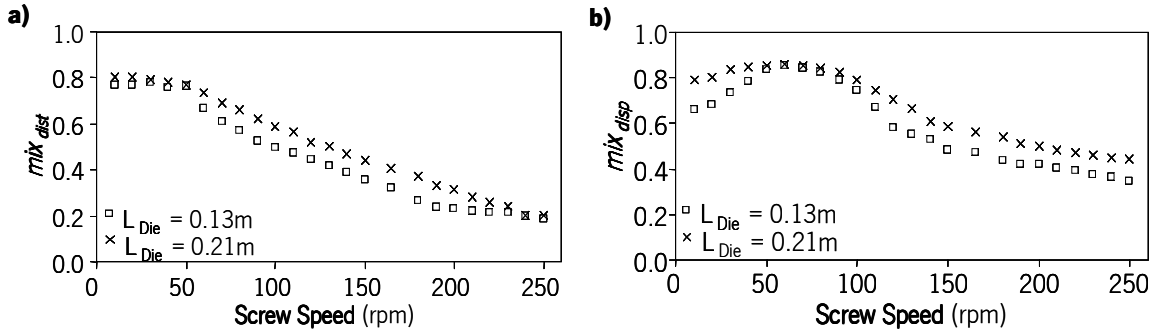

Figure 17: Effect of the die land length on the mixing of a solids-liquid system: a) distributive and b) dispersive mixing indices.

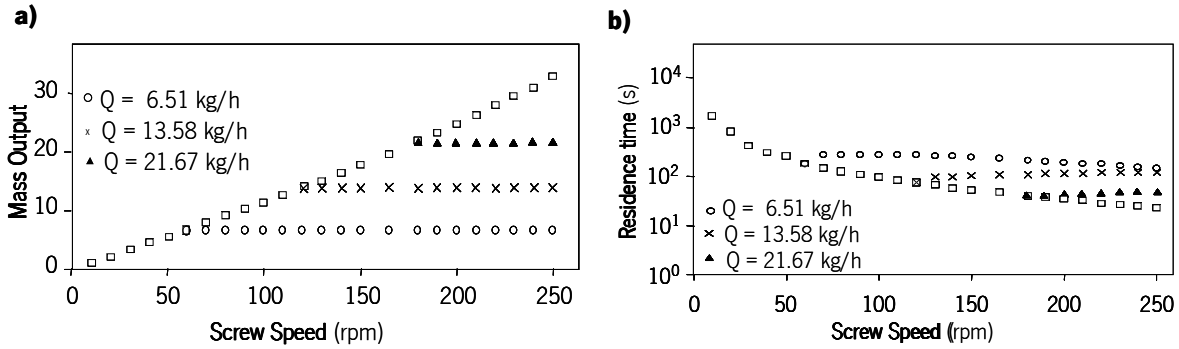

Figure 18: Using a die with a pressure regulator: a) Mass Output, b) Residence time for mixing.

The results depicted in Figure 19 and, especially, in Figure 20, for the liquid-liquid and solids-liquid systems, respectively, are in good agreement with the classical industrial practice of improving the quality of the extrudate obtained when operating at a certain operating condition, by simultaneously increasing the screw speed beyond the value necessary to obtain that output and the back pressure caused by the die. In

this way, the shear rate/stress levels increase but not at the expense of the residence time, which remains constant. For example, Figure 18a shows that for a screw speed of 180 rpm, the predicted output is slightly less than 22 kg/h. When processing the solids-liquid system under these conditions, the distributive mixing index is circa 0.26 and the dispersive mixing index circa 0.44. However, if the screw speed is raised to 250 rpm but the pressure is regulated so that the output is not changed, those two indices augment to 0.38 and 0.58, respectively, which is significant.

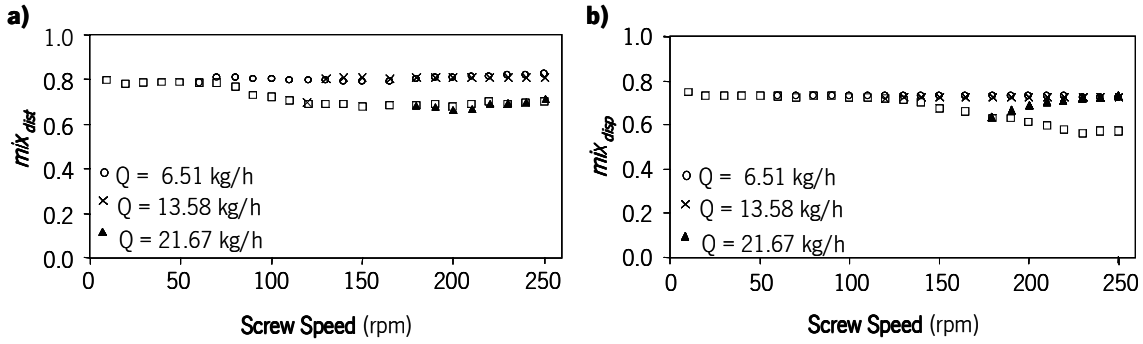

Figure 19: Effect of back pressure on mixing in solid-liquid system: a) distributive b) dispersive mixing indices.

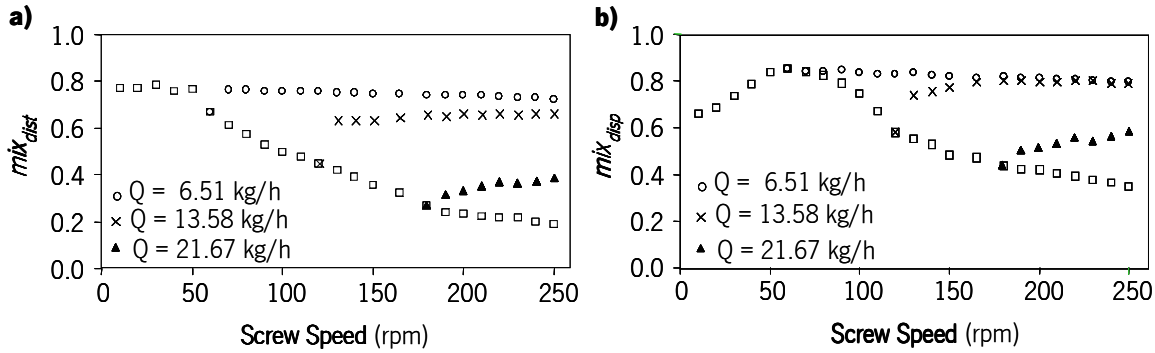

Figure 20: Effect of back pressure on mixing in solid-liquid system: a) distributive b) dispersive mixing indices.

4.6 Optimizing for mixing

The mixing indexes proposed in this work were used to determine the operating conditions and the screw geometry that maximizes the mixing performance for the liquid-liquid and solid-liquid systems studied. This was done adopting an optimization approach, where the indices are used as the objectives to be optimized.

The optimization algorithm contains three main components:

i. a modelling routine able to compute the values of the objectives chosen, which in this case is the software described above;

ii. a routine able to link those values to the optimization algorithm whilst enabling the possibility of dealing simultaneously with various objectives;

iii. an optimization algorithm (in this case, an Evolutionary Algorithm, EA, that uses a population of solutions representing the variables to be optimized).

The EA (a specific algorithm developed by the authors and denoted as RPSGA was used [38]) defines the solutions – operating condition and/or screw design – to be evaluated by the modelling routine (the initial solutions are generated randomly). The latter computes their corresponding behavior and passes this information back to the RPSGA algorithm via the objective function routine, which uses it to quantify the performance of each solution. In this way, the RPSGA is able to select the best solutions during the successive generations and, thus, progresses towards the best solutions. A more complete explanation of this algorithm and associated computations can be found in [38].

An important advantage of multi-objective algorithms, *i.e.*, algorithms that are able to optimize various objectives simultaneously, is their capacity to explicit the trade-of between objectives, usually via the use of Pareto Curves [39]. Pareto optimal plots relate the so called non-dominated solutions (*i.e.*, all the solutions that are at least as good as the remaining in relation to all objectives, but better with respect to at least one objective). Therefore, in the present optimization Pareto plots are 2D graphs containing the non-dominated solutions that maximize the distributive and dispersive mixing indices. Each solution in the plot corresponds to a set of operating conditions, screw geometry or both, depending on the type of the optimization problem solved.

Considering screw A (Table 2) and the same materials as above, the optimization of the operating conditions (screw speed and three barrel temperatures) in terms of distributive and dispersive mixing for the liquid-liquid (RUN 1) and solid-liquid system (RUN 2) was carried out. The operating conditions were allowed

to vary in the interval [50, 150] rpm for the screw speed and [190, 240] °C for the barrel temperatures. Figure 21 shows the resulting optimal Pareto plot. Within the range of the operating conditions searched, mix_{dist} varies between 0.73 and 0.97 and 0.77 and 0.81 for the liquid-liquid and solid-liquid systems, respectively, while mix_{disp} varies between 0.72 and 0.80 and 0.57 and 0.62, respectively. The two objectives are conflicting, *i.e.*, improvement of one deteriorates the other. Taking solid-liquid as example, this is probably due to the fact that bigger drops can attain higher deformations than smaller ones, that is, every time a drop breaks, a new spherical droplet is formed, a regression in distribution taking place. Although the values of the indices are always relatively high, for the material characteristics assumed the mixing capacity of the extruder is higher for the liquid-liquid system. The Figure also identifies two possible solutions to the problems. Solution 1 is located at the change in slope of the correlation, *i.e.*, neither distributive or dispersive mixing could be much better, even if considered individually, whereas solution 2 attempts to obtain a good balance between distribution and dispersion. The corresponding operating conditions are listed in Table 3. In the two cases, the screw speed and barrel temperatures are relatively low, which confirms that the most efficient mixing conditions require sufficiently high hydrodynamic stresses (moderate temperatures) and enough residence times (intermediate screw speeds).

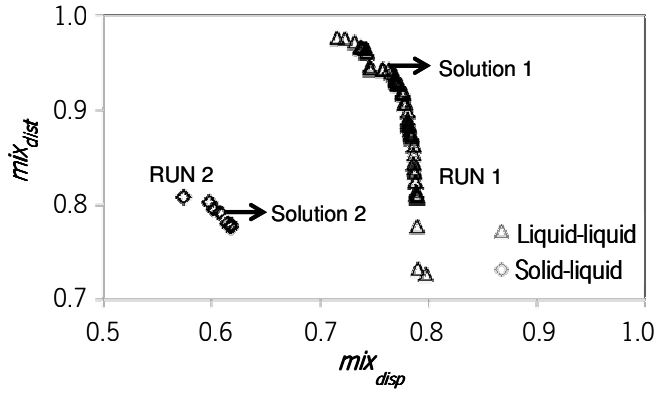

Figure 21: Pareto frontiers for runs 1 and 2, optimization of the operating conditions.

Table 3: Optimized operating conditions (N is screw speed and Tb_i is barrel temperature) and screw geometries (P is pitch and e is flight thickness). The solutions are identified in Figures 21 and 22.

Solution		1	2	3	4
Screw speed (rpm)	N	82	57	85	51
Barrel temperature profile (°C)	Tb_1	212	207	222	193
	Tb_2	208	229	207	207
	Tb_3	190	217	201	206
Extruder Length (m)	L_1			0.322	0.154
	L_2			0.353	0.386
	L_3			0.225	0.354
Barrel Diameter (m)	D			0.030	0.030
	D_1			0.023	0.023
	D_2			0.030	0.027
Pitch (m)	P			0.033	0.030
Flight thickness (mm)	e			3.5	3.8
Compression ratio				3.5	2.3

Figure 22 shows the optimal Pareto plot when the operating conditions and the screw geometry were simultaneously optimized. Again, two solutions were extracted (solutions 3 and 4), the corresponding data being presented in Table 3. The range of variation of the operating conditions was the same as before. The geometrical parameters optimized included the lengths of the feed and compression sections, L_1 [100, 400] mm and L_2 [170, 400] mm, the internal diameter of the feed and metering zones, D_1 [20, 24] mm and D_2, [24, 28] mm, the pitch P [28, 40] mm and the flight thickness, e [3, 4] mm, the numbers between square brackets representing the range of variation. Given the higher degrees of freedom granted to the optimization, not only the values of the mixing indices are higher than before, but the ability to converge to a single point also increased. The operating conditions proposed by the algorithm are not too different than those for solutions 1 and 2. Conversely, the screws for solutions 3 and 4 are quite different, and also distinct from screw A. These results are not easy to explain, but still it can be noted that the screw for solution 3 has a higher compression ratio than screw A (3.5 versus 2.5), while the screw for solution 4 has a lower CR, but the compression and metering zones are much longer. It is the combination of these parameters with the operating conditions that yields the mixing levels presented.

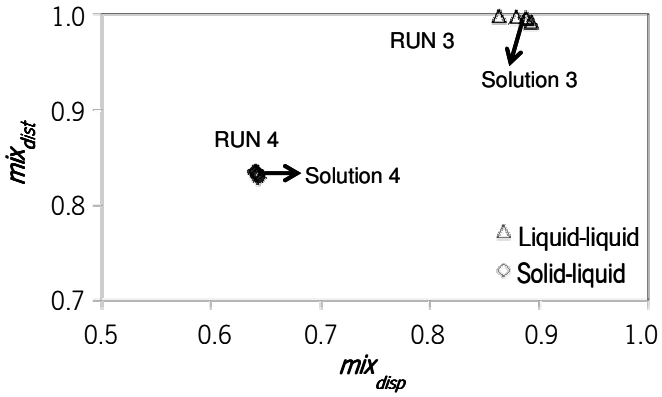

Figure 22: Pareto frontiers for runs 3 and 4, optimization of the operating conditions and screw geometry.

5 Conclusions

The present work uses available algorithms capable of predicting the evolution of the morphology of immiscible liquid-liquid systems, or the dynamics of filler size and spatial distribution of solids-liquid systems, to characterize the global mixing process performance of plasticating single screw extruders. Specifically, quantitative distributive and dispersive mixing indices were defined and made to range in the interval [0, 1], which makes them adequate to directly compare the aptitude for mixing of different screw profiles, to optimize operating conditions, to anticipate the behavior of a given compound, or to scale-up.

Although no direct comparison is made between predictions and experimental observations (these would be extremely complicated and laborious), the forecasted effects of material properties, operating conditions, screw and die geometry on mixing seem physically coherent and are in good agreement with the existing process understanding. In all cases, the methodology proposed evidenced good sensitivity to the parameter studied.

Generally, mixing improves with larger residence times in the melting and melt conveying zones and with higher hydrodynamic stresses (or, equivalently, higher shear rates). In practice, these two parameters are often conflicting, but specific operating techniques can be adopted to achieve a good compromise between them.

As an illustration of their usefulness, the mixing indices are used to set-up (via an optimization approach) the operating conditions and the screw geometry that maximize the mixing performance of single screw extrusion for a given material system.

References

1. C. Rauwendaal, *Polymer Mixing: A Self-Study Guide*, Hanser Publishers, New York (1998).
2. S.J. Kim and T. H. Kwon, *Adv. Polym. Techn.*, **15**, 41 (1996).
3. M. Gale, Adv. Polym. Techn., **16**, 251 (1997).
4. R.S. Spencer and R.M. Wiley, *J. of Colloid Sci.*, **6**, 133 (1951).
5. G. Pinto and Z. Tadmor, *Polym. Eng. Sci.*, **10**, 279 (1970).
6. D.M. Biggs and S. Middleman, *Ind. Eng. Chem. Fundam.*, **13**, 66 (1974).
7. D.M. Biggs, *Sci. Tech. Polym. Process.*, Int. Conference, 945 (1977).
8. I Manas-Zloczower, *Mixing and Compounding of Polymers: Theory and Practice*, Carl Hanser Verlag, Munich, Germany (2009).
9. H. Potente and M. Bastian, *Proceedings of Polyblends'97*, Canada, 397 (1997).
10. H. Potente and K. Kretschmer, *Polym. Eng. Sci.*, **42**, 19 (2002).
11. P. DeRoussel, D. V. Khakhar and J. M. Ottino, *Chem. Eng. Sci.*, 5**6**, 5511 (2001).
12. Z. Tadmor, C.G. Gogos, *Principles of Polymer Processing*, John Wiley & Sons, Novoken New Jersey, USA (2006).
13. S. Middleman S, *Fundamentals of Polymer Processing*, McGraw-Hill, New York (1977).
14. N. Harnby, M.F. Edwards and A.W. Nienow, *Mixing in the Process Industries*, Butterworth-Heinemann, Oxford (1992).
15. R.J. McDonough, *Mixing for the Process Industries*, Van Nostrand-Reinhold, New York (1992).
16. A.C.-Y. Wong and Y. Lam, *J. Polym. Res.,* **15**, 11 (2008).
17. M.H.G. Amin, L.D. Hall, W. Wang and S. Ablett, *Meas. Sci. Technol.*, **15**, 1871 (2004).
18. H. Benkreira, R.W. Shales and M.F. Edwards MF, *Intern. Polym. Proc.*, **7**, 126 (1992).
19. W. Wang, I. Manas-Zloczower and M. Kaufman, *AIChE Journal*, **49**, 1637 (2003).
20. M. Heniche and P.A. Tanguy, *Chem. Product and Process Modeling*, **3**, 1 (2008).

21. R.K. Connelly and J.L. Kokini, *J. of Food Eng.*, **79**, 956 (2007).

22. A. Lawal and D. Kaylon, *Polym. Eng. Sci.*, **35**, 1325 (1995).

23. P.G.M. Kruijt, O.S. Galaktionov, P.D. Anderson, G.W.M. Peters and H.E.H. Meijer, *AIChE Journal*, **47**, 1005 (2001).

24. W. Wang, I. Manas-Zloczower and M. Kaufman, *Int. Polym. Proc.*, **16**, 315 (2001).

25. K. Alemaskin, I. Manas-Zloczower and M. Kaufman, *Polym. Eng. Sci.*, **45**, 1011 (2005).

26. N. Domingues, A. Gaspar-Cunha and J.A. Covas, *Polym. Eng. Sci.*, **50**, 2194 (2010).

27. N. Domingues, A. Gaspar-Cunha, J.A. Covas, M. Camesasca, M. Kaufman and I. Manas-Zloczower, *Int. Polym. Proc.*, **25**, 188 (2010).

28. N. Domingues, M. Camesasca, M. Kaufman, I. Manas-Zloczower, A. Gaspar-Cunha and J.A. Covas, *Int. Polym. Proc.*, **25**, 251 (2010).

29. H.E.H Meijer and J.M.H. Janssen, *Mixing of Immiscible Liquids*, in *Mixing and Compouding of Polymers*, Manas-Zloczower, Z. Tadmor (Eds), Hanser Publishers, Germany, pp.85-147 (1994).

30. L. Delamare and B. Vergnes, *Polym. Eng. Sci.*, **36**, 1685 (1996).

31. C.E. Shannon and W. Weaver*, The Mathematical Theory of Communication*, Urbana, University of Illinois Press (1948).

32. A.I. Khinchin, *Mathematical Foundations of Information Theory*, New York, Dover (1957).

33. A. Scurati, D.L. Feke and Ica Manas-Zloczower, *Chem. Eng. Sci.*, **60**, 6564 (2005).

34. A. Gaspar-Cunha, *Modeling and Optimization of Single Screw Extrusion*, PhD Thesis, University of Minho (1999).

35. B. Elbirli, J.T. Lindt, S.R. Gottgetreu and S.M. Baba, *Polym. Eng. Sci.*, **24**, 988 (1984).

36. N. Domingues, M. Camesasca, M. Kaufman, I. Manas-Zloczower, A. Gaspar-Cunha and J. A. Covas, *ANTEC 2006*, Confer. Proceed, USA, 942 (2006).

37. H.P. Grace, *Chemical Engineering Communications*, **14**, 225 (1982).

38. Gaspar-Cunha A, Covas JA. *RPSGAe–Reduced Pareto Set Genetic Algorithm: Application to Polymer Extrusion*. In: Gandibleux X, Sevaux M, Sörensen K, T□kindt V, eds. Metaheuristics for Multiobjective Optimisation. Springer. Lecture Notes in Economics and Mathematical Systems Vol. 535; 221-249, 2004.

39. K. Deb, *Multi-Objective Optimization using Evolutionary Algorithms*, Wiley: Chichester, UK, 2001.

VI

Conclusions

Mixing models to quantify the mixing behaviour of liquid-liquid and solid-liquid systems in single screw extruders were proposed and implemented in computer. This was done through the linkage of the mixing models developed with an existing global modelling software able to compute all process functional zones (from the hopper until the end of the die). The routines developed are able to compute the mixing behaviour and the morphology development when a liquid or solid additive is incorporated in the polymeric matrix. Two mixing indexes were propose quantifying dispersive and distributive mixing for each material system.

The computational results were assessed experimentally and the results obtained generally indicate that the predictions are in line with reality. The influence of the process parameters (materials properties, system geometry and operating conditions) in the mixing performance was also studied. The program is sensitive to those changes. Therefore, this new computational tool was used for process optimization purposes. In the following, both systems will be discussed separately.

In the case of the liquid-liquid system, the model predicts the evolution of the morphology of drops suspended in a melt. Stretching, break-up and coalescence are considered. The non-isothermal two-dimensional flow of non-Newtonian fluid was. The computational results were compared with experimental observations by taking into account the morphology development of two immiscible polymers (HDPE and PP) along the extruder. The effect of different screw speeds and barrel temperatures was studied. For that purpose samples of cross-sections were collected and 10 μm of thick material carcasses were analysed under the microscope. The experimental results were shown to be in line with the model predictions.

An extensive study of the effect of material properties (*e.g.*, viscosity ratio and interfacial tension); operating conditions (*e.g.*, screw speed and barrel temperature) and screw geometry (*e.g.*, length of metering zone, compression ratio and channel depth) on the morphology development along the screw channel was performed. The main conclusions are:

i. Dispersion is easy to achieve for values of the viscosity ratio close to 1. For values ranging between 1 and 10^{-2} higher viscous hydrodynamic stresses are required for drop break-up but, in this case, the residence time required for break-up decreases. Coalescence is predicted for viscosity ratios of the order of 10^{-4}. Distributive mixing is less influenced by the viscosity ratio.

ii. Low interfacial tension implies lower dispersion because the time required for drop break-up increases, even with higher values for the viscous forces. Distributive mixing increases slightly for lower values of interfacial tension since, in this case, the higher hydrodynamic stresses together with less break-ups cause higher drop deformation.

iii. Dispersion and distribution decrease with increasing screw speed, since the effect of reducing the residence time for mixing (i.e., the residence time in the melting and melt conveying zones) is not compensated by the increase in shear rate.

iv. At constant screw speed changes in barrel temperature have little effect on mass output. Hence, on average, shear rate should decrease the hydrodynamic stress levels. However, as the barrel temperature increases, completion of melting is achieved earlier in the screw, resulting in increasing residence times for mixing. The balance between these opposing effects causes an overall small effect of barrel temperature on distribution and dispersion.

v. Longer metering zone causes lower mass output, hence the average shear rate decreases and the residence time for mixing increases. The balance between these two effects shows that distribution and dispersion increase for screws with a longer metering sections.

vi. Screws with higher compression ratio induce better mixing, as melting becomes more efficient and the residence time for mixing increases.

vii. Melting is more efficient in shallow screws. This means that more screw length is available for mixing. Simultaneously, the output capacity decreases and, thus, the residence time increases, but the average shear rates are higher. As a consequence, the mixing capacity increases when the channel height in the metering zone is decreased. This occurs especially for high screw speeds, where the effect of the residence time becomes predominant over that of the hydrodynamic stresses.

viii. A longer die will generate a higher back pressure, thus reducing the mass output and increasing the residence time for mixing. Therefore, this favours higher mixing levels.

As far the liquid-liquid system modelling of the morphology evolution of a solid-liquid system used the velocities profiles calculated with the existing flow modelling routine. Both rupture and erosion of the solid agglomerates were modelled. Modelling of erosion was essentially based on models taken from the literature, whereas a model for rupture was proposed. The trajectory of the particles was calculated from the velocity profiles by employing a tracking routine with an adaptive time step. This enabled the superposition of a Monte Carlo algorithm to model erosion and rupture using the dispersion probability, which is assumed to be dependent on the size of the agglomerate and on the shear stress. The quantification of the particles distribution was based on the Shannon entropy.

The model was coupled to a 3D Computational Fluid Dynamics software to simulate the melt conveying section of a single screw extruder. Taking into account that the results provided a good description of the dynamics of the mixing system along the channel and that they are sensitive to changes in the major parameters, the model was then applied to the existing global modelling single screw extrusion program.

As before, experimental data was generally in line with the model predictions.

The effect of material properties (*e.g.*, melt viscosity and cohesive strength of the solid particles), operating conditions (*e.g.*, screw speed and barrel temperature) and screw geometry (*e.g.*, length of metering zone, compression ratio and channel depth) on the morphology development along the screw channel were studied. The main conclusions were:

i. An increase in viscosity implies higher values for the average hydrodynamic stresses, which increase slightly the residence times. Consequently, better dispersive and distributive mixing are attained.

ii. When the cohesive strength increases, higher hydrodynamic stresses are required to cause dispersion. Therefore, the final levels of dispersion are lower. As a consequence, there are fewer particles in the system, causing lower distribution.

iii. The Distribution generally decreases with increasing screw speed, reflecting the decrease in residence time. The length of screw required for melting increases, but in spite of the higher hydrodynamic forces associated with higher screw speeds, lower screw speeds favour agglomerate dispersion. When the screw speeds are below a certain limit, the efficiency of dispersion deteriorates.

iv. Increasing barrel temperature entails the early completion of melting in the screw, increasing the residence times for mixing but, simultaneously, it reduces the intensity of the hydrodynamic forces. Taking this balance in consideration, when the barrel temperature increases the distributive mixing increases, while dispersion decreases.

v. As for the case of the liquid-liquid system:

   a. distribution and dispersion are higher for screws with a longer metering section;

   b. screws with higher compression ratio induce better mixing;

   c. shallower screws induce better mixing;

   d. longer die land length will generate higher mixing levels.

Suggestions for further work

The suggestions for further work are the following:

1. The study of flocculation of solid particles in the solid-liquid system was not taken into account. This involves the attraction between particles via Van der Waals forces and/or chemical connections. The integration of a model for flocculation in the global mixing model presented would complete physically and mathematically this study.

2. The agglomerate density (or porosity) affects the dispersive mixing as it requires different hydrodynamic forces to cause dispersion. The influence of the effect of the agglomerate density (which is different from the cohesive forces between particles) could be studied on the mixing degree of solid-liquid systems.

3. This study was proposed with the objective of designing new screw geometries and/or new mixing sections taking into account their mixing efficiency. This work will help any screw designer to understand the mixing efficiency of screw devices, leading to improve such design to achieve a better product quality.